LIST OF FIGURES ..... **III**

LIST OF EQUATIONS ..... **VI**

LIST OF TABLES ..... **VII**

ACKNOWLEDGEMENTS ..... **VIII**

ABSTRACT ..... **X**

DECLARATION ..... **X**

LIST OF ABBREVIATIONS ..... **XI**

CHAPTER 1 - INTRODUCTION **1-1**

MOLECULAR MECHANICS 1-1
TREATING TRANSITION METALS WITH MM 1-3
PREVIOUS WORK ON LIGAND EXCHANGE 1-6
PREVIOUS WORK WITH LFMM 1-8
REFERENCES 1-10

CHAPTER 2 - COMPUTATIONAL CHEMISTRY **2-1**

INTRODUCTION 2-1
FIRST PRINCIPLE METHODS – *AB INITIO* 2-1
Quantum Mechanics *2-1*
The Schrödinger[6] equation *2-2*
Hartree-Fock – Theory *2-4*
Density Functional Theory – DFT *2-8*
Local Density Approximation – LDA *2-11*
EMPIRICAL METHODS 2-12
MINIMUM ENERGY CROSSING POINTS (MECP) 2-13
INVESTIGATING MINIMUM ENERGY CROSSING POINTS: 2-14
MOLECULAR MECHANICS 2-16
Charge schemes *2-20*
LFMM – Ligand Field Molecular Mechanics *2-21*
AOM – The Angular Overlap Model *2-28*

CHAPTER 3 - MODELLING OF HEXAQUA COMPLEXES OF FIRST ROW DIVALENT TRANSITION METALS **3-1**

INTRODUCTION 3-1
COMPUTATIONAL DETAILS 3-2
DFT FUNCTIONALS 3-2
LFMM PARAMETERS 3-7
Charge scheme *3-15*
Morse Potential Parameters and Ligand-Ligand repulsion *3-23*
Final results for $[M(H_2O)_6]^{2+}$ *3-27*
CONCLUSIONS 3-29
REFERENCES 3-30

CHAPTER 4 - MODEL TRANSITION STATES **4-1**

INTRODUCTION 4-1
COMPUTATIONAL DETAILS 4-1
WATER EXCHANGE 4-2

Water Exchange Mechanisms *4-2*
Modelling water exchange *4-5*
LFMM exchange energy *4-10*
CONCLUSIONS 4-17
REFERENCES 4-18

CHAPTER 5 - TRANSITION STATES AND MINIMUM ENERGY CROSSING POINTS (MECP) 5-1

INTRODUCTION 5-1
COMPUTATIONAL DETAILS 5-3
MINIMUM ENERGY CROSSING POINTS (MECP) 5-4
TRUE TRANSITION STATES 5-4
TRANSITION STATES WITH LFMM 5-11
CONCLUSIONS 5-20
REFERENCES 5-21

CHAPTER 6 - COBALT (III) AND NITROGEN DONOR CAGE COMPLEXES 6-1

INTRODUCTION 6-1
COMPUTATIONAL DETAILS 6-4
RESULTS AND DISCUSSION 6-5
PARAMETER DEVELOPMENT 6-5
DFT WITH ADF: A NEW BASELINE 6-15
EXPANDED LIGAND TYPES 6-19
CONCLUSIONS 6-22
REFERENCES 6-23

CHAPTER 7 – MIXED LIGAND SYSTEMS OF CR^{3+} 7-1

INTRODUCTION 7-1
PARAMETER DEVELOPMENT 7-2
THE MIXED SYSTEM 7-8
CONCLUSIONS 7-13
REFERENCES 7-14

CHAPTER 8 – CONCLUSIONS 8-1

GENERAL CONCLUSIONS 8-1
FUTURE WORK 8-4
FINAL CONCLUSIONS – LFMM 8-5

List of Figures

Figure 1-1 Classical double hump in properties of the transition metals 1-5
Figure 1-2 Schematic representation of the exchange mechanisms with respect to the volume of activation. (modified from Figure 1[58]) 1-7
Figure 1-3 Early LFMM results for various Cu^{2+} complexes[80] 1-8
Figure 2-1 Diagrammatic representation of the SCF procedure 2-6
Figure 2-2 Distortion in Jahn-Teller active Cu(II) the classical Z extension and X,Y compression 2-18
Figure 2-3 Orbital splitting in tetragonal elongation Jahn-Teller distortion 2-19
Figure 2-4 Reference angles in representative compounds 2-19
Figure 2-5 Enthalpy of hydration for the divalent first row transition metal complexes from Ca to Zn 2-22
Figure 2-6 Ligand field splitting in octahedral Ca^{2+}, Mn^{2+} and Zn^{2+}, including electron distribution to show all systems stabilised by zero Δ_{oct} 2-23
Figure 2-7 LFSE in terms of Δ_{oct} for the metals between Mn and Zn 2-23
Figure 2-8 Schematic representation of the Morse potential parameters 2-25
Figure 2-9 Changes in M-O bond length and system energy as r_0 is changed 2-26
Figure 2-10 Changes in M-O bond length and system energy as α is changed 2-27
Figure 2-11 Changes in M-O bond length and system energy as D is changed 2-27
Figure 2-12 Changes in M-O bond length and system energy as $A_{//}$ is changed 2-28
Figure 2-13 O_h field splitting with reference to AOM parameters 2-29
Figure 2-14, Diagrammatic representation of the parameters θ and ϕ 2-29
Figure 3-1 Comparison of the DFT and experimental M-O distances (Å) 3-5
Figure 3-2 Plot of metal oxygen bond lengths with and without COSMO 3-6
Figure 3-3 Water has π bonding only in one direction 3-8
Figure 3-4 Classical splitting in T_h symmetry 3-8
Figure 3-5 Standard co-planar alignment of ligands T_h symmetry 3-9
Figure 3-6 Equatorial alignment of ligands, D_{2h} symmetry 3-10
Figure 3-7 Change in d orbital splitting upon adopting “equatorial” geometry 3-11
Figure 3-8 alignment of water molecules with axis frame 3-12
Figure 3-9 d orbitals showing alignment with π orbitals on ligands 3-12
Figure 3-10 Comparison of LFMM and DFT M-O bond lengths (Å) 3-18
Figure 3-11 Comparison of LFMM and DFT M-O bond lengths for Jahn-Teller active complexes(Å) 3-19
Figure 3-12 Total bonding energies calculated with LFMM and ADF (Kcal mol^{-1}) 3-19
Figure 3-13 Graphical representation of the motions required to find a true ground state for the hexaqua species 3-22
Figure 3-14 Showing favorable alignment in D_{2h} symmetry hexaqua complexes 3-23
Figure 3-15 Overlay of DFT (purple) and LFMM (green) structures, including the very important roll, pitch and yaw. 3-24
Figure 4-1 Associative (A) Exchange and intermediate 4-3
Figure 4-2 Interchange, associatively activated (I_a) 4-3
Figure 4-3 Dissociative (D) exchange and intermediate 4-4
Figure 4-4 Interchange, dissociatively activated (I_d) 4-4
Figure 4-5 Diagrammatic representation of the three different binding modes 4-6
Figure 4-6 DFT minimised structures of $[V(H_2O)_6]^{2+}$, V type binding 4-7

Figure 4-7 DFT minimised structures of $[V(H_2O)_6]^{2+}$, E type binding....4-7
Figure 4-8 DFT minimised structures of $[V(H_2O)_6]^{2+}$, F type binding....4-7
Figure 4-9 Relative energies (Kcal mol^{-1})....4-8
Figure 4-10 Comparison of selected structural parameters from DFT and LFMM optimisations. 4-9
Figure 4-11 Bound and unbound LFMM structures with seventh water 4-10
Figure 4-12 Schematic representation of the of how basic exchange process were modelled. 4-11
Figure 4-13 Structures with structural parameters for model complexes of $[V(H_2O)_6]^{2+}.H_2O$ 4-12
Figure 4-14 Activation energies (calculated) for the first row divalent elements, for both A and D pathways compared to the experimental –log*k,* where *k* is the experimental exchange constant. 4-13
Figure 4-15 Breakdown of associative activation energy into individual components: ligand-ligand repulsion (L-L), M-L bond stretching (Morse), LFSE and the parent force field terms. 4-15
Figure 4-16 Breakdown of dissociative activation energy into individual components: ligand-ligand repulsion (L-L), M-L bond stretching (Morse), LFSE and the parent force field terms. 4-15
Figure 4-17 Correlation between log *k* values and calculated activation energies, showing a 1 kcal mol^{-1} error 4-16
Figure 5-1 Schematic representation of what structures on the PES different methods locate....5-3
Figure 5-2 DFT transition state for $[V(H_2O)_5.(H_2O)_2]^{2+}$, Associative mechanism and with displacement vectors 5-6
Figure 5-3 DFT transition state for $[Mn(H_2O)_5.(H_2O)_2]^{2+}$. A mechanism, trans ligands exchanging....5-6
Figure 5-4 DFT transition state for $[Mn(H_2O)_4.(H_2O)_2]^{2+}$, Associative mechanism and with displacement vectors....5-7
Figure 5-5 DFT transition state for $[Mn(H_2O)_5...(H_2O)_2]^{2+}$, D mechanism and showing displacement vectors. However still based on seven water system....5-7
Figure 5-6 DFT transition state for $[Mn(H_2O)_5...H_2O]^{2+}$, D mechanism and with displacement vectors, based on a six water system....5-8
Figure 5-7 DFT transition state for $[Ni(H_2O)_4.(H_2O)_2]^{2+}$, A mechanism and with displacement vectors 5-8
Figure 5-8 DFT transition state for $[Ni(H_2O)_4...(H_2O)_2]^{2+}$, D mechanism and with displacement vectors....5-9
Figure 5-9 “Reactant” and “product” geometries used in standard MECP runs. Associative pathway 5-11
Figure 5-10 “Reactant” and “product” geometries used in standard MECP runs. Associative pathway – trans mechanism....5-12
Figure 5-11 “Reactant” and “product” geometries used in standard MECP runs. Dissociative pathway 5-12
Figure 5-12 LFMM transition state for V^{2+}, Associative mechanism....5-13
Figure 5-13 LFMM transition state for V^{2+}, Dissociative mechanism 5-13
Figure 5-14 LFMM transition state for Mn^{2+}, Associative mechanism 5-14
Figure 5-15 LFMM transition state for Mn^{2+}, Dissociative mechanism 5-14
Figure 5-16 LFMM transition state for Mn^{2+}, Associative mechanism 5-15
Figure 5-17 LFMM transition state for Ni^{2+}, Dissociative mechanism 5-15
Figure 5-18 Showing the dominant motion in each of the calculated LFMM transition states. 5-18
Figure 6-1 *Diamsar* a hexadentate ligand that causes distortion away from nominal octahedral shape with Co^{+3}....6-2
Figure 6-2 Cobalt cage complex showing significant DNA targeting and binding characteristics. 6-3
Figure 6-3 Octahedral geometry preferred by cobalt(II) complexes and trigonal prism often preferred by donor atoms in the pro-ligand....6-8
Figure 6-4 comparison of LFMM structures with crystallographic structures....6-10
Figure 6-5 Comparison of ADF and LFMM calculated frequencies for cobalt hexamine 6-11

Figure 6-6 Comparison of M-O bond lengths in LFMM and the Crystallographic data 6-12
Figure 6-7 Graph of LFMM M-N bond lengths against the crystal M-N bond lengths 6-14
Figure 6-8 Overlay of the LFMM(blue) and ADF (green) structures of (Cambridge crystal database refcode).6-16
Figure 6-9 Overlay of LFMM structure (calculated with counterion, ClO_4^-) with original crystal structure of CIXWUB 6-17
Figure 6-10 Key for Table 6-4 6-18
Figure 6-11 comparison of M-O bond lengths given the above stated correction, the circles highlight the outliers that were removed just on the correction of the two above structures. 6-18
Figure 6-12 OXAMCO structure (hydrogen atoms removed for clarity) with labeling key.....6-19
Figure 6-13 CAFHUN structure (hydrogen atoms removed for clarity) with labeling key.....6-20
Figure 6-14 WUGNUH structure (hydrogen atoms removed for clarity) with labeling key 6-21
Figure 7-1 $[Cr(NH_3)_5(H_2O)]^{3+}$ 7-1
Figure 7-2 LFMM (left) and ADF (right) structures for the hexaqua complexes of Cr^{3+}, both showing the roll, pitch and yaw found in earlier work 7-4
Figure 7-3 LFMM (left) and ADF (right) structures for the hexaammine complexes of C r^{3+} 7-4
Figure 7-4 LFMM (left) and ADF (right) structures for the methalyted hexaamine complexes of Cr^{3+} 7-5
Figure 7-5 diagrams of LFMM structures of the complexes with an associated seventh water molecule 7-6
Figure 7-6 I_a and I_d respectively, structures calculated with the LFMM MECP method 7-8
Figure 7-7 LFMM structures for the $[Cr(NH_3)_5(H_2O)]^{3+}$ complex and the $[Cr(NH_3)_6(H_2O)]^{3+}$ 7-8
Figure 7-8 I_a and I_d transition states calculated with the LFM method 7-10
Figure 7-9 I_a and I_d MECP structures for the exchange at $[Cr(NH_2CH_3)_5H_2O]^{3+}$ 7-11

List of Equations

Equation 1-1 Newton's second law 1-1
Equation 1-2 Hills original equation for calculating the conformational strain in a system, this is the original force field equation 1-2
Equation 2-1 Non-expanded version of Schrödinger equation 2-2
Equation 2-2 Schrödinger equation (time independent) with expanded Hamiltonian operator 2-3
Equation 2-3 Del-squared 2-3
Equation 2-4 Hamiltonian operator in terms of energy contributions to the total energy 2-3
Equation 2-5 Hamiltonian operator assuming Born-Oppenheimer approximation; the electronic Schrödinger equation. 2-4
Equation 2-6 Time dependant Schrödinger equation 2-4
Equation 2-7 Thomas-Fermi theory equation 2-9
Equation 2-8 Thomas-Fermi-Dirac equation 2-9
Equation 2-9 Kinetic energy functional, subscript s denotes Slater determinant 2-10
Equation 2-10 Density in term of one electron orbitals. 2-10
Equation 2-11 DFT energy equation with exchange-correlation term 2-10
Equation 2-12 Kohn-Sham equations 2-11
Equation 2-13 Dirac formula 2-12
Equation 2-14 VWN parameterisation of the correlation energy 2-12
Equation 2-15 Relationships that need to be satisfied to locate the MECP 2-13
Equation 2-16 Gradient difference vector in terms of the energies of the two states being minimised 2-15
Equation 2-17 Conditions to be met for the minimisation 2-16
Equation 2-18 F the step size and the functional relationship with previous terms 2-16
Equation 2-19 Simplified force field expression 2-16
Equation 2-20 Expanded force field expression 2-17
Equation 2-21 Force field equation with LFSE correction for d electrons 2-21
Equation 2-22 Morse Potential 2-24
Equation 2-23 Lennard-Jones equation 2-25
Equation 2-24 Pure 1,3-repulsive term for ligand-ligand interaction 2-25
Equation 2-25 AOM equations for nominally octahedral metal complexes 2-30
Equation 3-1 AOM equations for T_h symmetry 3-9
Equation 3-2 AOM equations for the equatorial D_{2h} geometry 3-10
Equation 3-3 Relationship between the splitting parameter Δ_{oct} and AOM parameters for normal D_{2h} symmetry 3-14
Equation 3-4 Relationship between the splitting parameter Δ_{oct} and AOM parameters for equatorial D_{2h} symmetry 3-14
Equation 4-1 Relationship between volume of activation and rate constant 4-5

List of Tables

Table 2-1 Scaling of different methods with respect to system size N. 2-7
Table 3-1 Calculated and experimental M-O bond lengths (Å) 3-4
Table 3-2 Bond lengths of the divalent transition metal aqua complexes $[M(H_2O)_6]^{2+}$, Jahn-Teller active have both the long and short bonds listed. 3-6
Table 3-3 Energies of the MOs (eV) from the equatorial geometry ADF calculations, values in parenthesis in cm^{-1} 3-13
Table 3-4 Calculated partial charges for various metals at different M-O bond lengths 3-16
Table 3-5 Compiled list of used charge schemes including standard TIP3P charges 3-17
Table 3-6 Compiled energetic data for LFMM calculations 3-20
Table 3-7 Compiled data, target energetic data 3-25
Table 3-8 Final LFMM parameters 3-26
Table 3-9 Compiled Results for LFMM minimisations; DFT underlined, Johnson and Nelson bold, LFMM italics 3-28
Table 5-1 Collection of the single negative frequencies found in the above geometries calculated with DFT 5-9
Table 5-2 Table showing comparison of energies for the different transition state pathways calculated with DFT 5-10
Table 5-3 LFMM energies for the different calculated MECP structures, kcal mol^{-1} 5-16
Table 5-4 Comparison of DFT and LFMM calculated structures and frequencies of the most favourable pathway for each metal. 5-19
Table 6-1 Early LFMM parameters and the final refined set based on full system property analysis (see later in this chapter) 6-6
Table 6-2 Calculated LFMM structures compared to crystal structures, sorted by reference code 6-7
6-3 Composition of starting test set, alphabetical by ccdc refcode 6-9
Table 6-4 Comparison of LFMM and DFT structural parameters for CIXWUB (Key for bond numbering shown below) 6-17
Table 6-5 Comparison of structural features for OXAMCO from the crystal structure and the LFMM structure 6-19
Table 6-6 Comparison of structural features for CAFHUN from the crystal structure and the LFMM structure 6-20
Table 6-7 Comparison of structural features for WUGNUH from the crystal structure and the LFMM structure 6-21
Table 7-1 Charges calculated for the $[Cr(H_2O)_6]^{3+}$ complex. 7-2
Table 7-2 Charges calculated for the $[Cr(NH_3)_6]^{3+}$ complex 7-3
Table 7-3 Charges used for all LFMM work that follows 7-3
Table 7-4 Table of key parameters calculated in both ADF and with LFMM using the developed parameter set 7-4
Table 7-5 Comparison of LFMM and DFT M-O bond lengths to the seventh ligand (in these a molecule of water) 7-6
Table 7-6 Energy comparison of different pathways for water exchange at $[Cr(H_2O)_6]^{3+}$ 7-7
Table 7-7 Comparison of M-O bond lengths in the $[Cr(NH_3)_5(H_2O)]^{3+}$ complex 7-9
Table 7-8 Comparison of exchange route energies from LFMM 7-10
Table 7-9 Comparison of LFMM and Rotzinger calculated bond lengths for the exchange pathways of $[Cr(NH_2CH_3)_5H_2O]^{3+}$ 7-11
Table 7-10 Comparison of exchange route energies from LFMM 7-12

Acknowledgements

There are many people who have influenced and aided me in the last three and half years and this is too small a space to do any of them real justice but I will try to thank all those I can.

The two people who I need to thank the most for keeping me sane and working are my beloved wife, Christine, and my Supervisor Dr Rob Deeth.

My wife has been by my side constantly throughout the last three and a half years, giving me support and encouragement whenever I needed it, and making sure that I stayed grounded keeping in mind what had to be done both academically and in life as a whole. Christine has also made the finishing of this thesis a lot easier as she has done enough worrying for both us leaving me to remain fairly calm and do the writing.

My supervisor Rob has been an immense help to me in all that I have done for this PhD. His overwhelming and infectious enthusiasm for the subject is impossible to resist and has resulted in many fond memories of excited discussions in the pub, well known to be the best location for significant scientific development. The social down time hosted by Rob and his wife Pam is always a great event for the group and has maintained the excellent atmosphere within the office.

There are many people within the theory and computational cluster that deserve my thanks. James Burnside, who was the ICCG when I joined it, deserves thanks for helping me settle quickly and providing great distraction especially at the end of the day in enemy territory. Christian Diedrich, who joined the group at the end of my first year, who constantly helped with his support, encouragement and knowledge of computational theory. Anna Anastasi , for making sure I was organised and always being willing to lend a hand with any problem. David Quigley, for always being approachable, helpful and far too modest.

Next I have to thank the rest of my family especially my parents who have always been supportive and encouraging in everything I have ever done, without this support I would not have made it this

far. My brothers Jack and Connor, for understanding what I had to do when I moved away and always being tolerant when I could not make it back to see them. My Nan and Granddad, for always believing in me no matter what the challenge, sadly my Grandad is not here to see me finally submit this thesis. To the rest of my family, you have my thanks for always being there and encouraging.

Finally to everyone else that has been a part of the last three and half years, both socially and academically, thank you.

Abstract

In this thesis the use of LFMM and the application of it to problems not typical tractable within a classical framework are detailed.

The parameterisation of LFMM through the AOM is shown for a number of different metal ligand complexes. The developed parameters are then used to investigate numerous problems, structures and energies of first row divalent metal complexes, energies of the water exchange pathways using model structures, investigation of the true transition states of water exchange and the selectivity for different pathways, structures and behaviour of cobalt (III) cage complexes and finally ligand exchange on mixed donor chromium (III) complexes.

The work in chapters one – three has been published as:

Deeth, R. J.; Randell, K. *Inorg Chem* **2008**, *47*, 7377-7388

An overview of the LFMM method and other comparable methods has been published as:

R. J. Deeth, A. Anastasi, C. Diedrich and K. Randell, *Coord. Chem. Rev.*, 2009, **253**, 795-812.
Molecular Modelling for Transition Metal Complexes: Dealing with d-Electron Effects

The preprint of a publication that is grounded in this work is also included as an appendix.

R. J. Deeth, A. Anastasi, and K. Randell, Ligand field torque: a π-type electronic driving force for determining ligand rotation preferences, Submitted

Declaration

The work in this thesis is my own and has not been submitted for degree at any other university.

The guidelines followed in the preparation of this thesis were those described in the Postgraduate Research Degree Studies booklet, obtainable from the department of Chemistry.

Signed..... Date.....

List of Abbreviations

ADF	Amsterdam Density Functional
AO	Atomic Orbital
AOM	Angular Overlap Model
CFT	Crystal Field Theory
CLF	Cellular Ligand Field
COSMO	Conductor Like Screening Model
DFT	Density Functional Theory
DommiMOE	D-Orbitals Molecular Mechanics in the Molecular Operating Environment
DOMMINO	D-Orbitals in Molecular Mechanics of INOrganics
GGA	Generalized Gradient Approximation.
HF	Hartree-Fock
I_a	Associative Interchange
I_d	Dissociative Interchange
ICCG	Inorganic Computational Chemistry Group
LDA	Local Density Approximation
LFMM	Ligand Field Molecular Mechanics
LFSE	Ligand Field Stabilisation Energy
LFT	Ligand Field Theory
MM	Molecular Mechanics
MOE	Molecular Operating Environment
PES	Potential Energy Surface
TM	Transition Metal
TS	Transition State

Chapter 1 - Introduction

Molecular mechanics

The development of the theories and equations that underpin theoretical chemistry started over three centuries ago with Isaac Newton's Principia Mathematica[1]. This seminal work contained Newton's Laws which form the core of what we now call classical mechanics. Newton's second law relates the forces *F*, of an object to the mass *m* and acceleration $\frac{d\vec{v}}{dt}$, of said object. Although these laws were written based on observations of planetary bodies they have been applied, with differing degrees of success, to chemical systems.

Newton's laws in terms of mathematical mechanics are applied to atoms in a chemical system, the other part of modern mathematical mechanics is that of quantum mechanics (QM). QM acts on more fundamental particles in the chemical hierarchy; electrons and nuclei. QM involves the solving of the Schrödinger equation for a set of particles. However, this is less than trivial and can only be achieved completely for one electron systems. In many electron systems approximations must be used to gain solutions to the Schrödinger equation (more details in Chapter 2). Given the methods that have been developed to treat systems quantum mechanically are still too computationally costly for large or complex systems we need to look to classical molecular mechanics.

$$\vec{F} = \frac{d}{dt}(m\vec{v})$$

Equation 1-1 Newton's second law

The terms in Equation 1-1 are: $\vec{F}$ the force vector, *t* is the time, *m* is the mass of the particle and $\vec{v}$ is the velocity vector.

The use of classical mechanics equations on chemical bodies (atoms) was originally called conformational analysis and was initially proposed by Hill[2] (at this point there was no such thing as a geometry optimisation). The equation proposed by Hill is for a single pair of interacting groups and assumes that the Lennard-Jones potential is appropriate and that Hooke's law is valid at large separations.

$$E = u_0\left(\frac{r_0}{r}\right)^{12} - 2u_0\left(\frac{r_0}{r}\right)^{6} + \frac{1}{2}k_a(l-l_0)^2 + \frac{1}{2}k_b(\theta-\theta_0)^2$$

Equation 1-2 Hill's original equation for calculating the conformational strain in a system, this is the original force field equation

The terms in Equation 1-2 are, U_0 the minimum of the interaction energy (i.e. when $r = r_0$), *r* the distance between two interacting groups, *l* the bond length, θ the bond angle, k_a the bond stretch force constant and k_b the bond angle force constant with r_0, l_0 and θ_0 being the reference values for *r*, *l* and θ.

This conformational analysis was first applied to transition metals by Corey and Bailar[3] and very soon after by others[4-6]. It was not until much later that a method for calculating this conformation strain in a "free" system was developed[7-10], although these methods were still primarily used for fixed coordinate systems with common geometric translocations. However, the techniques required took until 1965 before the first method for the automated minimisation of a system was developed[11,12]. This was the steepest decent method of energy minimisation. Steepest decent requires the calculation of the derivatives of the energy with respect to movements in the 3N coordinates of the system, where N is the number of atoms.

A slightly later improvement to the steepest decent method is that of modified Newton-Raphson[13]. The main difference between the two is the modified Newton-Raphson technique is capable of moving all atoms at once in a concerted minimisation, whereas the steepest decent has to move each atom in turn. This means that the modified Newton-Raphson technique requires far fewer iterations to find the minimum. Dependent on the starting geometry, this may be a local or the global minimum. Also with the modified Newton-Raphson method, it is much simpler to calculate thermodynamic data and vibrational frequencies, as the derivatives of the energy with respect to the displacements are calculated for the step before the minimum. While these methods are all successful in finding the minima of a system (given a suitable starting geometry) they are more suited to organic systems which have easily definable parameters for the structural information. In most transition metal systems this is not the case, and so a more sophisticated method is required.

Treating Transition Metals with MM

A significant amount of the initial molecular mechanics work for transition metals was carried out on cobalt amines[14-22]. This may have been because the initial work in computational coordination chemistry was based on the systems that Werner had studied. Also cobalt(III) hexaam(m)ines are almost always low-spin d^6 and fairly rigorously octahedral. However, these original calculations were based in Boyd's[13] earlier techniques, which treated the system based on electrostatics and steric strain. While this pragmatic approach worked well for a lot of the systems studied, it is not universally applicable to coordination chemistry problems. The stumbling block for classical molecular mechanics is in the treatment of d electrons, since the coordination geometry and spatial relationship of ligands around a metal is not always that of equal bonds and equal spacings[23-28]. To apply the MM method to transition metal complexes a correction is required.

Originally conventional molecular mechanics was applied to transition metal systems. This method had some flaws, one of the biggest being that of unique labelling (unique labelling is covered in more detail in Computational Chemistry Chapter 2). As it can be seen in Equation 2-20 there is only one "space" for the reference bond length but this is not sufficient in many transition metal systems. However, there are examples in the literature of groups using conventional MM to treat transition metals. Two of the larger groups doing this are that of Comba[17,29-32] and Landis[33-37]. The Comba group used certain technical methods to overcome some of the shortcomings of the MM method. These included typing axial and equatorial ligands as different to overcome the unique labelling problems, as well as using the fairly common idea of replacing the angle terms with the metal as the second atom with pure 1-3 repulsive interactions. The Landis group used the valence bond theory to develop the VALBOND force field.

As stated, most earlier work with MM was done on organic systems. However, transition metals have some distinguishing features that separate their behaviour from organic systems. The behaviour of transition metal complexes is largely dictated by the d orbitals. They are responsible for the bond behaviour, bond order and relative energetics of the complexes. For a sound theoretical treatment of transition metals, a method is required that accounts for the behaviour and influence of these d electrons.

In 1929 the CFT (Crystal Field Theory) was published by Bethe[38]. This theory was developed by applying group theory to electrostatic theory by investigating how the strength and symmetry of a crystal field affect the electronic levels of gaseous metal ions. This early postulate by Bethe was ratified very quickly after publication by numerous groups[39-42]. The initial communication by Gorter[39] was the first work to state that the orbital splitting was the same for a tetrahedron as an octahedron but with the order reversed. This initial work also contained the proof that hydrated iron was surrounded by six water ligands.

CFT was developed as a method of describing the effect on the d orbitals of an electrostatic interaction. It does not inherently consider any bonding. A more chemically intuitive system was developed to do just this. This was LFT (Ligand Field Theory)[43]. LFT can be thought of as a combination of MO (molecular orbital) theory[44,45] and CFT. LFT was used extensively by the Gerloch group[46-49].

The exact method used was the AOM (Angular Overlap Model). The AOM differs from CFT in that it is a bond centred approach and that it has a different barycentre to the other models. The AOM method is used as the basis for the LFMM (Ligand Field Molecular Mechanics) method[50,51]. The motivation behind most of this method is the seminal work of Basolo and Pearson[52] which links the properties of the transition metals to the LFSE (Ligand Field Stabilisation Energy) and is often characterised by the common double hump in observable properties. The work of Basolo and Pearson, while of great significance is not unique in the observations made linking the LFSE to other chemical properties. In 1960 Leslie Orgel published his work on transition metal chemistry: ligand field theory[53]. In 1962 Carl Ballhausen published his book on an Introduction to Ligand Field Theory[54].

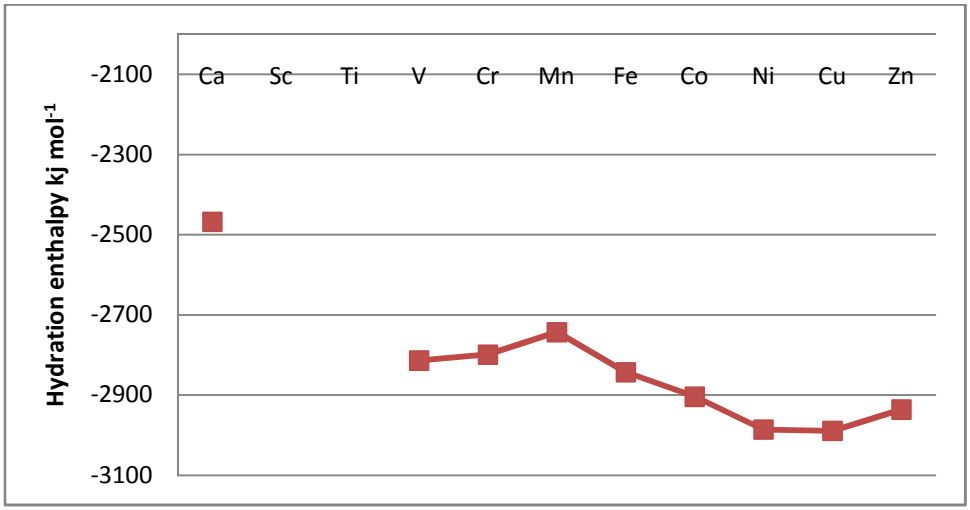

Figure 1-1 Classical double hump in properties of the transition metals

To validate the LFMM method, the "simple" reaction of ligand exchange has been chosen to be modelled (full details in Results chapter one). The exchange of water molecules at transition metal elements is not as simple a process as it first seems: firstly the exchange rates span a significant range, secondly there are scientific disagreements as to the exact mechanism of these exchanges, which will be returned to later.

Previous work on ligand exchange

The exchange of one ligand with another at a metal centre has been studied extensively for at least the last fifty years. Surprisingly, given that it is such a simple process to imagine there has been considerable conjecture on the matter. The conjecture is over the mechanism of ligand exchange in these metal complexes. The types of mechanism possible are: associative, dissociative and concerted, with the concerted pathways having either associative (I_a) or dissociative (I_d) character.

The original mechanistic discussion for the exchange of water ligands at transition metal centres was published by Eigen and Wilkins[55,56]. This work compared the exchange of aquo ligands at different metal sites. The early work concludes a I_d mechanism for all divalent and trivalent first row transition metal ions preceded by the formation of a stable outer sphere complex. This mechanism was arrived at by a comparison of the rates of reaction between the interchange and water exchange at different metal ions.

Over a decade later, following advances in NMR spectrometry, contrary conclusions were drawn. This direct investigation into the mechanism of water exchange, utilising high pressure NMR[57], found that the Mn^{2+} ion actually exchanged via an I_a mechanism[58-62]. This conclusion was drawn from the negative volume of activation (-6.2 $cm^3\ mol^{-1}$) seen for this species as opposed to the positive volume of activation for Ni^{2+} (+7.1 $cm^3\ mol^{-1}$). A diagrammatic explanation of the

activation volume is provided in Figure 1-2. Only a few years later the same group reported a negative volume of activation for the V^{2+} system[63], supposedly ending the arguments about the mechanism of water exchange.

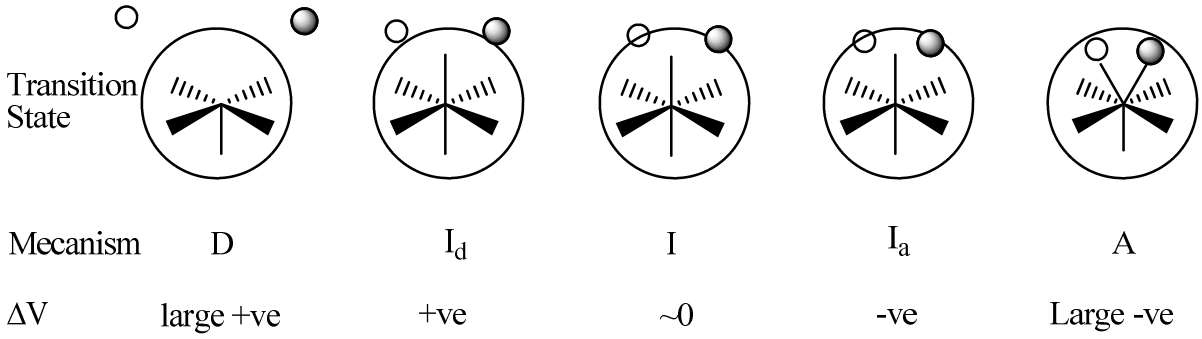

Figure 1-2 Schematic representation of the exchange mechanisms with respect to the volume of activation. (modified from Figure 1[58])

Still more recently, a series of publications have been made that disputed the validity of the NMR results and tried to reset the mechanism of exchange to one that is unanimously I_d in nature. These calculations were performed by Akesson *et al*[64,65]. These theoretical results were quickly argued against by Rotzinger[66-68] who performed a series of high level QM calculations to ascertain that there is a mechanistic changeover upon going from V^{2+} to Mn^{2+} to Ni^{2+} in agreement with the experimental volumes of activation. This later work is backed up by the inclusion of transition states and normal mode analysis. An alternative approach to the work carried out by Rotzinger and others is contained within this thesis.

In choosing to look at the reactions and behaviour of water molecules it is important to see how water is treated in other simulation methods. There exist at present a number of ways to treat water computationally. These range from very large scale bulk methods that treat many water molecules as one simulation entity (such as the MARTINI[69,70] coarse grained[71] force field for biological simulations), to more complex models with multiple sites on each water molecule,

designed to maximise the amount of complex water behaviour recovered from the simulation, the most widely used of these being the TIP[72-75] series (TIPnP, where n is the number of sites used to represent the water potential).

Previous Work with LFMM

The Ligand Field Molecular Mechanics[51] (LFMM) method (covered in detail in Computational Chemistry chapter) is implemented within the MOE package[50]. LFMM has been used previously to successfully investigate a range of transition metal systems[76-79]. The complexes and behaviours of Cu^{2+} have always been of high interest to the group[77-81], due to the computational challenges posed by these systems to classical MM. The LFMM method has been successful in calculating the structures of various Cu^{2+} ammine structures (Figure 1-3).

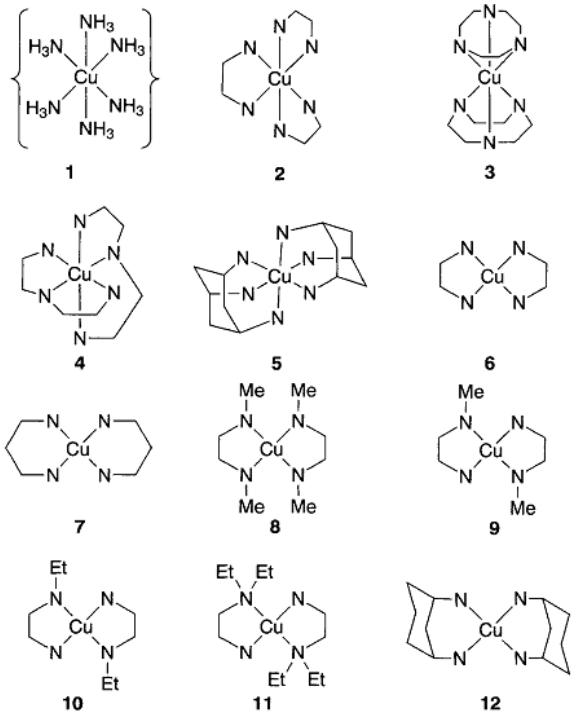

Complex	Cu–N_{eq} Calc.	Cu–N_{eq} Obs.	Cu–N_{ax} Calc.	Cu–N_{ax} Obs.	N–Cu–N Calc.	N–Cu–N Obs.	Ref.
1	2.04	(2.15[a])	2.48	(2.45[a])	90.0	(90.0[a])	12
2	2.09	2.10	2.44	2.41	86.4	85.1	13
	2.03	1.99					
3	2.06	2.06	2.36	2.32	83.3	83.3	14
4	2.11	2.10	2.44	2.41	84.6	82.1	15
	2.01	2.04					
5	2.01	2.07	2.29	2.35	83.4	85.4	16
6	2.02	2.02			85.4	84.1	17
7	2.00	2.04			84.8	86.7	18
8	2.04	2.06			86.7	85.3	19
9	2.01	2.01			86.3	85.9	20
	2.04	2.06					
10	2.03	2.02			86.2	85.0	21
11	2.02	2.01			85.2	84.9	22
	2.10	2.08					
12	2.00	2.02			85.5	87.6	23

Figure 1-3 Early LFMM results for various Cu^{2+} complexes[80].

LFMM has also been used in calculating the bite angle in Cu^{2+} bis-oxazaline complexes, that are of interest for asymmetric catalysis but were not investigable by synthetic means[82]. More recently the group's interests have taken a more bio-inorganic form, with the investigation of type 1 copper centres[77,83] and the modelling of more complex bridged copper oxo structures[79], such as those found in the oxidised form of the type 3 copper proteins.

References

(1) Newton, I. **1687**.
(2) Hill, T. L. *J Chem Phys* **1946**, *14*, 465.
(3) Corey, E. J.; Bailar, J. C. *J Am Chem Soc* **1959**, *81*, 2620-2629.
(4) Williams, O. F.; Bailar, J. C., Jr. *J Am Chem Soc* **1959**, *81*, 4464-9.
(5) Cooley, W. E.; Liu, C.-F.; Bailar, J. C., Jr. *J Am Chem Soc* **1959**, *81*, 4189-95.
(6) Selbin, J.; Bailar, J. C., Jr. *J Am Chem Soc* **1960**, *82*, 1524-6.
(7) Gollogly, J. R.; Hawkins, C. J. *Inorg Chem* **1969**, *8*, 1168-1173.
(8) Gollogly, J. R.; Hawkins, C. J. *Inorg Chem* **1970**, *9*, 576-582.
(9) Beattie, J. K.; Gollogly, J. R.; Hawkins, C. J. *Inorg Chem* **1971**, *10*, 317-323.
(10) Gollogly, J. R.; Hawkins, C. J. *Inorg Chem* **1972**, *11*, 156-61.
(11) Wiberg, K. B. *J Am Chem Soc* **1965**, *87*, 1070-1078.
(12) Fletcher, R.; Reeves, C. M. *The Computer Journal* **1964**, *7*, 149-154.
(13) Boyd, R. H. *J. Chem. Phys.***1968**, *49*, 2574-2583.
(14) Brubaker, G. R.; Johnson, D. W. *Coord Chem Rev* **1984**, *53*, 1-36.
(15) Hambley, T. W.; Searle, G. H. *Acta Crystallogr C* **1984**, *40*, 383-386.
(16) Bond, A. M.; Hambley, T. W.; Snow, M. R. *Inorg Chem* **1985**, *24*, 1920-1928.
(17) Comba, P.; Hambley, T. W.; Zipper, L. *Helv Chim Acta* **1988**, *71*, 1875-1880.
(18) Comba, P.; Maeder, M.; Zipper, L. *Helv Chim Acta* **1989**, *72*, 1029-1037.
(19) Comba, P.; Hormann, A.; Martin, L. L.; Zipper, L. *Helv Chim Acta* **1990**, *73*, 874-882.
(20) Curtis, N. F.; Robinson, W. T.; Weatherburn, D. C. *Aust J Chem* **1992**, *45*, 1663-1680.
(21) Hambley, T. W.; Lawrance, G. A.; Martinez, M.; Skelton, B. W.; White, A. H.*Dalton Trans* **1992**, 1643-1648.
(22) Comba, P.; Sickmuller, A. F. *Inorg Chem* **1997**, *36*, 4500-4507.
(23) Bacci, M. *Chem Phys* **1986**, *104*, 191-199.
(24) Brown, M. F.; Cook, B. R.; Sloan, T. E. *Inorg Chem* **1975**, *14*, 1273-1278.
(25) Cotton, S. A. *Coord Chem Rev* **1972**, *8*, 185-&.
(26) Hambrigh.P *Coord Chem Rev* **1971**, *6*, 247-&.
(27) Melson, G. A.; Stotz, R. W. *Coord Chem Rev* **1971**, *7*, 133.
(28) Vleck, J. H. V. *J. Chem. Phys.***1939**, *7*, 72-84.
(29) Comba, P. *Inorganic Chemistry* **1989**, *28*, 426-431.
(30) Bernhardt, P. V.; Comba, P. *Inorg Chem* **1992**, *31*, 2638-2644.
(31) Bernhardt, P. V.; Comba, P.; Hambley, T. W.; Massoud, S. S.; Stebler, S. *Inorg Chem* **1992**, *31*, 2644-2651.
(32) Comba, P.; Remenyi, R.*Coord Chem Rev* **2003**, *238*, 9-20.
(33) Root, D. M.; Landis, C. R.; Cleveland, T. *J Am Chem Soc* **1993**, *115*, 4201-4209.
(34) Landis, C. R.; Cleveland, T.; Firman, T. K.; Root, D. M. *Abstr Am Chem Soc*, **1995**, *210*, 67-COMP.
(35) Cleveland, T.; Landis, C. R. *J Am Chem Soc* **1996**, *118*, 6020-6030.
(36) Landis, C. R.; Cleveland, T.; Firman, T. K. *J Am Chem Soc* **1998**, *120*, 2641-2649.
(37) Firman, T. K.; Landis, C. R. *J Am Chem Soc* **2001**, *123*, 11728-11742.
(38) Bethe, H. a. *Ann Phys* **1929**, *3*.
(39) Gorter, C. J. *Phys Rev* **1932**, *42*, 437.
(40) Jordahl, O. M. *Phys Rev* **1934**, *45*, 87.
(41) Schlapp, R.; Penney, W. G. *Phys Rev* **1932**, *42*, 666.
(42) Van Vleck, J. H. *Phys Rev* **1932**, *41*, 208.
(43) C.J., B. *Introduction to Ligand Field Theory*; McGraw-Hill: New York, 1962.
(44) Mulliken, R. S. *Phys Rev* **1932**, *40*, 55.
(45) Van Vleck, J. H.; Sherman, A. *Reviews of Modern Physics* **1935**, *7*, 167.
(46) Gerloch, M.; Woolley, R. G.*Dalton Trans* **1981**, 1714-1717.
(47) Gerloch, M.; Woolley, R. G. *Prog Inorg Chem* **1983**, *31*, 371-446.

(48) Deeth, R. J.; Gerloch, M. *Inorg Chem* **1984**, *23*, 3853-3861.
(49) Gerloch, M. *Inorg Chem* **1981**, *20*, 638-640.
(50) Deeth, R. J.; Fey, N.; Williams-Hubbard, B. *J Comput Chem* **2005**, *26*, 123-130.
(51) Deeth, R. J.; Foulis, D. L.; Williams-Hubbard, B. J. *Dalton Trans* **2003**, 3949-3955.
(52) Basolo, F. P., R. G *Mechanisms of Inorganic Reactions*; John Wiley & Sons Inc:: New York, 1967.
(53) Orgel, L. E. *An Introduction to the Transition-Metal Chemistry Ligand-Field Theory.*; Methuen: London, 1960.
(54) Ballhausen, C. *Introduction to Ligand Field Theory*; McGraw-Hill: London and New York, 1962.
(55) Wilkins, R. G. *Acc Chem Res* **1970**, *3*, 408-&.
(56) Eigen, M. *Pure Appl Chem* **1963**, *6*, 97-116.
(57) Merbach, A. E.; Vanni, H. *Helv Chim Acta* **1977**, *60*, 1124-1127.
(58) Meyer, F. K.; Newman, K. E.; Merbach, A. E. *J Am Chem Soc* **1979**, *101*, 5588-92.
(59) Ducommun, Y.; Earl, W. L.; Merbach, A. E. *Inorg Chem* **1979**, *18*, 2754-2758.
(60) Meyer, F. K.; Newman, K. E.; Merbach, A. E. *J Am Chem Soc* **1979**, *101*, 5588-5593.
(61) Ducommun, Y.; Newman, K. E.; Merbach, A. E. *Helv Chim Acta* **1979**, *62*, 2511-2516.
(62) Vanni, H.; Merbach, A. E. *Inorg Chem* **1979**, *18*, 2758-2762.
(63) Ducommun, Y.; Zbinden, D.; Merbach, A. E. *Helv Chim Acta* **1982**, *65*, 1385-90.
(64) Akesson, R.; Pettersson, L. G. M.; Sandstrom, M.; Siegbahn, P. E. M.; Wahlgren, U. *J Phys Chem* **1993**, *97*, 3765-3774.
(65) Aakesson, R. P., Lars G. M.; Sandstroem, Magnus; Wahlgren, Ulf *J Am Chem Soc* **1994**, *116*, 8691-8704.
(66) Rotzinger, F. P. *J Am Chem Soc* **1996**, *118*, 6760-6766.
(67) Rotzinger, F. P. *J Am Chem Soc* **1997**, *119*, 5230-5238.
(68) Rotzinger, F. P. *Chimia* **1997**, *51*, 97-99.
(69) Marrink, S. J.; Risselada, H. J.; Yefimov, S.; Tieleman, D. P.; de Vries, A. H. *J Phys Chem B* **2007**, *111*, 7812-7824.
(70) Monticelli, L.; Kandasamy, S. K.; Periole, X.; Larson, R. G.; Tieleman, D. P.; Marrink, S. J. *J Chem Theory Comput* **2008**, *4*, 819-834.
(71) Wang, H.; Junghans, C.; Kremer, K. *Eur Phys J E* **2009**, *28*, 221-229.
(72) Jorgensen, W. L.; Chandrasekhar, J.; Madura, J. D.; Impey, R. W.; Klein, M. L. *J Chem Phys* **1983**, *79*, 926-935.
(73) Mahoney, M. W.; Jorgensen, W. L. *J Chem Phys* **2000**, *112*, PII [S0021-9606(00)50820-4].
(74) Mahoney, M. W.; Jorgensen, W. L. *J Chem Phys* **2001**, *115*, 10758-10768.
(75) Rick, S. W. *J Chem Phys* **2004**, *120*, 6085-6093.
(76) Piquemal, J. P.; Williams-Hubbard, B.; Fey, N.; Deeth, R. J.; Gresh, N.; Giessner-Prettre, C. *J Comput Chem* **2003**, *24*, 1963-1970.
(77) Deeth, R. J. *Chemical Communications* **2006**, 2551-2553.
(78) Bentz, A.; Comba, P.; Deeth, R. J.; Kerscher, M.; Seibold, B.; Wadepohl, H. *Inorg Chem* **2008**, *47*, 9518-9527.
(79) Diedrich, C.; Deeth, R. J. *Inorg Chem* **2008**, *47*, 2494-2506.
(80) Burton, V. J.; Deeth, R. J. *J. Chem. Soc., Chem. Commun.* **1995**, 573-574.
(81) Burton, V. J.; Deeth, R. J.; Kemp, C. M.; Gilbert, P. J. *J Am Chem Soc* **1995**, *117*, 8407-8415.
(82) Davies, I. W.; Deeth, R. J.; Larsen, R. D.; Reider, P. J. *Tetrahedron Lett* **1999**, *40*, 1233-1236.
(83) Deeth, R. J. *Inorg Chem* **2007**, *46*, 4492-4503.

Chapter 2 - Computational Chemistry

Introduction

The earlier introduction chapter dealt with why a computational approach is often used to investigate chemical systems, for example, in gaining mechanistic information or for developing a predictive tool. This chapter deals with the theories that underpin the methods that have been used within this work.

Molecular modelling is a term often used to describe any research into chemical problems using computers. Computational chemistry is the study of molecular properties using mathematical formulae. Many of these formulae are now too complex to be solved by hand, and so increasingly larger resources are needed to look at interesting systems.

The area of computational chemistry can be broadly split into two areas that define the methods used; Quantum Mechanics (QM), the study of the interaction of atomic and subatomic particles treated with quantum theory; Molecular Mechanics (MM), the study of atomic systems with interactions treating by classical mechanics.

First Principle methods – *ab initio*

Quantum Mechanics

Quantum mechanics derives its name originally from the fact that the energy emitted by black bodies is quantised. It takes discrete values which is in opposition to the classical mechanics (Newtonian physics) view. The idea of quantisation was proposed in 1900 by Max

Planck[1] and was later extended by various scientists to cover many aspects of scientific theory.

One of the most significant of these was the Rutherford[2]-Bohr[3-5] model of the atom which was the first model to accurately account for the emission spectra of the hydrogen atom. The Rutherford-Bohr model says that the energy levels that electrons can occupy are quantised.

The Schrödinger[6] equation

The Wavefunction, Ψ, exists for any chemical system. This is one of the fundamentals of quantum physics and hence chemistry. Ψ gives the expectation value of a property when acted upon by the corresponding operator. The most commonly used operator in modern quantum mechanics is $\hat{H}$, the Hamiltonian operator, which is the energy operator.

$$\hat{H}\Psi = E\Psi$$

Equation 2-1 Non-expanded version of Schrödinger equation

The non-expanded representation of the Schrödinger equation[7], Equation 2-1, states that to solve the equation you need; values of E, the energy, and Ψ, the wavefunction, such that when Ψ is acted upon by $\hat{H}$ it returns the wavefunction multiplied by the energy.

If we expand the Hamiltonian operator we get

$$\left\{\frac{-\hbar^2}{2\mathrm{m}}\nabla^2+\gamma\right\}\Psi(r)=E\Psi(r)$$

Equation 2-2 Schrödinger equation (time independent) with expanded Hamiltonian operator

The above equation is still not fully expanded as ∇^2 is an operator in itself.

$$\nabla^2=\frac{\partial^2}{\partial x^2}+\frac{\partial^2}{\partial y^2}+\frac{\partial^2}{\partial z^2}$$

Equation 2-3 Del-squared

Given the above expansions it is also prudent to say that the Hamiltonian operator includes in it all of the terms needed to calculate the total energy of the system Equation 2-4; the kinetic energy of the electrons T_e and neutrons T_n, the potential energy from the interelectron and internuclear repulsion, the electrostatic attraction between electrons and the nuclei.

$$H = T_e + T_n + V_{ee} + V_{nn} + V_{en}$$

Equation 2-4 Hamiltonian operator in terms of energy contributions to the total energy

However, the Born-Oppenheimer approximation states that, with respect to the electrons the nucleus is stationary. Therefore, the kinetic energy of the neutrons T_n is assumed to be zero, this simplifies the Hamiltonian operator.

$$H = T_e + V_{ee} + V_{nn} + V_{en}$$

Equation 2-5 Hamiltonian operator assuming Born-Oppenheimer approximation; the electronic Schrödinger equation.

Equation 2-2 is the time independent Schrödinger equation. This is the most common form of the equation applied to quantum mechanical calculations. However, it is still an approximation. The approximation that enables the time independent Schrödinger equation is that the external field γ is independent of time.

When the potential is not independent of time, then the full time dependant Schrödinger equation, Equation 2-6, is used.

$$\left\{\frac{-\hbar^2}{2m}\frac{\partial^2}{\partial x^2}\frac{\partial^2}{\partial y^2}\frac{\partial^2}{\partial z^2}+v\right\}\Psi(r,t)=i\hbar\frac{\partial\ \Psi(r,t)}{\partial t}$$

Equation 2-6 Time dependant Schrödinger equation

Hartree-Fock – Theory

Hartree-Fock (HF) theory is considered the branching point of theories and solutions to the Schrödinger equation, and as such is the basis for all *ab initio* computational chemistry. HF theory is an independent particle model. The interaction of one particle in a system is only considered against an average potential of all interactions. This means that the HF method fails to account fully for electron correlation.

The HF method[7] describes each electron as an orbital with the total wavefunction being a product of all of these orbitals. However, the total wavefunction must be antisymmetric. This is achieved by arrangement of the orbitals within a single Slater determinant. The variational principle states that any trial wavefunction will have an energy expectation value equal to or higher than the true ground state wavefunction.

The shape of a given orbital describes the probability of finding an electron with a particular propability (often 95% chance) within a given space. It includes the attraction to the nuclei and the averaged repulsion from all other electrons. However, all other electrons are described by their own respective orbitals. Hence, the HF equations depend on their own solutions and solution is an internally iterative process. This iterative process is why the HF method was originally called the Self Consistent Field (SCF) method. To solve the HF equations the one electron (molecular orbital) coefficients are needed. This is achieved by the SCF method. First an initial guess at the coefficients is made, forming the density matrix. Then the Fock matrix is formed from this initial guess. This Fock matrix is then diagonalized, which leads to a new set of coefficients and a new density matrix. The process is continued until the change of the coefficients falls below a certain threshold and a self consistent field has been formed.

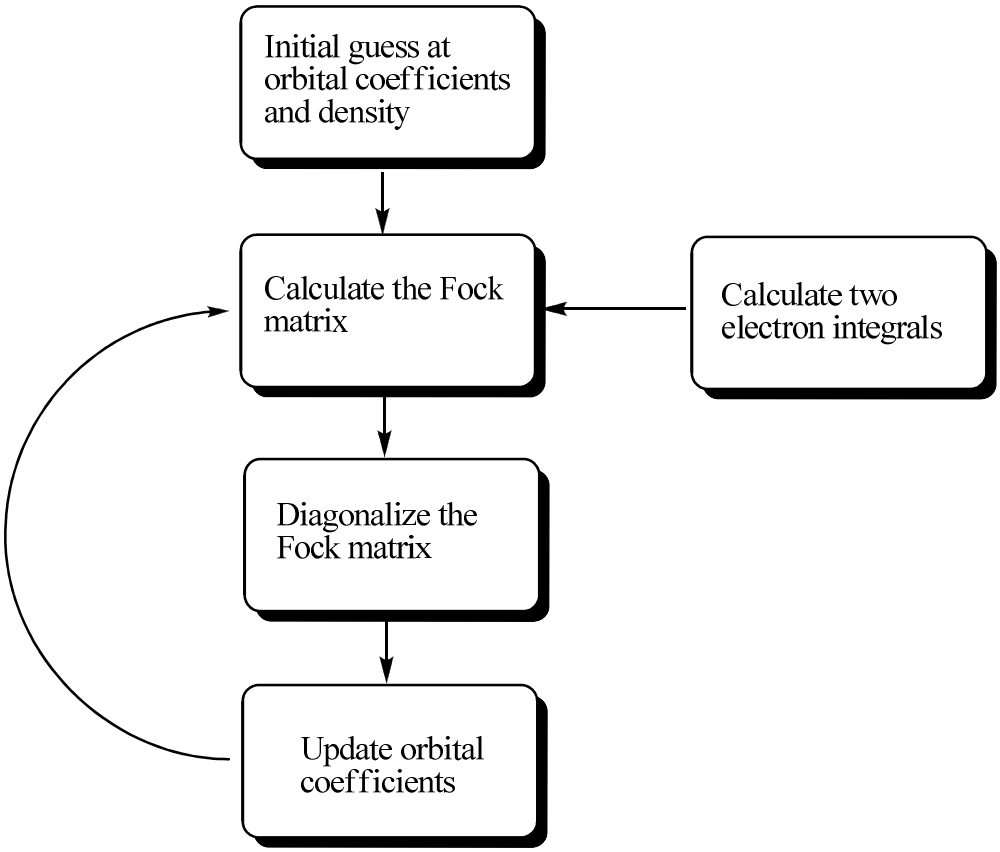

Figure 2-1 Diagrammatic representation of the SCF procedure

Methods that make some attempt to account for the correlation energy are collectively referred to as post Hartree-Fock methods and include; CI, configuration interaction; CC, coupled custer; MP2/3/4…, Möller-Plesset perturbation theory; MCSCF, Multi configurational self consistent field. However, these methods are considerably more computationally costly than HF. Each of the varying methods scales, in terms of computational cost, based on the size of the system N.

Method	Scaling factor
DFT	N^3
HF	N^4
MP2	N^5
CCSD	N^6
CCSD(T)	N^7
MP4	N^8
CI-SDTQ	N^{10}

Table 2-1 Scaling of different methods with respect to system size N.

Methods that use the wavefunction as the principle target quantity are severely limited by the size of the system, due to the fact the wavefunction is dependent on 4n variables for each electron, three spatial variables and one spin variable.

It is for this reason that methods that scale more favourably with the system size have become more attractive. The most popular of these seems by far to be DFT.

Density Functional Theory – DFT

DFT can be considered analogous to HF in that they are both independent particle models. However, DFT takes into account the many body effect of correlation energy by modelling the correlation of one electron against the electron density.

DFT is based on the Hohenberg-Kohn theorem[8], which states that the ground state density ρ(r) of a system of interacting electrons in an external field *V*(r) describes the ground state energy in a unique way; there is a one to one correlation between the electron density and the energy in any given system.

This makes DFT an attractive method as the electron density only ever depends on three spatial variables, regardless of the number of electrons in the system.

The first problem with DFT is that although the density yields the ground state energy the functional to connect these two properties is not known. There has been significant work in this area to design functionals for this purpose. The second is the inability within DFT to improve in a systematic manner upon previous results.

Early work was based on orbital-free DFT with the energy functional divided into its three constituent parts; T[ρ], the kinetic energy; E_{np}[ρ], the attraction between electrons and nuclei; T_{ee}[ρ], the repulsion between electrons. Under the Born-Oppenheimer approximation E_{nn}[ρ] is a constant. Using a HF theory formalism it is possible to separate T_{ee}[ρ] into a Coulomb, J[ρ], and exchange, K[ρ], part

The earliest form of this model was the Thomas-Fermi (TF) theory Equation 2-7 which did not include any exchange.

$$E[\rho] = T[\rho] + E_{ne}[\rho] + J[\rho]$$

Equation 2-7 Thomas-Fermi theory equation

The inclusion of the exchange term lead to the Thomas-Fermi-Dirac (TFD)[9,10] model.

$$E[\rho] = T[\rho] + E_{ne}[\rho] + J[\rho] + K[\rho]$$

Equation 2-8 Thomas-Fermi-Dirac equation

However, there is a serious chemical flaw in the orbital-free TF and TFD models, in that neither of them predict any bonding within molecules. Also, the orbital free methods have a very poor representation of the kinetic energy.

Modern DFT is based on the work of Kohn and Sham (KS)[11] that stated that the electron kinetic energy should be calculated from a set of redundant orbitals used to describe the electron density. Under this basis the only unknown is the exchange-correlation functional, of which there are many now available.

KS DFT splits the kinetic energy functional into two parts. One can be calculated exactly while the other is a minor correction term. The reintroduction of orbitals means that KS DFT scales as 3N rather than just 3.

In KS theory the electrons are treated as non-interacting and so the kinetic energy is expressed in terms of a Slater determinant composed of molecular orbitals, ϕ_i. This is an

exact solution to the Schrödinger equation and yields the exact kinetic energy functional which depends only on the density.

$$T_S[\rho] = \sum_i^N \left\langle \phi_i \left| -\frac{1}{2}\nabla^2 \right| \phi_i \right\rangle$$

Equation 2-9 Kinetic energy functional, subscript s denotes Slater determinant

However, the kinetic energy functional requires the exact density which would require an infinite number of natural orbitals. Fortuitously, as the exact density is not known it can be represented by a set of one-electron orbitals.

$$\rho_{approx} = \sum_{i=1}^{N_{elec}} \left| \phi_i \right|^2$$

Equation 2-10 Density in term of one electron orbitals.

In reality electrons are not non-interacting and as such the DFT answer is not absolute. However, it does remain one of the most popular methods in modern quantum chemistry. The remaining kinetic energy is incorporated into the exchange-correlation energy.

$$E_{DFT} = T_s[\rho] + E_{NE}[\rho] + J[\rho] + E_{xc}[\rho]$$

Equation 2-11 DFT energy equation with exchange-correlation term

The expansion of the above orbital terms leads the Kohn-Sham equations which can be solved iteratively to yield the optimal set of orbitals and hence the "best" electron density.

$$\left[-\frac{1}{2}\nabla^2 + V_{en}(r_1) + \int \frac{\rho(r_2)}{|r_1 - r_2|} \mathrm{d}r_2 + V_{\mathrm{xc}}(r_1)\right] \phi_i(r_1) = \epsilon_i \, \phi_i(r_1)$$

Equation 2-12 Kohn-Sham equations

The task in modern DFT is to find the exact functional for the exchange-correlation energy. The exact exchange-correlation functional would yield the exact energy from DFT. However, at the moment only approximations exist.

Despite the approximate nature of these exchange-correlation functionals, DFT is still more attractive than orbital free theory. This is due to the fact that in orbital free theory one must find approximation for the kinetic, exchange and correlation functionals, whereas in DFT one only needs the XC functional. The energy of the XC functional is around 10% that of the kinetic energy functional, so KS DFT is a lot less sensitive to inaccurate approximations.

Local Density Approximation – LDA

The LDA is the simplest model for approximating the XC functional. In the LDA the local density is treated as a uniform electron gas with density ρ. From this the XC functional can be calculated based on the [ρ] at a given point in the system.

The exchange energy of a uniform electron gas is given by the Dirac formula Equation 2-13 Dirac formula.

$$E_x^{LDA}[\rho] = -C_x \int \rho^{4/3}(r)dr$$

Equation 2-13 Dirac formula

The correlation energy in a uniform electron gas, a purely dynamical correlation, has been interpolated analytically by Vosko, Wilk and Nusair[12] (VWN), and Perdew and Wang [13](PW). All of the work herein has used the VWN version.

$$\varepsilon_c^{VWN}(r_s,\zeta) = \varepsilon_c(r_s,0) + \varepsilon_c(r_s)\left[\frac{f_2(\zeta)}{f_2^{"}}\right](1-\zeta^4) + [\varepsilon_c(r_s,1) - \varepsilon_c(r_s,0)]f_2(\zeta)\zeta^4$$

$$f_2(\zeta) = \frac{(f_1(\zeta)-2)}{(2^{1/3}-1)}$$

Equation 2-14 VWN parameterisation of the correlation energy

Empirical Methods

An empirical approach involves basing the model only on what is physically observable or experimentally achievable; many force field methods are empirically based, and of those that are not purely empirical many are semi-empirical, meaning that they were parameterised based on both observable properties and for example quantum chemical calculations.

Molecular Mechanics (MM) is empirically based and is treated within the classical mechanics ideas of balls connected with springs. The strengths of these springs are defined by the force field parameters which are empirically derived. The justifications for using MM and other

empirical models are many. Practicality; they are based on actual systems not abstract theories and so are directly comparable to experiment. Computational cost; empirical methods are significantly faster than *ab initio* methods. Applicability; force fields can be tuned for new problems, often with little problem.

Minimum Energy Crossing Points (MECP)

An MECP[14,15] is the point at which the Potential energy surfaces (PES) of different isomers (electronic isomers) cross. Normal isomerism involves interconversion between isomers on the same PES. However cases do exist of the isomerisation between 2 different PES's, the conversion between these 2 isomers is therefore a non-adiabatic process.

In diatomic molecules the PES will only intersect if the states have different spin or spatial symmetry, this rule however breaks down when the system is more complicated than a diatomic, because in a diatomic the only independently variable nuclear coordinate is the interatomic distance and to solve the equations for crossing two independently variable nuclear coordinates are required.

This comes about from the fact that the energy of the 2 states can be derived from the Schrödinger equation for the electronic waveform, and that the energies of the 2 states E_1 and E_2 respectively depend upon the matrix elements $H_{11,}$ H_{22} and H_{12} derived from the secular eigenvalue equation and to have degenerate solutions (a crossing point) you need to satisfy the relationships:

$$H_{11} = H_{22}$$
$$H_{12}(= H_{21}) = 0$$

Equation 2-15 Relationships that need to be satisfied to locate the MECP

Therefore in a diatomic H_{12} is always zero and the non crossing rule is maintained, however as stated in a polyatomic system there are enough degrees of freedom to choose values for 2 nuclear coordinates while the other degrees of freedom (3N-8) can be freely changed without leaving the region of the crossing.

When these two variables defined as X_1 and X_2 are used in the region that satisfies the above equations the solution yields an equation with the form of a double cone with the vertex as the origin. For this reason the crossing is called a conical intersection, a molecular funnel of a diabolic point.

From this the statement can be made that "in a polyatomic molecule, even with the same spatial or spin symmetry, 2 states can intersect along an *n*-2 dimensional hyperline as the energy is plotted against the *n* nuclear coordinates.Where *n* is the degrees of freedom (3N-6).

Investigating Minimum energy crossing points:

Due to the non-adiabatic nature of these transitions they cannot be investigated by normal means such as analysing of the molecular motion (vibrations etc). The MECP is the point on the hyperline where the 2 PES's cross. The energies of the 2 PES's and the gradients of the energies with respect to nuclear coordinates can be combined to yield two new gradients, (f,g) these gradients are orthogonal to each other and go to zero at the MECP.

Until recently the methods for finding the MECP of a system involved analytical gradients using constraints based on the LaGrange multipliers [16], and some more recent methods reqing the Hessian of the LaGrange to be evaluated numerically[17]. These methods are

indirect and computationally costly, therefore a more expedient method to find the MECP was required.

Early work on this was reported by Bearpark *et al*[18] who describes a method for locating the MECP of 2 PES without using any constraints, making it a more direct method. The method also only uses normal Hessian updating techniques which are found as standard in many quantum chemical programs, the author states that Gaussian 92 works without modification, and that optimisation is possibly in the region of the crossing without the need to calculate the Hessian.

As stated above the energy of the two PES's is equal in *n*-2 directions, moving in the 2 other directions X_1 and X_2 lifts the degeneracy of the energies, so at the lowest point on the hyperline the energy of the excited state is minimised in *n*-2 variable and the gradients of the PES's are zero in *n*-2 space orthogonal to the plane defined by X_1 and X_2.

The vectors X_1 and X_2 lie parallel to the gradient difference vector defined by:

$$X_1 = \frac{d(E_1 - E_2)}{dq}$$

Equation 2-16 Gradient difference vector in terms of the energies of the two states being minimised

So of the two methods of minimisation, they require one to minimise the energy orthogonal to the plane X_1, X_2 while obeying E_1=E_2, so you can either minimise E_2 subject to 2 constraints, which requires the LaGrangian functions to be solved.

The alternative is to minimise the function E_1-E_2 in the plane spanned by X_1, X_2 while simultaneously minimising E_2 in the remaining *n*-2 dimensional space that is orthogonal to the X_1, X_2 plane. From this the one condition for minimisation is

$$\frac{d(E_1 - E_2)^2}{dq_a} = 2(E_1 - E_2)X_1 = 0$$

Equation 2-17 Conditions to be met for the minimisation

where X_1 is the difference vector shown above. For the minimisation the size of the vector X_1 has no meaning, the step size purely depends on the function E_1-E_2, with the following relationship:

$$F = 2(E_1 - E_2)\frac{X_1}{\sqrt{X_1 X_1}}$$

Equation 2-18 F the step size and the functional relationship with previous terms

Molecular mechanics

A standard force field, and by extension MM, can be described by a single simplified equation.

$$E_{total} = \Sigma(E_b + E_\theta + E_\phi + E_{nb} + E_\varepsilon)$$

Equation 2-19 Simplified force field expression

The total energy of the system E_{total} is composed from the sums of E_b, the bond stretching potential; E_θ, the angle bending potential; E_ϕ, the torsional potential; E_{nb}, the non-bonded potential; E_ε, the electrostatic potential.

The lowest combination of all potentials in the system corresponds to the E_{total} of the ground state geometry. This definition and method works well for many systems, but does have its weaknesses.

If we expand the above Equation 2-19, we get Equation 2-20.

$$E_{tot} = \sum_{i,j} k_{ij}(r_{ij} - r_{0,ij})^2 + \sum_{i,j,k} k_{ijk}(\theta_{ijk} - \theta_{0,ijk})^2 + \sum_{i,j,k,l} k_{ijkl}[1 + \cos(n_{ijkl}\tau - \phi_{ijkl})] + \left[\sum_{i<j} \frac{\rho_i \rho_j}{\varepsilon d_{ij}} + \sum_{i<j}\left(\frac{A_{ij}}{d_{ij}^{12}} - \frac{B_{ij}}{d_{ij}^{6}}\right)\right]$$

Equation 2-20 Expanded force field expression

The first problem encountered with this implementation is that the Hooke's law equation only has one value for the reference bond length. While this is suitable for many complexes it is obviously deficient for Jahn-Teller active species such as Cu^{2+}. Classical MM would need to have two reference bond lengths to treat systems such as Cu^{2+} as it is commonly found to have a distorted geometry with two long bonds and four short bonds. To use the classical Hooke's law you would need to have a different bond stretch term for each set of bonds. While this would work if the "axial" and "equatorial" ligands were different, it would not work if the ligands were all equivalent. The Jahn-Teller theorem states "any non-linear molecular system in a degenerate electronic state will be unstable and will undergo distortion to form a system of lower symmetry and lower energy thereby removing the

degeneracy". However, the Jahn-Teller theorem does not state in what sense this distortion will be. The common distortion in d^9 Cu^{2+} is a tetragonal elongation. Assuming the elongation is along the global *z* axis and that the axial bonds elongate by length 2*x* and the equatorial bonds shorten by *x* then the d-orbitals split as in Figure 2-2. The tetragonal elongation causes the d_{z^2} orbital to drop in energy while $d_{x^2-y^2}$ rises in energy. The stabilisation comes from the lowering in energy of two electrons while only one electron is raised in energy.

The second problem arises from the nature of the Jahn-Teller distortion, a purely electronic effect, in that classical mechanics does not treat electrons in any explicit way.

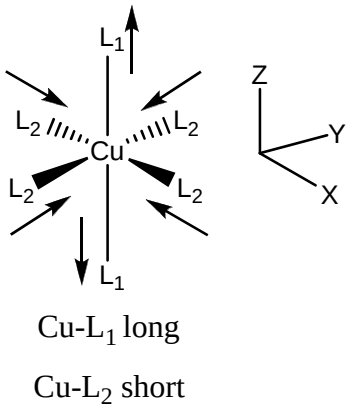

Figure 2-2 Distortion in Jahn-Teller active Cu(II) the classical Z extension and X,Y compression

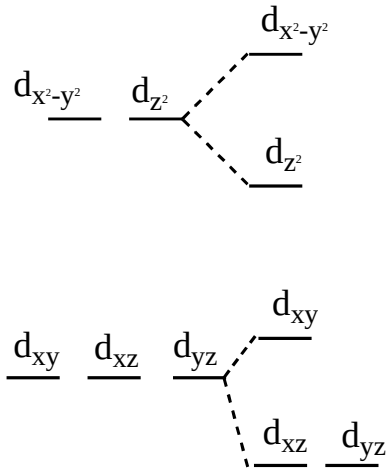

Figure 2-3 Orbital splitting in tetragonal elongation Jahn-Teller distortion

The third problem with the implementation of the above equation is again that of unique labelling: this time in the second force field term. In many common systems the rules for the angle are fairly rigid, carbon – methane, 109.5°; nitrogen – ammonia, 107°; oxygen – water, 104.5°; they are defined by one reference value. However, in transition metal complexes this is not always the case, as not all internal angles are the same.

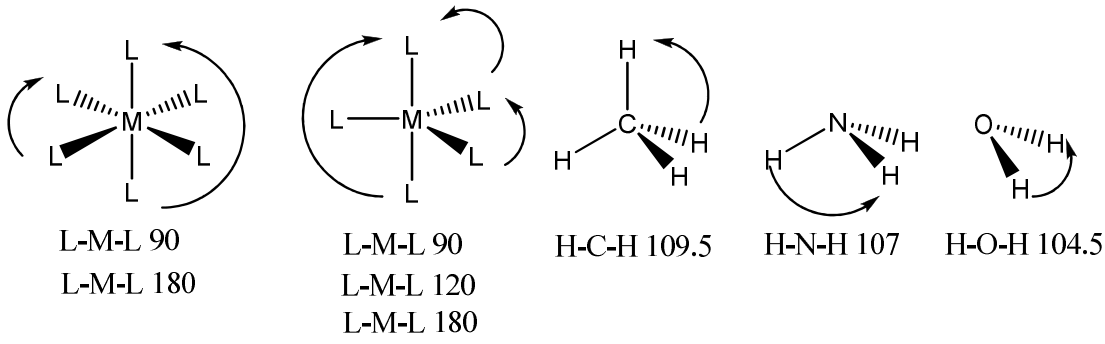

Figure 2-4 Reference angles in representative compounds

This unique labelling problem, together with the fact that conventional force field methods cannot take into account any of the d electron effects, means that an extension is needed if

classical methods are to be used for transition metal systems. The inclusion of d electrons is covered explicitly in *ab initio* methods and so the above issues do not apply to such techniques. However, they are considerably slower than classical methods and hence the maximum system size is more limited.

Charge schemes

When parameterising and designing a force field a set of charges must be decided. Charge schemes exist within many of the commercially available packages; CHARMM, AMBER and MMFF as examples. These force fields have been developed with set charges and deviation from these charges may cause deviation from the expected performance. There are a number of ways to construct the charges in molecules. However, the three to be covered are the ones available in the ADF software; Mulliken[19,20], Hirshfeld[21] and Voronoi[21].

In Mulliken population analysis the number of electrons N is divided over all of the basis functions in the system. For the diagonal elements of the population matrix this method is fine. However, the problem arises because the electrons are divided equally over any of the off diagonal elements. This separation over off diagonal elements gives an often greater charge separation than is expected.

Hirshfeld charges are calculated by firstly separating the molecule into atomic fragments. Then the electron density at any point in space is divided among the nearby fragments proportionally to their free atom density at that distance from their respective centres. An integration of these densities (bonded minus free atoms) gives the atomic charges.

Voronoi deformation density charges are computed based on a compartmentalisation of the atomic units into Voronoi cells. A Voronoi cell is defined by the midplane on each of the

bond vectors. The atom in the Voronoi cell is then treated as a neutral unbound atom. The deformation density is then calculated by "switching on" the atomic interactions of the neighbouring atoms and monitoring the flow of charge into and out of the cell. If the neighbouring atoms differ greatly in size then the Voronoi method starts to break down, although it does still give an idea of the polarisation of a chemical bond.

LFMM – Ligand Field Molecular Mechanics

LFMM[22] is a solution to the unique labelling and inclusion of d orbital effect problems. It uses the concept of the ligand field stabilisation energy (LFSE) to account for the d electron effects.

$$E_{total} = \Sigma(E_b + E_\theta + E_\phi + E_{nb} + E_\varepsilon) + LFSE$$

Equation 2-21 Force field equation with LFSE correction for d electrons

The LFSE[23,24] is the stabilisation that arises from the fact that the d orbitals on metal ions do not remain degenerate when placed in a non-spherical field. The orbitals split depending on the arrangement of ligands around the metal and the possible overlap between orbitals.

The effect of the LFSE can be clearly seen when a comparison of, for example, the enthalpy of hydration is made for hexaaqua complexes of the divalent first row metal ions.

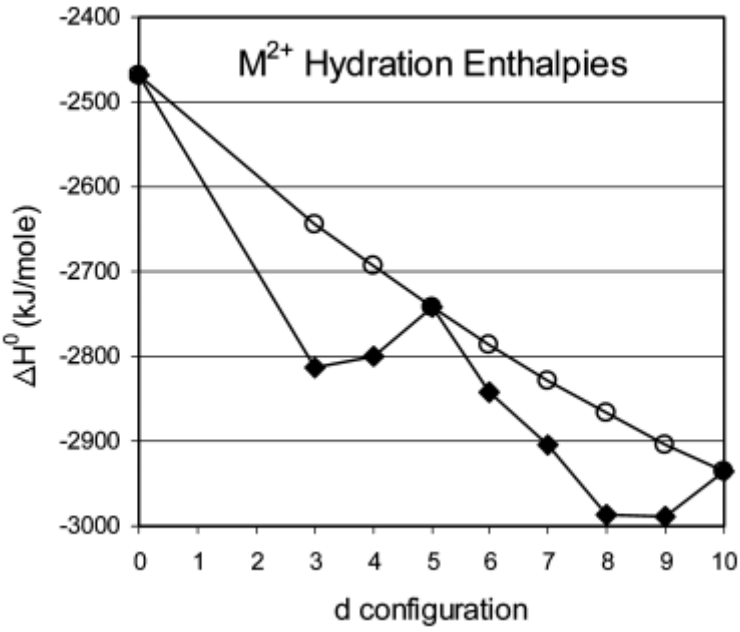

Figure 2-5 Enthalpy of hydration for the divalent first row transition metal complexes from Ca to Zn

The hydration enthalpies show the typical “double hump”, a very common feature when looking at properties of the transition metals going across a period.

The above Figure 2-5 shows the energies of the actual complexes as well as the extrapolated line from Ca^{2+} to Mn^{2+} and on to Zn^{2+} which is the line upon which the energies would be expected to lie if there were no electronic effects.

Ca^{2+}, Mn^{2+} and Zn^{2+} are the 3 metals in the first row that have zero LFSE, the further the actual energy is from this line then the higher the LFSE for that complex.

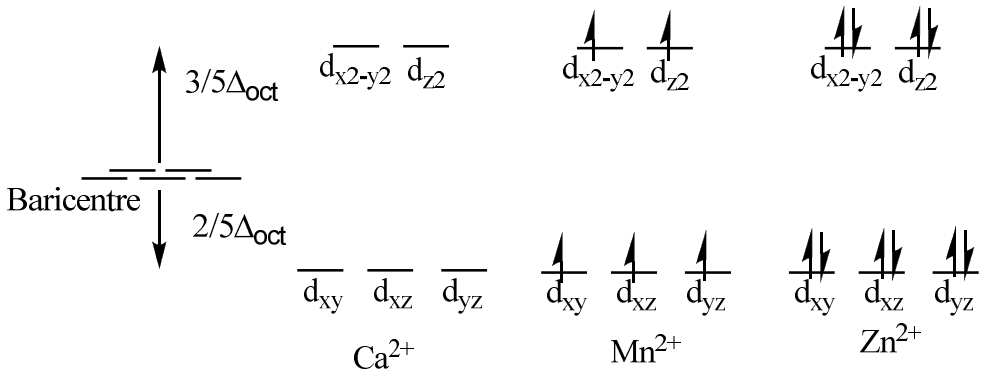

Figure 2-6 Ligand field splitting in octahedral Ca^{2+}, Mn^{2+} and Zn^{2+}, including electron distribution to show all systems stabilised by zero Δ_{oct}

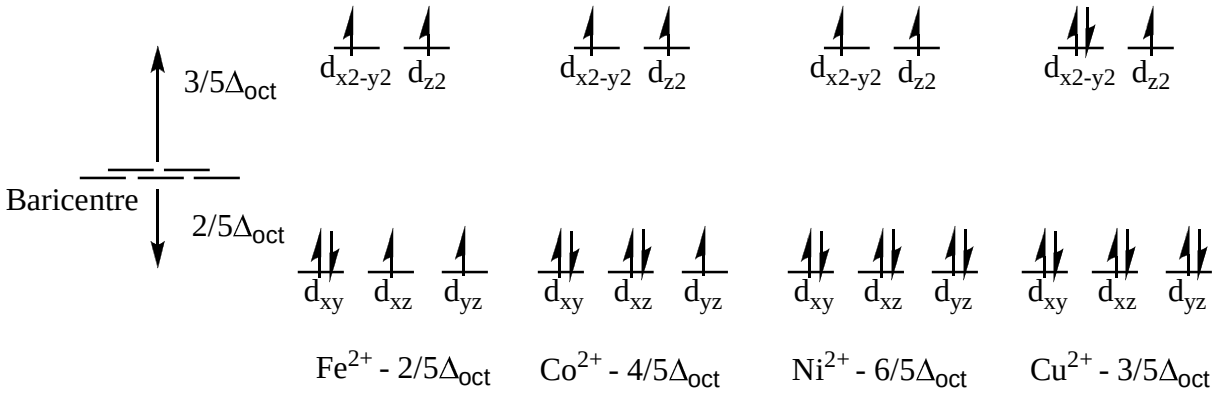

Figure 2-7 LFSE in terms of Δ_{oct} for the metals between Mn and Zn

To be successful in the treatment of transition metal complexes the above behaviours need to be included. This is achieved within LFMM using the Angular Overlap Model[25-27] (AOM). The AOM is a bond centred orbital approach. The benefit of this compared to a global orbital approach is that the parameters are defined based on the one metal ligand bond and not on the geometry and environment of the whole system. This bond centred approach means that force field parameters developed for a ligand should be independent of the molecular environment. Hence, LFMM is capable of treating mixed systems and systems away from the

classical ideal geometry; two very important features considering the unique labelling problems already mentioned.

In addition to using the AOM LFMM also uses some different equations to the ones presented earlier (Equation 2-20).

The first term in the expanded equation deals with the energy of deforming bond from its "ideal" value, and was presented earlier in the form of Hooke's law. However, within LFMM, the Morse potential is used instead. The Morse potential has the benefit that it allows a more realistic behaviour of the chemical bond. As the bond is compressed, the energy rises sharply and as the bond is stretched the energy rises asymptotically towards a dissociation limit. The benefit of this is that the system can more easily explore conformational space away from the ideal geometry, this is especially important in transition metal systems given the large difference in bond lengths in Jahn-Teller active complexes. The Morse potential still suffers from the problem of unique parameters.

$$E_{Morse} = D[1 - e^{-\alpha(r - r_0)}]^2$$

Equation 2-22 Morse Potential

The parameters in the Morse potential are chosen in parallel with the other LFMM parameters to best reproduce the available data (for a detailed breakdown of LFMM parameterisation see Chapter 3). They are; D, the bond dissociation energy; α, the curvature of the well; r_0, the reference bond length.

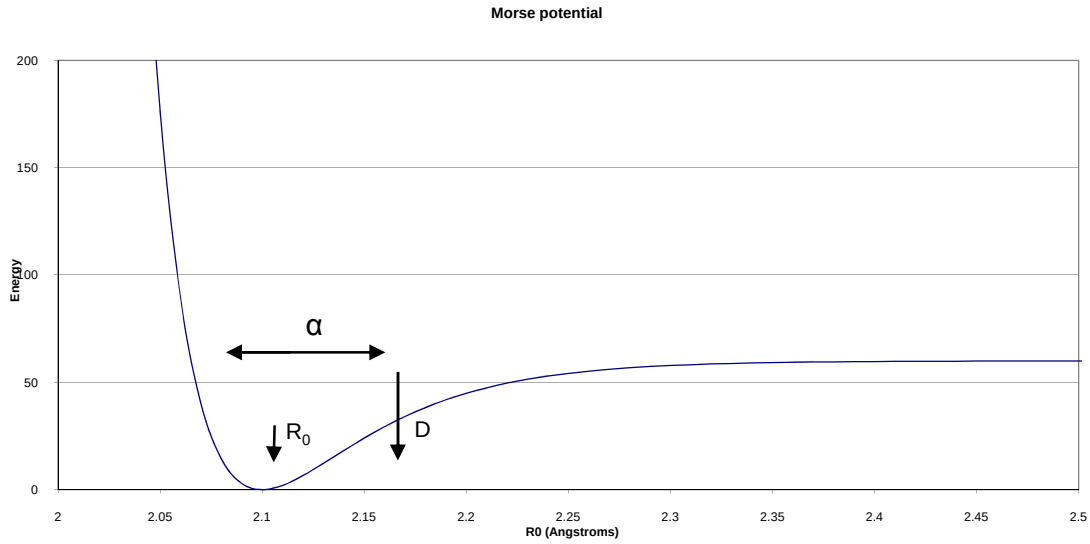

Figure 2-8 Schematic representation of the Morse potential parameters

The second term in the expanded in force field equation (Equation 2-20) is that for angle bending. LFMM does not use this potential in the area around the metal instead a 1,3 purely repulsive term is used, based on the points on a sphere model. However, this was not how the angular geometry was originally treated. Originally a Lennard-Jones like potential based on the van der Waals (VDW) forces, was used, but was discarded since the VDW energies were insufficient.

$$E = \frac{A}{r_{ij}^{12}} - \frac{B}{r_{ij}^{6}}$$

Equation 2-23 Lennard-Jones equation

$$E = \frac{A_{LL}}{r^{n}}$$

Equation 2-24 Pure 1,3-repulsive term for ligand-ligand interaction

Each of the force field parameters (r_0, α, D and A_{LL}) has an effect on the calculated properties of the system and it is important to know what magnitude and direction of response is seen when a parameter is changed. Figures 2-9 through 2-12 are all based on changes observed in $[M(H_2O)_6]^{2+}$ complex, where M = V^{2+} for all except Figure 2-11 where M = Cu^{2+}.

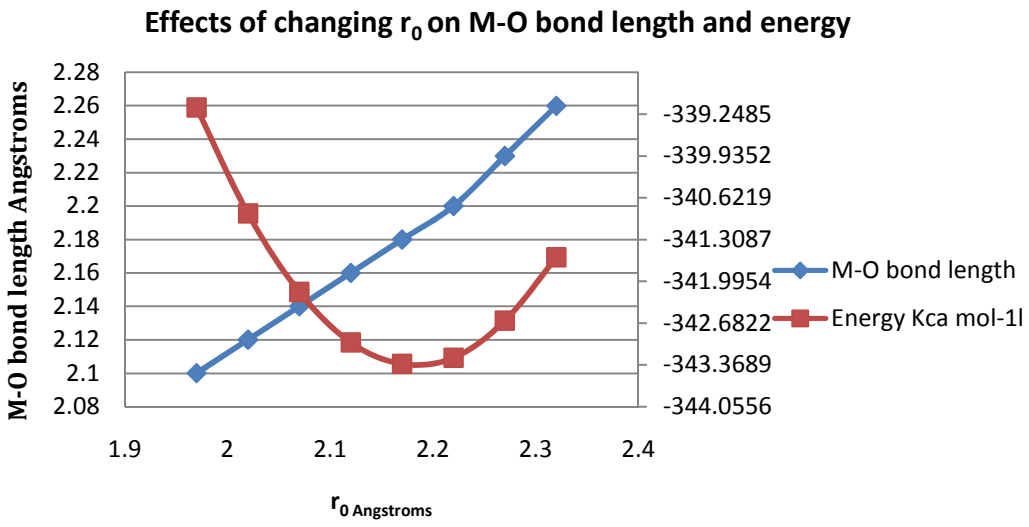

Figure 2-9 Changes in M-O bond length and system energy as r_0 is changed

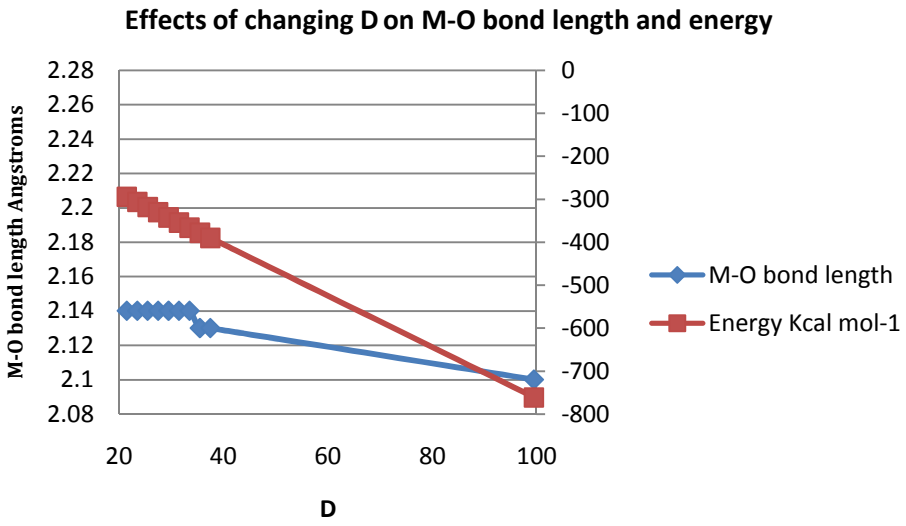

Figure 2-10 Changes in M-O bond length and system energy as α is changed

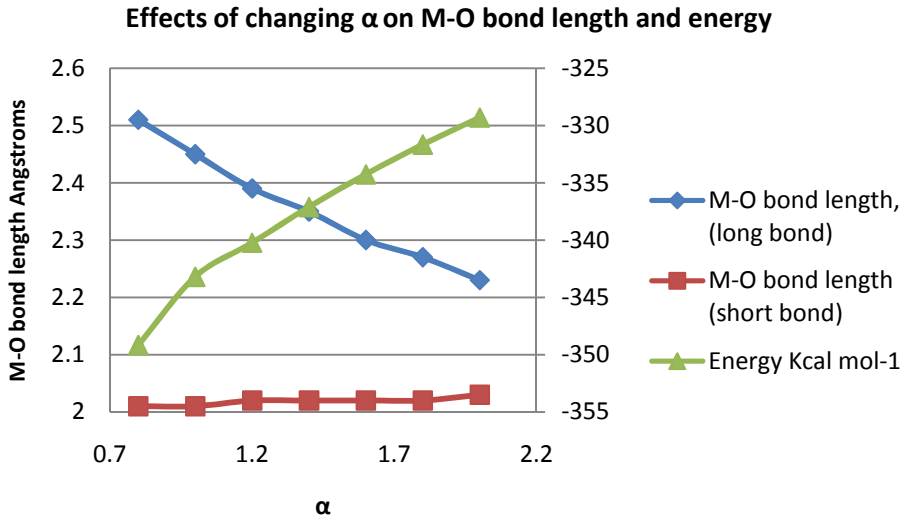

Figure 2-11 Changes in M-O bond length and system energy as *D* is changed

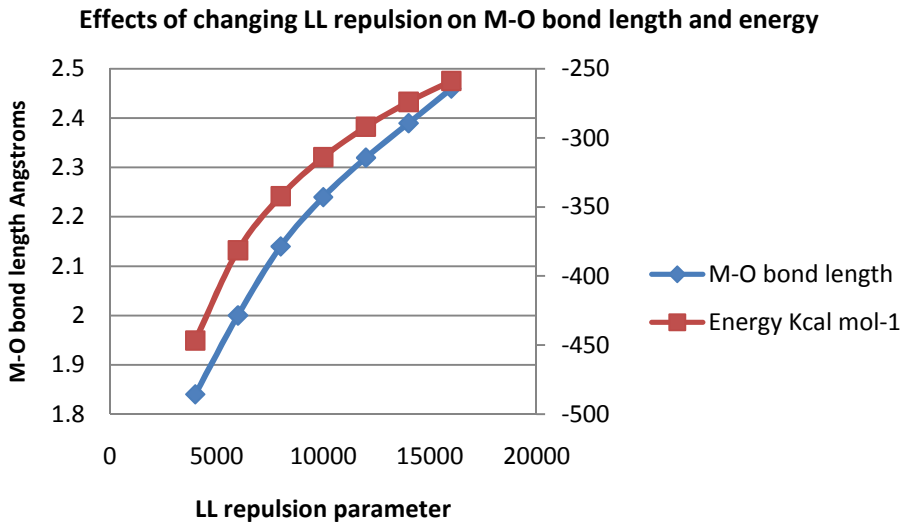

Figure 2-12 Changes in M-O (Å) bond length and system energy (kcal mol^{-1}) as A_{ll} is changed

AOM – The Angular Overlap Model

The AOM is used within LFMM to incorporate the d-electron effects and hence capture the LFSE.

As previously stated, the AOM is a bond centred approach, which allows parameters to be developed for individual ligand metal combinations and gives the method a wide degree of transferability.

The AOM has essentially 4 parameters; $e_{\sigma,}$ the full energy of a perfect σ type overlap; $e_{\pi x}$ and $e_{\pi y}$, the full energy of a perfect π type overlap; e_{ds}, the amount the mixing between the metal d_z2 orbital and an s type metal valence orbital.

The values of e_{σ} and $e_{\pi x/y}$ can be derived from spectroscopic measurements of the d-d splitting or from alternative theoretical means (see Results).

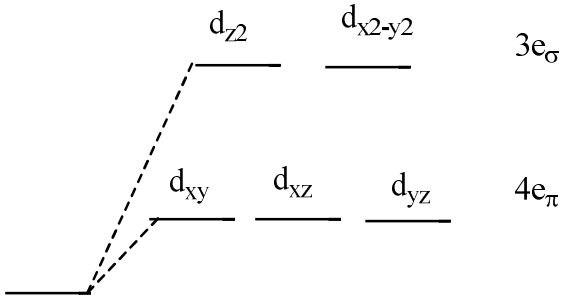

Figure 2-13 O_h field splitting with reference to AOM parameters

The maximum overlap for any ligand with a metal d orbital can be obtained from the AOM matrix. The AOM matrix relates the overlap of a ligand orbital with a particular metal orbital in terms of the internal polar coordinates, θ and ϕ. ϕ is the angle between the projection of the bond vector on the xy plane and global x axis. θ is the angle between the global z axis and bond vector.

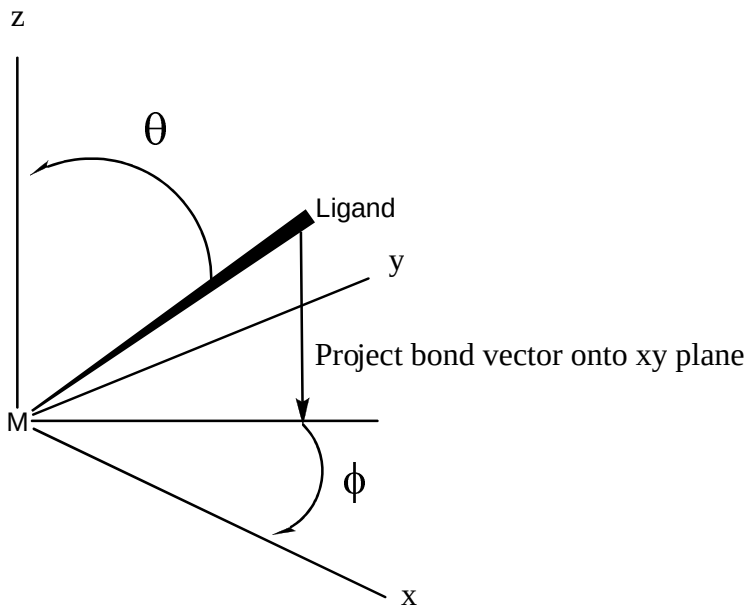

Figure 2-14, Diagrammatic representation of the parameters θ and ϕ

When the AOM matrix is used to derive the AOM equations for a molecule with octahedral symmetry with six molecules, having π bonding in both *x* and *y* directions, the following interactions are expected (Equation 2-25), where the subscripts x+/x-, y+/y- and z+/z- denote ligands on the positive or negative direction of the respective global direction.

$$E(d_{x2-y2}) = \tfrac{3}{4}\{ e_\sigma (L_{X+}) + e_\sigma (L_{Y+}) + e_\sigma (L_{X-}) + e_\sigma (L_{Y-})\}$$
$$E(d_{z2}) = e_\sigma (L_{z+}) + e_\sigma (L_{z-}) + \tfrac{1}{4}\{ e_\sigma (L_{X+}) + e_\sigma (L_{Y+}) + e_\sigma (L_{X-}) + e_\sigma (L_{Y-})\}$$
$$E(d_{xy}) = e_\pi(L_{x+}) + e_\pi(L_{x-}) + e_\pi(L_{y+}) + e_\pi(L_{y-})$$
$$E(d_{xz}) = e_\pi(L_{x+}) + e_\pi(L_{x-}) + e_\pi(L_{z+}) + e_\pi(L_{z-})$$
$$E(d_{yz}) = e_\pi(L_{y+}) + e_\pi(L_{y-}) + e_\pi(L_{z+}) + e_\pi(L_{z-})$$

Equation 2-25 AOM equations for nominally octahedral metal complexes

The sign of the AOM parameters positive or negative, e_σ and e_π, demotes whether the interaction is destabilising or stabilising respectively. A positive e_π denotes a π donor while a negative e_π is a π acceptor.

References

(1) Planck, M. *Verhandlungen der Deutschen Physikalischen Gesellschaft* **1900**, *2*, 237-245.
(2) Rutherford, E. *Philos. Mag. (1798-1977)* **1911**, *21*, 669-89.
(3) Bohr, N. *Philos. Mag. (1798-1977)* **1913**, *26*, 1-25,476-502.
(4) Bohr, N. *Philos. Mag. (1798-1977)* **1914**, *26*, 857-75.
(5) Bohr, N. *Nature (London, U K)* **1921**, *108*, 208-9.
(6) Schrödinger, E. *Phys Rev* **1926**, *28*, 1049-70.
(7) Jensen, F. *Introduction to Computational Chemistry - 2nd Edition*; Second ed.; J. Wiley, 2007.
(8) Hohenberg, P.; Kohn, W. *Phys Rev* **1964**, *136*, B864.
(9) Umeda, K. *Phys Rev* **1940**, *58*, 92.
(10) Chandramohan, D.; Balasubramanian, S. *Phys Rev B* **1987**, *35*, 2750.
(11) Kohn, W.; Sham, L. J. *Phys Rev* **1965**, *140*, A1133.
(12) Vosko, S. H.; Wilk, L.; Nusair, M. *Can J Phys* **1980**, *58*, 1200-11.
(13) Perdew, J. P.; Chevary, J. A.; Vosko, S. H.; Jackson, K. A.; Pederson, M. R.; Singh, D. J.; Fiolhais, C. *Phys Rev B: Condens Matter Mater Phys* **1992**, *46*, 6671-87.
(14) Harvey, J. N.; Aschi, M.; Schwarz, H.; Koch, W. *Theor Chem Acc* **1998**, *99*, 95-99.
(15) Harvey, J. N.; Poli, R.; Smith, K. M. *Coord Chem Rev* **2003**, *238*, 347-361.
(16) Koga, N.; Morokuma, K. *Chem Phys Lett* **1985**, *119*, 371-4.
(17) Manaa, M. R.; Yarkony, D. R. *J Chem Phys* **1993**, *99*, 5251-6.
(18) Bearpark, M. J.; Robb, M. A.; Schlegel, H. B. *Chem Phys Lett* **1994**, *223*, 269-74.
(19) Mulliken, R. S. *J. Chem. Phys.***1955**, *23*, 1833-1840.
(20) Mulliken, R. S. *Phys Rev* **1932**, *40*, 55.
(21) Célia Fonseca Guerra, J.-W. H., Evert Jan Baerends, F. Matthias Bickelhaupt, *J Comput Chem* **2004**, *25*, 189-210.
(22) Deeth, R. J.; Fey, N.; Williams-Hubbard, B. *J Comput Chem* **2005**, *26*, 123-130.
(23) Burton, V. J.; Deeth, R. J.; Kemp, C. M.; Gilbert, P. J. *J Am Chem Soc* **1995**, *117*, 8407-8415.
(24) Basolo, F.; Pearson, R. G. *Mechanisms of Inorganic Reactions, A Study of Metal Complexes in Solution. 2nd Ed*, 1967.
(25) Schoenherr, T.; Atanasov, M.; Adamsky, H. *Comprehensive Coordination Chemistry II* **2004**, *2*, 443-455.
(26) Gerloch, M.; Woolley, R. G. *Prog Inorg Chem* **1983**, *31*, 371-446.
(27) Gerloch, M.; Woolley, R. G. *Dalton Trans* **1981**, 1714-1717.

Chapter 3 - Modelling of Hexaqua Complexes of First Row Divalent Transition Metals

Introduction

The majority of interest in metal complexes comes from their varied and often unique behaviour in a number of solvents. The most common and probably beneficial solvent to consider is water, as it is found in many well investigated systems: water is the main solvent present in the human body, the planet is covered mostly in water and reactions that can be performed in water, as opposed to other solvents such as alcohols, are environmentally friendlier.

The divalent first row transition metal ions can be considered to be octahedral in aqueous solvent, although there is some contention about Cu^{2+}. It is not clear from the literature whether Cu^{2+} is six, five or four coordinate[1-3], due to large distortion caused by the strong Jahn-Teller effect[4,5].

As the aquated species of the divalent first row transition metals are important in such a broad spectrum of areas, it is important to make sure that a good baseline of comparison is obtained between LFMM and either experiment or DFT. Where possible the experimental structures and energies were used; however, in cases where these data were not available, or were not as accurate as other data used, then DFT structures and energies have been substituted in.

The aim of the initial work was to not only to develop a force field for these complexes but to test how LFMM performs for structures and energies. Based on the conclusions drawn in

the seminal work by Basolo and Pearson, if the LFMM method can accurately account for the Crystal Field Activation Energy (CFAE) then it should be able to quantitatively reproduce the experimental data, such as Δ_H (the enthalpy change of formation, for example) and structural features as well as qualitatively reproducing the rate constants of a process.

Computational details

All calculations in this chapter were performed using LFMM[6,7] and ADF[7].

Geometry optimisations performed using ADF were done using various gradient corrected functionals; PW91[8], BLYP[9,10], RPBE[11], as well as the LDA. LDA calculations were performed using the Vosko-Wilke-Nusair[12] equations for the electron correlation energy.

ADF allows imposed symmetries. However, due to the exact symmetry of the hexaqua complexes, there are complications, which are discussed in full detail later in the chapter.

Charges were calculated using the Natural Atomic Orbital (NOA) method in Jaguar and the Mulliken population analysis in ADF.

The default ADF options were used for all minimisations, with the COSMO[13] scheme being employed where solvation was to be included. An integration level of 4.0 was used for simple minimisations and a level of 6.0 for frequency calculations.

DFT Functionals

The aim of the first part of this chapter is to develop a set of force field parameters for the complexes of the divalent first row transition metal ions.

It is important that there is a constant and reliable set of data that is self consistent, available throughout the whole of this research. To guarantee this DFT structures and energies will be used in concert with experimental results. Due to the large number of possible methods that can be used within modern QM, it is imperative to find a method that works well for all of the systems that will be looked at. This is to minimise the chances of creating a set of force field parameters that do not perform in the same way across the whole of the transition metal series.

The experimental metal-oxygen bond lengths are well known for the hexaqua complexes of the first row transition metal ions[14,15]. The metal-oxygen distances that are commonly available in the literature are given as one distance for all metals, Vanadium to Zinc. This single value is not in fact correct as four of the metal complexes; Chromium, Iron, Cobalt and Copper, are nominally Jahn-Teller active.

The reason that these distances are often reported as one value is due to the fact that the many methods for measuring the bond length take some average. This effect is known as the dynamic Jahn-Teller effect and comes from the fact that the Jahn-Teller active complex are in constant flux and most measurements are taken over a long time scale and so see the averaged structure.

Taking these averaged experimental bond lengths as a baseline for comparison, the minimum energy structures of the whole series of complexes was calculated using DFT. These calculations used a global restraint to ensure that while the bond lengths could change, and hence minimise, they could not differ from one another. This approach guaranteed six equal bond lengths, which could be used to decide on the functional that was best suited for use as the general functional. With six equal bond lengths and water molecules as ligands, the highest available symmetry the system can have is T_h symmetry. However, this symmetry is not implemented within ADF so D_{2h} was used instead as the

symmetry for these minimisations. For the complexes that would have had orbitally degenerate ground states non integral occupations were used. The ability to set non integral occupations is one of the strengths of DFT, as the calculation only requires the density of the electrons, whereas, in HF theory an orbital is either full or empty.

	Exp	LDA	PW91	BLYP	RPBE
V	2.13	2.061	2.124	2.151	2.156
Cr	2.17	2.082	2.148	2.172	2.183
Mn	2.18	2.11	2.174	2.191	2.21
Fe	2.13	2.058	2.123	2.145	2.16
Co	2.09	2.018	2.084	2.105	2.118
Ni	2.06	1.985	2.067	2.081	2.094
Cu	2.09	2.009	2.075	2.098	2.109
Zn	2.1	2.034	2.093	2.112	2.132

Table 3-1 Calculated and experimental M-O bond lengths (Å)

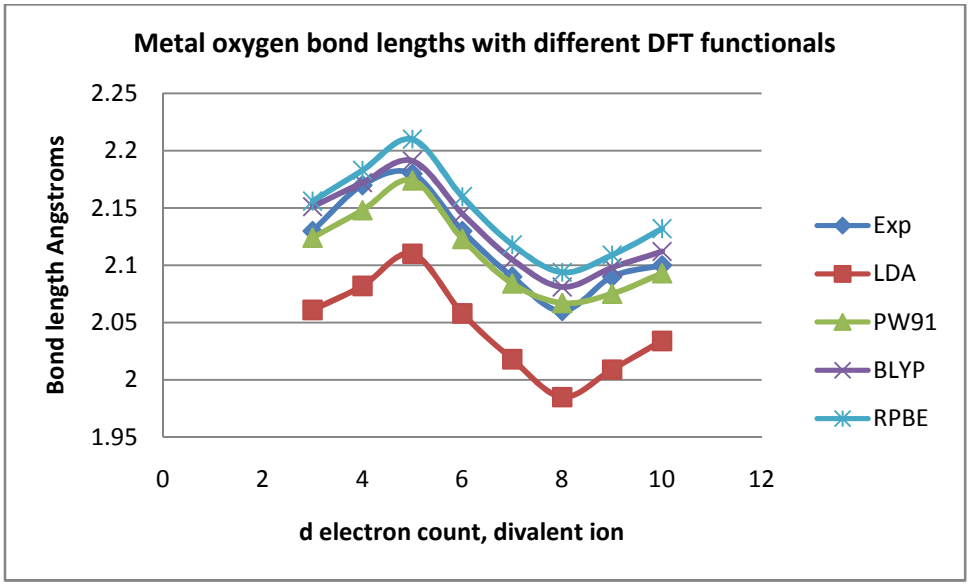

Figure 3-1 Comparison of the DFT and experimental M-O distances (Å)

It is clearly shown above (Figure 3-1) that all of the functionals tried are equally precise, while none of them are absolutely accurate.

The LDA systematically overbinds the water molecules in the complex, leading to shorter bond lengths than expected. It is interesting to note, however, that if the COSMO field had not been used, then the LDA values would have appeared even further from the experimental data than any of the GGA functionals, due to the fact that the COSMO solvation effect causes a contraction of the M-O bond lengths.

d Electrons		No Solvation		Cosmo	
3	V	2.14		2.12	
4	Cr	2.09	2.39	2.06	2.33
5	Mn	2.19		2.17	
6	Fe	2.11	2.21	2.09	2.17
7	Co	2.01	2.09	2	2.06
8	Ni	2.07		2.05	
9	Cu	2.01	2.31	1.97	2.26
10	Zn	2.11		2.09	

Table 3-2 Bond lengths (Å) of the divalent transition metal aqua complexes $[M(H_2O)_6]^{2+}$, Jahn-Teller active have both the long and short bonds listed

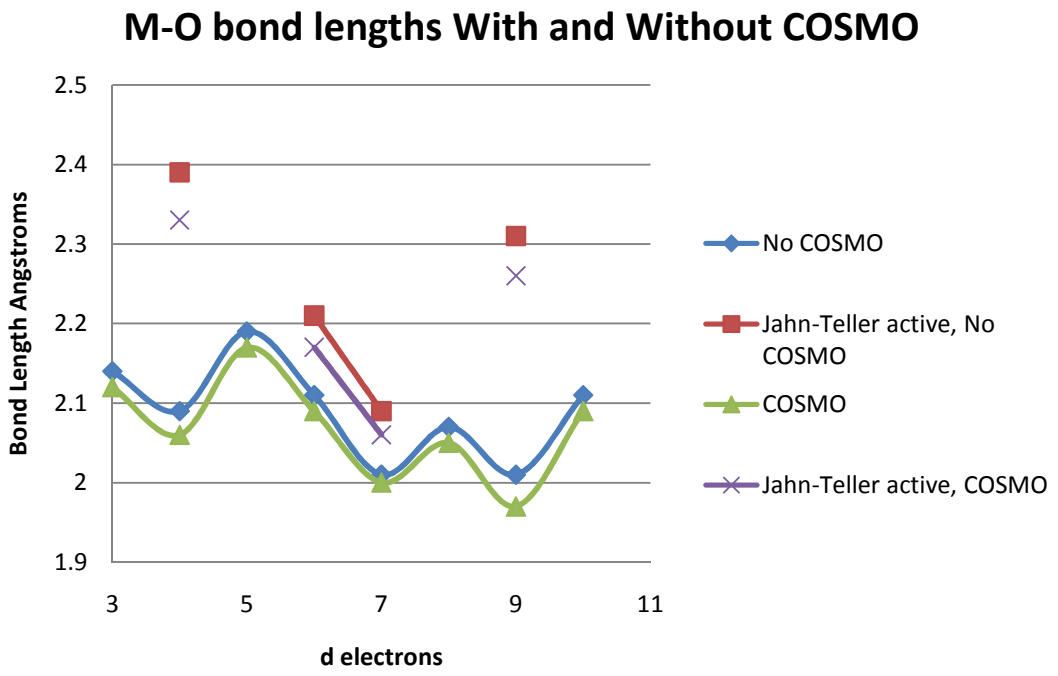

Figure 3-2 Plot of metal oxygen bond lengths (Å) with and without COSMO

None of the GGA functionals showed any major benefit or difference to the other ones. Therefore PW91 was chosen as the computational standard. PW91 was marginally more accurate than the other functionals, although this "accuracy" may be within the theoretical noise of the calculation. With these considerations it would have been defensible to have chosen any of the functionals, and to move forward with that choice. In the shown functionals, there is a small discrepancy at chromium and copper. This stems from the fact that the six equal bond lengths are highly averaged, as these complexes are in fact strongly Jahn-Teller active.

LFMM Parameters

Now that a suitable functional has been chosen a set of force field parameters needs to be developed (for details on LFMM and its implementation see Computational Chemistry).

To account for the d-orbital stabilisation energy a set of AOM parameters that accurately and precisely model the structural and energetic properties of these complexes is required[16]. As stated earlier the three parameters needed for the AOM contribution to the force field are; $e_{\sigma,}$ $e_{\pi x}$ and $e_{\pi y,}$. However, water only has the ability to σ bond and form π bonds in one plane, either *x* or *y* (this *x,y* direction is based on the local axis frame, not the global axis frame), but not both.

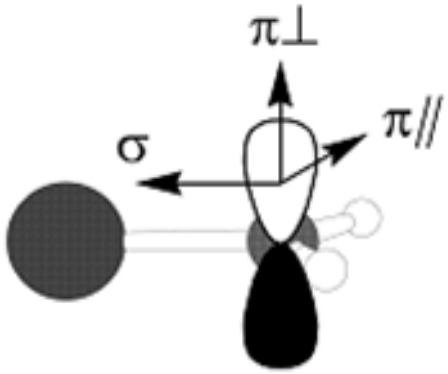

Figure 3-3 Water has π bonding only in one direction

Assuming that water is sp^2 hybridised, Figure 3-3, and hence is planar with the metal ion, then there is only the one π direction for bonding consideration as the other π type orbitals are involved in bonding between the oxygen and hydrogens.

This non cylindrical π bonding means that water only needs one e_π parameter. This parameter will be referred to as $e_{\pi\perp}$.

As stated earlier the highest symmetry for the hexaqua complexes is T_h Figure 3-5. In this symmetry there is the classical "octahedral" splitting of the d orbitals that gives the lower energy triply degenerate t_g set, and the higher energy doubly degenerate e_g set Figure 3-4, leaving only one degree of freedom, with which to assign the two AOM parameters.

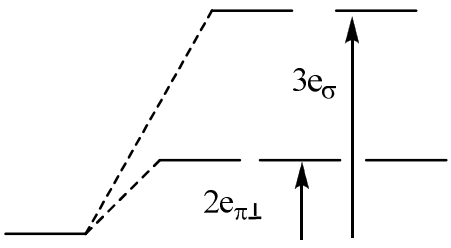

Figure 3-4 Classical splitting in T_h symmetry

$$E(d_{x2-y2}) = \tfrac{3}{4}\{ e_\sigma (L_{X+}) + e_\sigma (L_{Y+}) + e_\sigma (L_{X-}) + e_\sigma (L_{Y-})\} = 3e_\sigma$$

$$E(d_{z2}) = e_\sigma (L_{z+}) + e_\sigma (L_{z-}) + \tfrac{1}{4}\{ e_\sigma (L_{X+}) + e_\sigma (L_{Y+}) + e_\sigma (L_{X-}) + e_\sigma (L_{Y-})\} = 3e_\sigma$$

$$E(d_{xy}) = e_\pi (L_{x+}) + e_\pi (L_{x-}) = 2e_{\pi\perp}$$

$$E(d_{xz}) = e_\pi (L_{z+}) + e_\pi (L_{z-}) = 2e_{\pi\perp}$$

$$E(d_{yz}) = e_\pi (L_{y+}) + e_\pi (L_{y-}) = 2e_{\pi\perp}$$

Equation 3-1 AOM equations for T_h symmetry

The splitting of the d orbitals is determined by the arrangement of the ligands around the metal centre, so by changing the alignment of the ligands it is possible to create a d orbital splitting that allows us to derive a value for the e_π parameter from DFT calculations. The alignment that is needed to get this splitting is an "equatorial" D_{2h} arrangement, Figure 3-6.

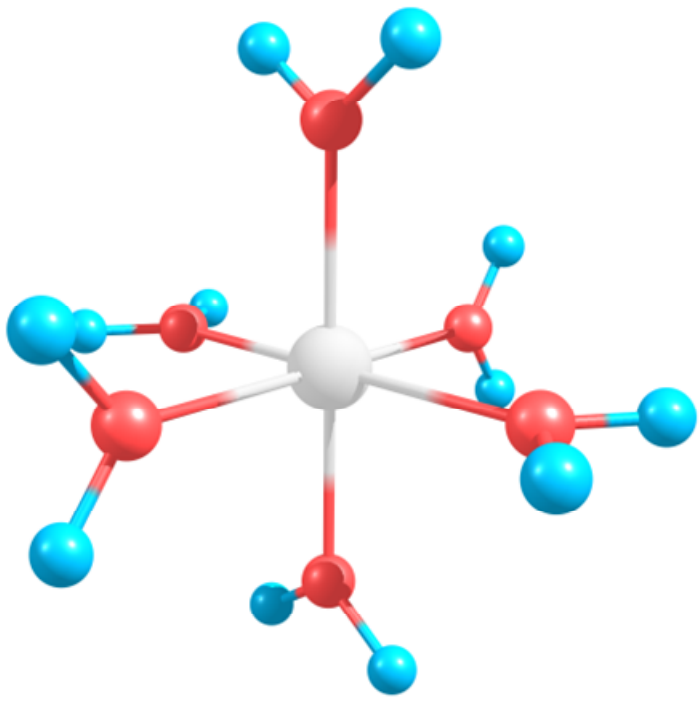

Figure 3-5 Standard co-planar alignment of ligands T_h symmetry

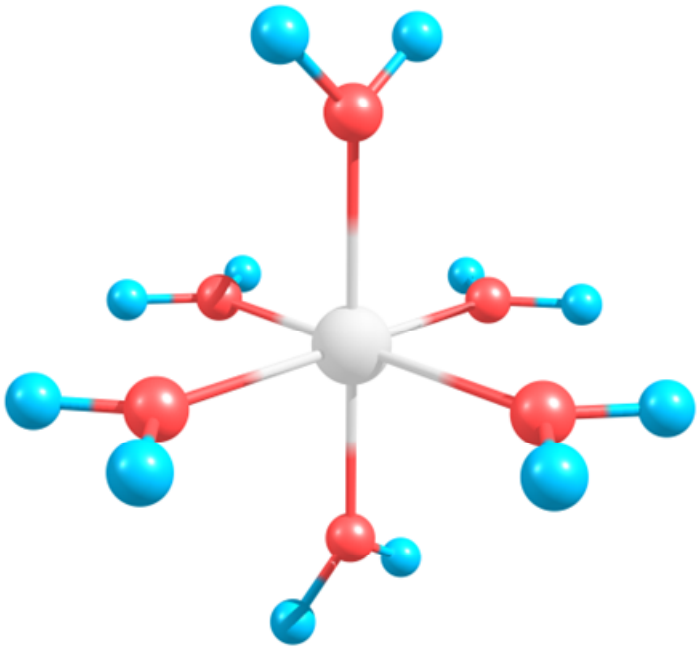

Figure 3-6 Equatorial alignment of ligands, D_{2h} symmetry

The equatorial arrangement of ligands results in a change of the d orbital splitting pattern, resulting in one d orbital at zero e_π, one at two e_π and one at four e_π (Figure 3-7). The exact order of the d orbitals is dependent on the chosen axis frame, and on the alignment of the ligands with respect to the axis frame.

$$E(d_{x2-y2}) = \tfrac{3}{4}\{ e_\sigma (L_{X+}) + e_\sigma (L_{Y+}) + e_\sigma (L_{X-}) + e_\sigma (L_{Y-})\} = 3e_\sigma$$
$$E(d_{z2}) = e_\sigma (L_{z+}) + e_\sigma (L_{z-}) + \tfrac{1}{4}\{ e_\sigma (L_{X+}) + e_\sigma (L_{Y+}) + e_\sigma (L_{X-}) + e_\sigma (L_{Y-})\} = 3e_\sigma$$
$$E(d_{xz}) = e_{\pi\perp}(L_{z+}) + e_{\pi\perp}(L_{z-}) + e_{\pi\perp}(L_{x+}) + e_{\pi\perp}(L_{x-}) = 4e_{\pi\perp}$$
$$E(d_{yz}) = e_{\pi\perp}(L_{y+}) + e_{\pi\perp}L_{y-}) = 2e_{\pi\perp}$$
$$E(d_{xy}) = 0e_{\pi\perp}$$

Equation 3-2 AOM equations for the equatorial D_{2h} geometry

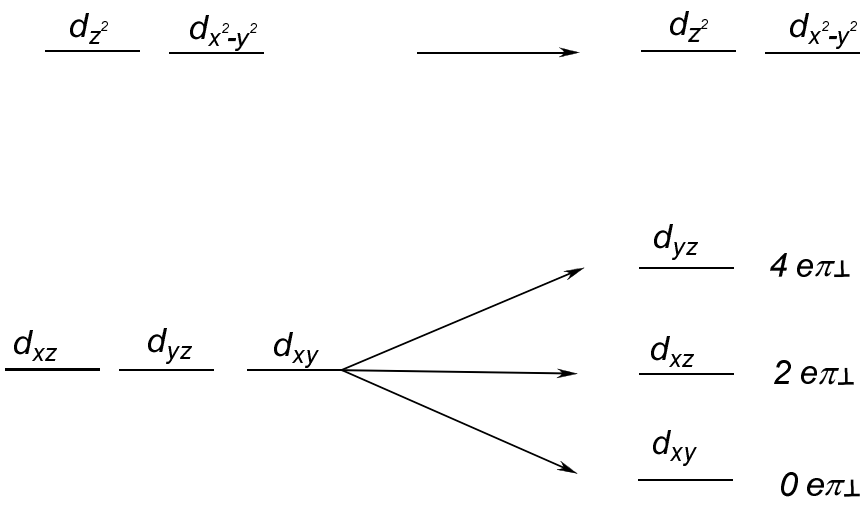

Figure 3-7 Change in d orbital splitting upon adopting "equatorial" geometry

Assuming a standard axis frame with the four equatorial waters lying in the *xy* plane and the two axial waters lying in the *xz* plane (Figure 3-8), then the d orbital ordering is as above (Figure 3-7). The overlaps between the ligand orbitals and the d orbitals on the metal are depicted in Figure 3-9. The overlaps for the d_{z^2} and $d_{x^2-y^2}$ are not shown as the contribution that causes them to change in energy is σ in nature.

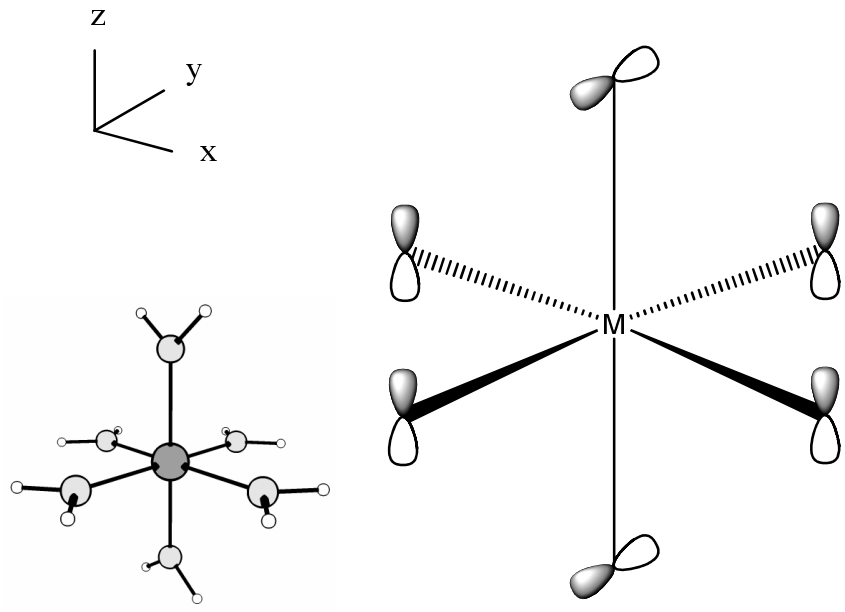

Figure 3-8 alignment of water molecules with axis frame

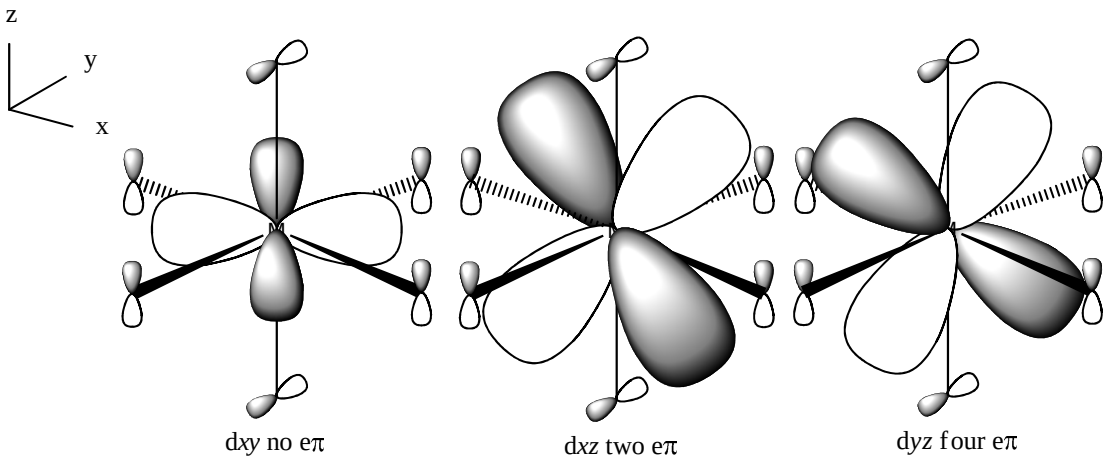

Figure 3-9 d orbitals showing alignment with π orbitals on ligands

The presence of this unidirectional π bonding means that the crystal field splitting parameter Δ_{oct} is no longer equal to $3e_\sigma - 4e_\pi$ but is now $3e_\sigma - 2e_\pi$.

Given the above it was possible to minimise the equatorial geometry and use the orbital energies to estimate the value of $e_{\pi\perp}$. The orbital energies were taken from the Kohn-Sham orbitals with the largest d_{xy}, d_{xz} and d_{yz} contributions.

	V	Mn	Ni
E(dxy)	-12.221	-15.314	-15.396
	0.000	0.000	0.000
E(dxz)	-11.834	-14.935	-14.977
	0.387 (3121)	0.38 (3065)	0.419 (3380)
E(dyz)	-11.517	-14.619	-14.681
	0.704 (5678)	0.695 (5606)	0.716 (5775)

Table 3-3 Energies of the MOs (eV) from the equatorial geometry ADF calculations, values in parenthesis in cm^{-1}

The calculated orbital energies above (Table 3-3), show both the absolute energy of the orbital as well as the energy relative to the lowest MO for that metal system. It is interesting to note that the splittings are remarkably alike even though the splitting parameter, Δ_{oct} for the metals is very different; 12300 cm^{-1} for $[V(H_2O)_6]^{2+}$ and 8500 cm^{-1} for $[Ni(H_2O)_6]^{2+}$.

Given that the above energy levels are so similar, the same value for $e_{\pi\perp}$ can be used for the whole first row divalent series. Either the total of the relative energies is two $e_{\pi\perp}$ or the difference between successive energy levels is two $e_{\pi\perp}$. Either way the value for $e_{\pi\perp}$ is Calculated to be 1480 ± 50 cm^{-1}.

Using the obtained value of $e_{\pi\perp}$ it is simple to calculate the value of e_{σ} using the experimental values for Δ_{oct}. However, some provisos need to be added to this expectation, as described below.

$$\Delta_{oct} = 3e_{\sigma} - 4e_{\pi_{\perp}}$$

Equation 3-3 Relationship between the splitting parameter Δ_{oct} and AOM parameters for normal D_{2h} symmetry

$$\Delta_{oct} = 3e_{\sigma} - 2e_{\pi_{\perp}}$$

Equation 3-4 Relationship between the splitting parameter Δ_{oct} and AOM parameters for equatorial D_{2h} symmetry

Ultimately the values used for e_{σ} were derived based on hydration enthalpies. However, this was not the expectation when these calculations were carried out. The derivation of the e_{σ} value is detailed later in this chapter when all force field parameters are discussed.

Having established a values for our e_{σ} and $e_{\pi\perp}$(going forward from the original idea that it could be based solely on the Δ_{oct}), the distance dependence of the AOM parameters needs to be established. The AOM parameters have an inverse fifth power dependence on the bond lengths, so a calculated value of 1400cm^{-1} for e_{π} gives an AOM parameter of 57177, at a bond length of 2.1 Angstroms. While this power dependence is backed up by crystal field theory and the electrostatic behavior, it is somewhat arbitrary as any power dependence could be used. Likewise the AOM parameters for e_{σ} and $e_{\pi\perp}$ could be somewhat redundant as any value of e_{σ} could be used as long as the e_{π} chosen reproduced the required Δ_{oct}.

For the LFMM force field there are eight parameters that need to be optimised (for each different metal). The parameters to be optimized are: the AOM parameters e_{σ} and e_{π}, the Morse function parameters (D, r_0,α), the ligand-ligand repulsion parameter, A_{LL}, and the partial atomic charges ρ(O) and ρ(H).

Most of the parameters above are derived based on an iterative method, and so it was attractive to define values for as many parameters as possible that could be evaluated independently before the relatively time consuming iterative process.

It was decided that the most likely variables (after the e_σ and e_π), that could be decided upon independently were the partial atomic charges.

Charge scheme

The charge scheme for the hexaqua complexes was derived from QM calculations.

To calculate possible charge schemes Jaguar was used as it was able to utilise the full T_h symmetry for the orbitally nondegenerate ground states of Mn(II) and Zn(II). In addition Cu(II) was investigated as a strongly Jahn-Teller active system, to see the effect that long and short bonds had on the charges seen.

		ρ(M)		ρ(O)		ρ(H)	
Metal	M-O Å	Mulliken	NAO	Mulliken	NAO	Mulliken	NAO
Mn	2.10	1.05	1.53	-0.81	-1.01	0.48	0.55
Mn	2.20	1.02	1.60	-0.81	-1.02	0.49	0.54
Mn	2.19	0.98	1.58	-0.82	-1.03	0.50	0.55
Mn	2.40	0.99	1.68	-0.80	-1.02	0.49	0.54
Zn	2.13	1.13	1.68	-0.83	-1.03	0.49	0.54
Zn	2.16	1.33	1.75	-1.00	-1.08	0.56	0.56
Cu	2.26			-0.79	-1.02	0.47	0.53
Cu	2.02	0.86	1.53	-0.78	-1.01	0.50	0.55
Cu	2.03			-0.79	-1.01	0.50	0.55
Bare water				-0.77	-0.93	0.39	0.47
Water(aq)				-0.88	-1.01	0.44	0.51

Table 3-4 Calculated partial charges for various metals at different M-O bond lengths

It is seen from Table 3-4, that even fairly large bond length changes do not perturb the observed charge distribution. This observation could be argued away for the Mn(II) and Zn(II) cases as the 6 bond lengths were the same and so the overall electrostatic pull on each molecule would be fairly uniform. However in the case of Cu(II), with two long and four short bonds, there is still no significant difference to the partial charges seen even though four of the water molecules are 0.2 Å closer to the metal.

The observed Mulliken populations give charges that are more covalent in character than the charges seen in the more complex NAO scheme. However, it is seen that the charge scheme does not change much, which leads to the conclusion that a single charge scheme would suffice in describing the divalent hexaqua complexes. Earlier the spurious methods involved in the calculation of the Mulliken charges were discussed. From this it is more attractive to use the more theoretically sound NAO charge scheme. However, due to later calculations a third charge scheme, “intermediate”, was introduced. This third charge

scheme was “attractive” as it did not have the harsh charges of the NAO method and was more in line with the electro neutrality principle. In addition it was able to reproduce in LFMM several structural features that were found to be significant. These are detailed later in the chapter. The LFMM method uses partial point charges to approximate the electrostatics of a complex. Whereas QM charges are set to give the correct electrostatic potential, because of this it is not surprising that the charges used within LFMM our different from those that are calculated with QM.

Scheme	ρ(M)	ρ(O)	ρ(H)
Mulliken	1.22	-0.55	0.34
Intermediate	1.4	-0.82	0.46
Natural	1.64	-1.02	0.54
TIP3P		-0.84 (-0.834)	0.42 (0.417)

Table 3-5 Compiled list of used charge schemes including standard TIP3P charges

The charge schemes shown above include TIP3P[17] charges as these were the charges used in LFMM when bare water molecules are considered. TIP3P is covered in more detail in the introduction.

When the work on metal aqua complexes was started, and the parameters first developed, the charge scheme used was the NAO scheme. This charge scheme worked perfectly well for the initial work. It correctly reproduced all of the geometric features of the DFT structures, as well as relative energy differences.

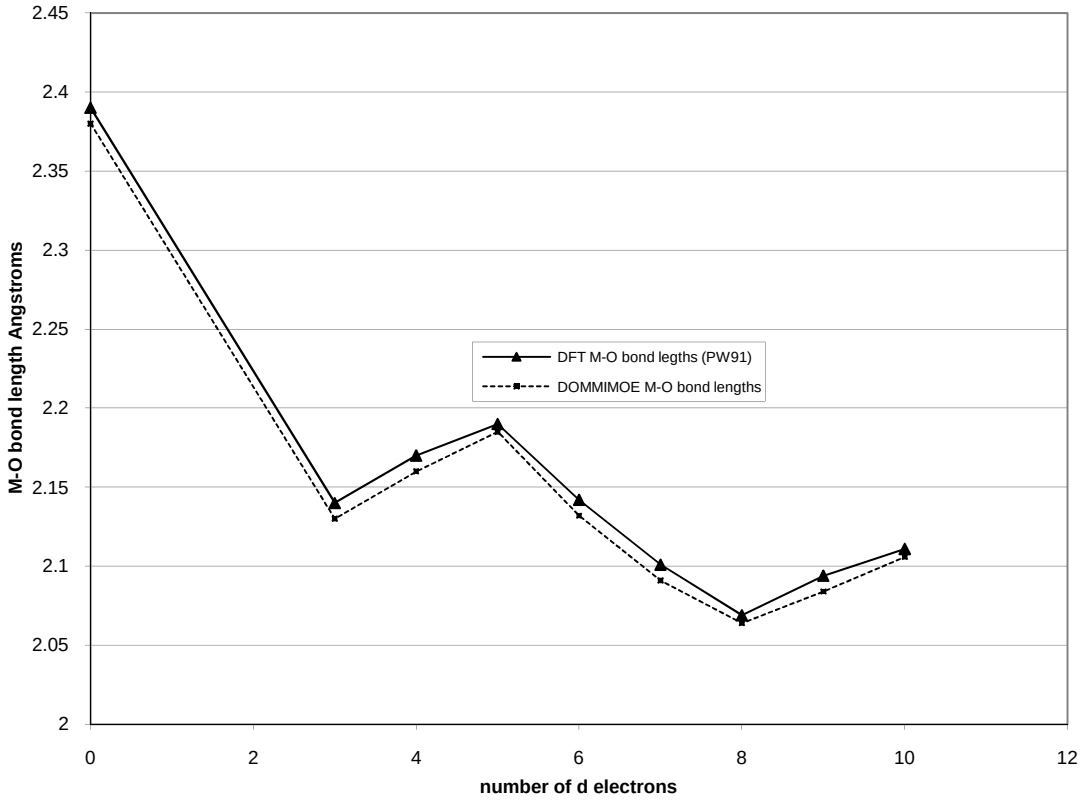

Figure 3-10 Comparison of LFMM and DFT M-O bond lengths (Å)

While this initial result was encouraging, it still was not accurate as none of the systems so far were allowed to relax. When allowed to relax, the expected strong Jahn-Teller distortion is seen in d^4 Cr(II) and d^9 Cu(II), as well as the weaker Jahn-Teller distortion in d^6 Fe(II) and d^7 Co(II). Turning on the Jahn-Teller effect in LFMM was achieved by inclusion of the AOM parameters and slight parameter changes.

LFMM performs as well with the Jahn-Teller effect considered as it did with purely symmetrical complexes.

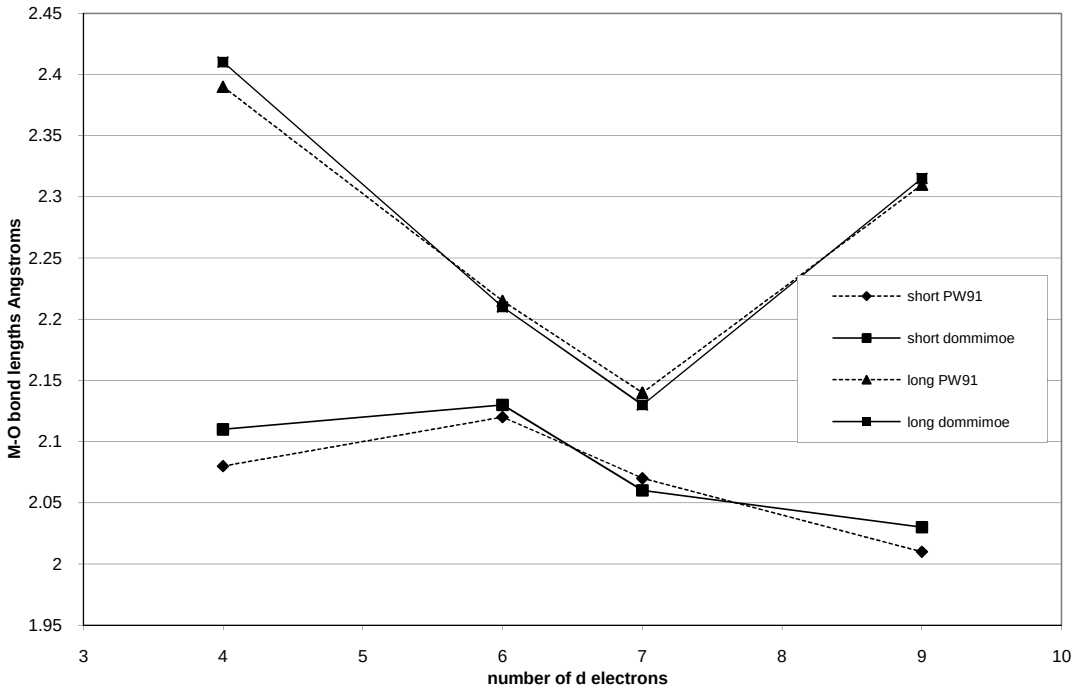

Figure 3-11 Comparison of LFMM and DFT M-O bond lengths (Å) for Jahn-Teller active complexes

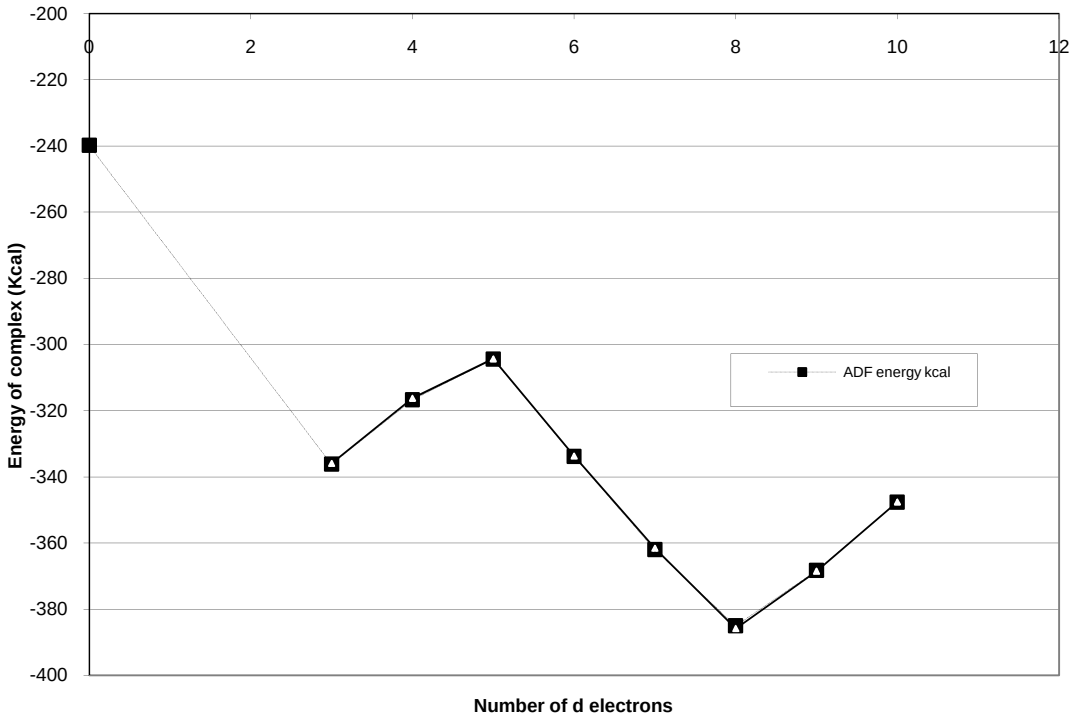

Figure 3-12 Total bonding energies calculated with LFMM and ADF (Kcal mol^{-1})

d electrons	Metal	ADF energy kcal mol^{-1}	DOMMIMOE energy kcal mol^{-1}
0	Ca	-239.81	
3	V	-336.14	-335.96
4	Cr	-316.68	-316.24
5	Mn	-304.42	-304.35
6	Fe	-333.80	-333.73
7	Co	-361.94	-361.57
8	Ni	-385.00	-385.82
9	Cu	-368.27	-368.52
10	Zn	-347.68	-347.59

Table 3-6 Compiled total bonding energy data for LFMM calculations

The above energies Figure 3-12 were calculated using the first set of parameters and the NAO charge scheme. The energies were compared to the raw data output from ADF. There were no corrections made to the energy at this point. This was a trial to see if LFMM could reproduce absolute numbers while maintaining the ability to accurately get a structure for a minimised complex. The bond lengths and energies shown (Figure 3-10, Figure 3-11, Figure 3-12) were all calculated using the same initial parameter set.

After this initial success, the bar for comparison was raised. Transition states within LFMM were the next target, covered in full detail in a later chapter. To accomplish this, the true minima and transition states for the water exchange species had to be found. Many papers by Rotzinger[18-21] *et al*[22-25] cover the process of water exchange, and the states and geometries involved in the process. In these earlier studies a common theme was found,

that the starting geometries for these exchange processes (i.e. the hexaqua complex) was not in fact a true minimum on the PES. This lead to the reinvestigation of the LFMM structures to test if they were indeed true minima. Using the LFMM structures as a starting point for DFT single point frequency calculations confirmed that the LFMM structures also were not true minima. To obtain true minima for these hexaqua complexes, the complexes must be allowed to relax. In ADF this relaxation is accomplished by setting a lower symmetry, and having no restraints to regulate bond lengths.

Having calculated the frequencies for all of the hexaqua complexes in D_{2h} symmetry it was easy to see the distortions that needed to occur by animating the output. In each case there were three negative frequencies, all around -50 wave numbers.

The motion that was required to remove the negative frequencies is described by three different, but coupled motions. The three motions needed to make a true ground state are shown in Figure 3-13; a pitch, a movement of the hydrogen atoms out of the metal water plane; a yaw, a rotation of the water molecule keeping the H-O-H angle the same, with an increase in one H-O-M angle and a decrease in the opposite angle; a roll, a rotation of the water molecule about the M-O bond.

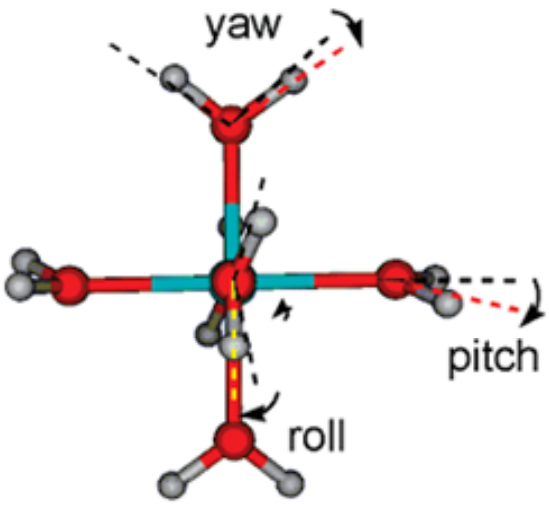

Figure 3-13 Graphical representation of the motions required to find a true ground state for the hexaqua species

The discovery of these structural features that are required for true ground states, lead to another criteria in all of the LFMM optimisations, that the molecules should show this distortion and so be true minima. At this point the low charge scheme was discarded since it could not, with any set of parameters, reproduce the required motions in the water molecules and so could not give true minima on the PES. The LFMM structures while not the global minimum were all local minimum with no negative frequencies. The observation that the "low" charge scheme could not reproduce the required structural features leads to the conclusion that these distortions are mainly electrostatically controlled. The roll, pitch and yaw of the water molecules exposes the "back" of one molecule to the "face" of another creating weak pseudo hydrogen bonds. These hydrogen bonds are made more likely by the co-planar nature of the water bonds, where the hydrogen atoms on one water molecule point at the oxygen atoms on its two neighbouring molecules. At this point these interactions are considered only in the scope of the six directly bound water molecules, as there is considerable contention in the literature about the required number of "outer sphere" water molecules to accurately reproduce the water complex.

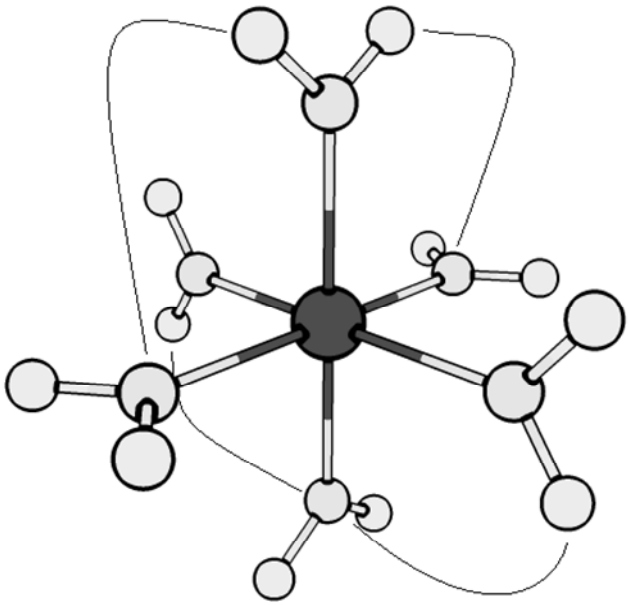

Figure 3-14 Showing favorable alignment in D_{2h} symmetry hexaqua complexes

The remaining two charge schemes were both used throughout the rest of the work carried out on hexaqua complexes, and are covered in detail in following chapters.

Morse Potential Parameters and Ligand-Ligand repulsion

The Morse potential (α, r_0 and D) and the ligand-ligand repulsion term, A_{LL}, are considered together because they are the four parameters that directly affect the geometry of the system in the most straightforward way. The AOM parameters also affect the geometry of the molecule but a change in one of the AOM parameters is not necessarily as easy to make to get the structural change you want, as a lot of the AOM parameters have switch-over points so it is not a smooth progression like it is with the Morse potential parameters.

As shown in the introduction, the Morse potential parameters have a fairly linear and predictable effect on the structure of the complex. For this reason, the initial optimisation of these parameters was fairly straightforward. The initial parameterisation was performed by hand using an iterative process until the structure in LFMM agreed with that calculated by DFT or provided by experiment.

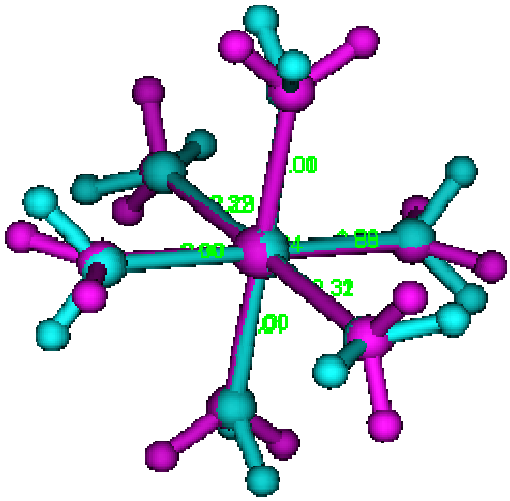

Figure 3-15 Overlay of DFT (purple) and LFMM (green) structures, including the very important roll, pitch and yaw.

While the structural overlay (Figure 3-15) may look different from each other. Both of the above structures have the roll, pitch and yaw in the same magnitude. They appear different due to different internal directions for these motions.

After the initial work to devise a set of parameters that accurately reproduced the structural details was deemed successful a new criteria was added to include the energetics of the

systems. The energetic parameters were to see how well LFMM could perform with absolute energies as a benchmark, not just relative energies.

The absolute energies were calculated from the enthalpy of hydration (ΔH_{hydr}) with a correction to remove the solvation energy. The solvation energy was calculated using COSMO in ADF. However, COSMO is designed to reproduce solvation free energies. The entropic contributions to the total energy are known to be small (~2%) for hydrated metal ions and so the COSMO method can be considered accurate for these needs.

Johnson and Nelson[26-28] include a further breakdown to the energy scheme by further splitting the U_t, into U_{res} and LFSE. Where U_t is the internal energy (chemical potential) of the system. U_{res} is the energy of the metal complexes in the absence of a ligand field stabilisation effect; the interpolated points between Ca^{2+}, Mn^{2+} and Zn^{2+} represent this value.

Metal	ΔH_{hydr}	E(COSMO)	U_{res}	LFSE	U_t
Ca	-377	-203	-174	0	-174
V	-458	-207	-211	-40	-251
Cr	-455	-207	-222	-25	-247
Mn	-440	-206	-233	0	-233
Fe	-465	-208	-244	-13	-256
Co	-477	-209	-254	-17	-268
Ni	-503	-210	-264	-29	-293
Cu	-502	-209	-273	-20	-293
Zn	-489	-207	-282	0	-282

Table 3-7 Energy decomposition of target energetic data (kcal mol^{-1})

The D parameter allows very easy tuning of the energy given by LFMM, while having minimum effects on the structural results. The r_0 and A_{LL} are tuned to reproduce the bond

length once the D parameter has been set. Finally the α parameter is set based on reproducing the normal mode vibrational frequencies calculated in ADF.

At the start of this chapter the minimisation of $e_{\pi\perp}$ and e_{σ} was discussed and the fact that e_{σ} could be set based on the calculated $e_{\pi\perp}$. However, it was stated that it would be refined based on later requirements and practicalities. That requirement is that the e_{σ} needed to be tuned to reproduce the required LFSE based on the Johnson and Nelson break down.

All of the above work leads to the final set of LFMM parameters (Table 3-8) that were used for the rest of the work involving water as a ligand in the later chapters.

Metal	*D* kcal mol^{-1}	r_0 *Å*	α	A_{LL} kcal mol^{-1}	$a_5(e_s)^a$ *kcal mol^{-1} Å^{-5}*	$a_5(e_\pi)$ *kcal mol^{-1} Å^{-5}*	Δ_{oct}*(fit)* *cm^{-1}*	Δ_{oct}*(exp)*[29] *cm^{-1}*
V	22.3	2.13	1.6	5350	228000	60500	13024	**12300**[26], 12400
Cr	23.5	2.19	1.5	5300	263000	64000	14455	**9250**[26], 14000[a]
Mn	26.4	2.08	1.7	5250	-	-	-	**8300**
Fe	28.6	2.04	1.7	5200	115000	60300	5203	**9350**[26], 10400
Co	30.8	2	1.7	5150	105000	55000	5125	**8400**[26], 9300
Ni	32	2.02	1.6	5100	150000	51000	9542	**8600**[26], 8500
Cu	33.9	1.97	1.4	5050	161000	53900	9754	**7850**[26], 13000[a]
Zn	37.5	1.93	1.5	5400	-	-	-	**-**

Table 3-8 Final LFMM parameters, [a] Value based on position of absorption maximum

The above parameters were designed to specifically reproduce the absolute energetic data (U_t and U_{res}) and the target M-O bond lengths for the divalent hexaqua metal ions. Given the above it seems that the parameters fail to reproduce the Δ_{oct} values expected for these complexes. The worst failures are seen for Cu^{2+} and Cr^{2+}, the two strongest Jahn-Teller distorted complexes, for which the experimental data cannot be interpreted within octahedral symmetry. In contrast to this are the Fe^{2+} and Co^{2+} complexes for which the d-d spectra is readily analyzed in octahedral symmetry, even though the experimental data are quite different to that calculated with LFMM. Again this is attributed to the Jahn-Teller effect in these systems.

Final results for $[M(H_2O)_6]^{2+}$

The above parameters were used to optimise the series of first row divalent hexaqua metal complexes (Table 3-9).

Metal	r_{sph} Å	r_{oct}^{JN} Å	r_{min} Å r1	r2	r3	ν_s (a_1) / cm^{-1}
V	2.2 **2.235** *2.21*	**2.137**		2.14 *2.13*		335 *352*
Cr	2.18 **2.205** *2.24*	**2.167**	2.08 *2.08*	2.07 *2.08*	2.41 *2.37*	- -
Mn	2.18 **2.178** *2.18*	**2.178**		2.18 *2.18*		332 *337*
Fe	2.14 **2.155** *2.15*	**2.126**	2.12 *2.12*	2.15 *2.12*	2.13 *2.12*	- -
Co	2.13 **2.135** *2.14*	**2.093**	2.12 *2.05*	2.09 *2.05*	2.11 *2.14*	- -
Ni	2.12 **2.119** *2.13*	**2.06**		2.08 *2.08*		347 *353*
Cu	2.12 **2.106** *2.13*	**2.087**	2.02 *1.97*	2.02 *1.97*	2.32 *2.31*	- -
Zn	2.12 **2.097** *2.13*	**2.097**		2.12 *2.13*		328 *363*

Table 3-9 Compiled Results for LFMM minimisations; DFT underlined, Johnson and Nelson bold, LFMM italics, all bond lengths in Angstroms (Å)

Conclusions

A set of parameters has been successfully developed for the treatment of the $[M(H_2O)_6]^{2+}$ type complexes. This set of parameters has been improved upon and refined based on the consideration and inclusion of additional important features. Throughout this research the targets for the LFMM method to meet have been raised after each success. This has led to an increased appreciation and understanding what features are important to parameterise against. The early expectations of the LFMM method were that reproduction of the metal – ligand bond length would be sufficient for the parameterisation of the system. However, for flexibility and applicability it is important to consider extra data.

Utilising the LFMM force field the structures and energies for the first row divalent transition metal series have been quantitatively reproduced, including the Jahn-Teller active species (Cr^{2+}, Fe^{2+}, Co^{2+} and Cu^{2+}).

References

(1) Bacci, M. *Chem Phys* **1986**, *104*, 191-199.
(2) Pasquarello, A.; Petri, I.; Salmon, P. S.; Parisel, O.; Car, R.; Toth, E.; Powell, D. H.; Fischer, H. E.; Helm, L.; Merbach, A. E. *Science (Washington, DC, U S)* **2001**, *291*, 856-859.
(3) Bryantsev, V. S.; Diallo, M. S.; van Duin, A. C. T.; Goddard III, W. A. *J. Phys. Chem. A* **2008**, *112*, 9104-9112.
(4) Gerloch, M. *Inorg Chem* **1981**, *20*, 638-640.
(5) Magini, M. *Inorg Chem* **1982**, *21*, 1535-8.
(6) Deeth, R. J.; Fey, N.; Williams-Hubbard, B. *J Comput Chem* **2005**, *26*, 123-130.
(7) Te Velde, G.; Bickelhaupt, F. M.; Baerends, E. J.; Fonseca Guerra, C.; Van Gisbergen, S. J. A.; Snijders, J. G.; Ziegler, T. *J Comput Chem* **2001**, *22*, 931-967.
(8) Perdew, J. P.; Burke, K.; Ernzerhof, M. *Phys Rev Lett* **1996**, *77*, 3865-3868.
(9) Becke, A. D. *Phys Rev A: At, Mol, Opt Phys* **1988**, *38*, 3098-100.
(10) Lee, C.; Yang, W.; Parr, R. G. *Phys Rev B* **1988**, *37*, 785.
(11) Hammer, B.; Hansen, L. B.; Norskov, J. K. *Phys Rev B: Condensr Mater Phys* **1999**, *59*, 7413-7421.
(12) Vosko, S. H.; Wilk, L.; Nusair, M. *Can J Phys* **1980**, *58*, 1200-11.
(13) Pye, C.; Ziegler, T. *Abstr. Am. Chem. Soc.* **1999**, *218*, 223-230.
(14) F. Albert Cotton, L. M. D., Carlos A. Murillo, and Jaime F. Quesada *Inorg Chem* **1993**, *32*, 4861-4867.
(15) Aakesson, R. P., Lars G. M.; Sandstroem, Magnus; Wahlgren, Ulf *J Am Chem Soc* **1994**, *116*, 8691-8704.
(16) Deeth, R. J.; Randell, K. *Inorg Chem* **2008**, *47*, 7377-7388.
(17) Jorgensen, W. L.; Chandrasekhar, J.; Madura, J. D.; Impey, R. W.; Klein, M. L. *J Chem Phys* **1983**, *79*, 926-935.
(18) Rotzinger, F. P. *J Am Chem Soc* **1996**, *118*, 6760-6766.
(19) Rotzinger, F. P. *J Am Chem Soc* **1997**, *119*, 5230-5238.
(20) Rotzinger, F. P. *Chimia* **1997**, *51*, 97-99.
(21) Rotzinger, F. P. *Helv Chim Acta* **2000**, *83*, 3006-3020.
(22) Kang, S. K.; Lam, B.; Albright, T. A.; O'Brien, J. F. *New J Chem* **1991**, *15*, 757-62.
(23) Akesson, R.; Pettersson, L. G. M.; Sandstroem, M.; Siegbahn, P. E. M.; Wahlgren, U. *J Phys Chem* **1993**, *97*, 3765-74.
(24) Helm, L.; Merbach, A. E. *Coord Chem Rev* **1999**, *187*, 151-181.
(25) Inada, Y.; Mohammed, A. M.; Loeffler, H. H.; Rode, B. M. *J Phys Chem A* **2002**, *106*, 6783-6791.
(26) Johnson, D. A.; Nelson, P. G. *Inorg Chem* **1995**, *34*, 5666-5671.
(27) Johnson, D. A.; Nelson, P. G. *Inorg Chem* **1995**, *34*, 3253-3259.
(28) Johnson, D. A.; Nelson, P. G. *Inorg Chem* **1999**, *38*, 4949-4955.
(29) Griffiths, J. S. *The theory of transition metal ions first edition*; Cambridge University Press: Cambridge, 1961.
(30) Rotzinger, F. P. *J Phys Chem B* **2005**, *109*, 1510-1527.

Chapter 4 - Model Transition States

Introduction

Successfully reproducing the ground state geometries of transition metal complexes was not a trivial matter, especially when the Jahn-Teller effect was included. However, there are many more facets of aqua complexes that would prove a much more exciting test of the method. With the MOE platform as the major tool it seems sensible to look at process that have far reaching and interesting implications. One such feature of metal complexes is ligand exchange.

In the divalent hexaaqua first row transition metal complexes there is a very interesting spread of exchange rates (k / s^{-1}), from $8.7 * 10^{1}$ for V^{2+} to $4.4 * 10^{9}$ for Cu^{2+} .

In the previous chapter it was shown that LFMM can calculate absolute energies of ground state structures.

Computational details

All calculations in this chapter were performed using DOMMIMOE and ADF.

Geometry optimisations performed using ADF were done using various gradient corrected functionals; PW91, BLYP, RPBE, as well as the LDA. LDA calculations were performed using the Vosko-Wilke-Nusair equations for the electron correlation energy.

The default ADF options were used for all minimisations, with the COSMO scheme being employed where solvation was to be included. An integration level of 4.0 was used for

simple minimisations and a level of 6.0 for frequency calculations as well as transition state optimisations

Water Exchange

The LFMM force field was developed using both empirical data (observable and measurable quantities) and DFT calculated data. This, coupled with the bond centered, approach means that the force fields developed herein are applicable to any problem with an aqua metal bond.

The interesting range of ligand exchange rates makes an interesting target for investigation by LFMM as well as compelling validation that the method satisfactorily includes the ability to deal with more complex problems.

In the now seminal work by Basolo and Pearson a qualitative relationship between the crystal field activation energy and the rate constant for water exchange was established. However, Basolo and Pearson [1] were using a crude model for the prediction of the CFSE. It is hoped that LFMM which explicitly treats the "true" LFSE should be able to reliably model these exchange processes.

Water Exchange Mechanisms

There are currently three accepted mechanisms for the exchange of an aqua molecule bound to a metal centre with an associated water molecule in the complex's first solvation sphere[2,3].

These three process are associative (A), dissociative (D) and interchange (I). The first two process A and D respectively proceed via a stable intermediate of higher or lower coordination number than the parent complex. The I process can be further described by whether it proceeds via an associative (I_a) or dissociative (I_d) activation.

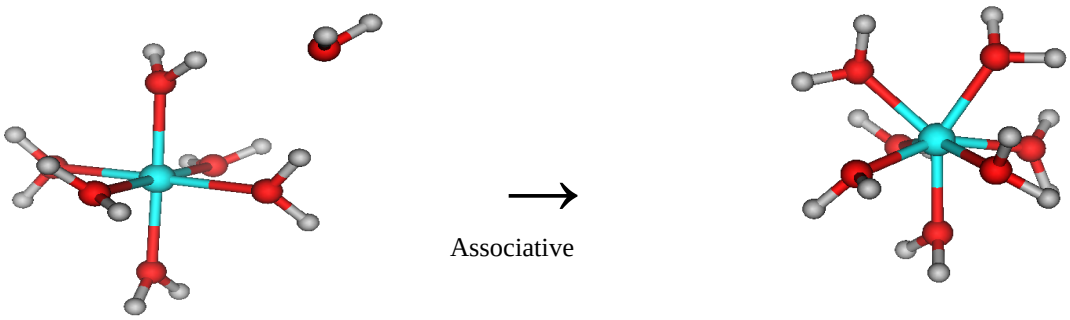

Figure 4-1 Associative (A) exchange and intermediate

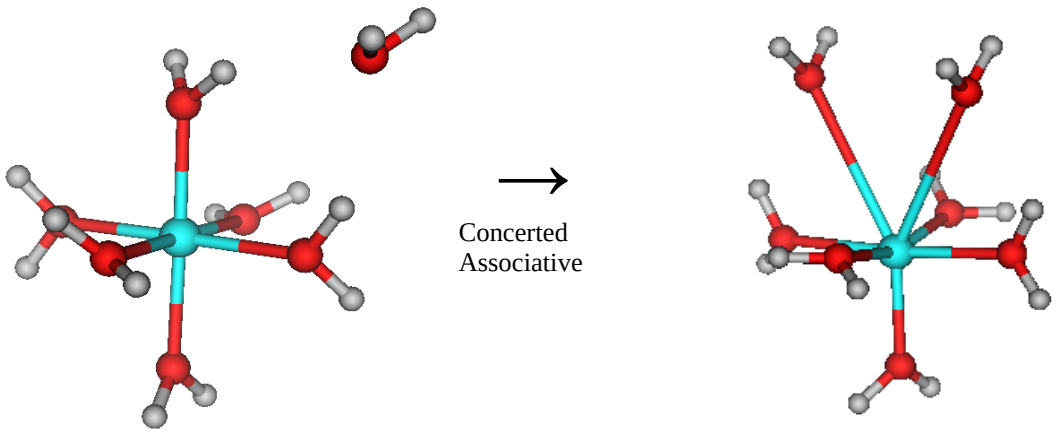

Figure 4-2 Interchange, associatively activated (I_a)

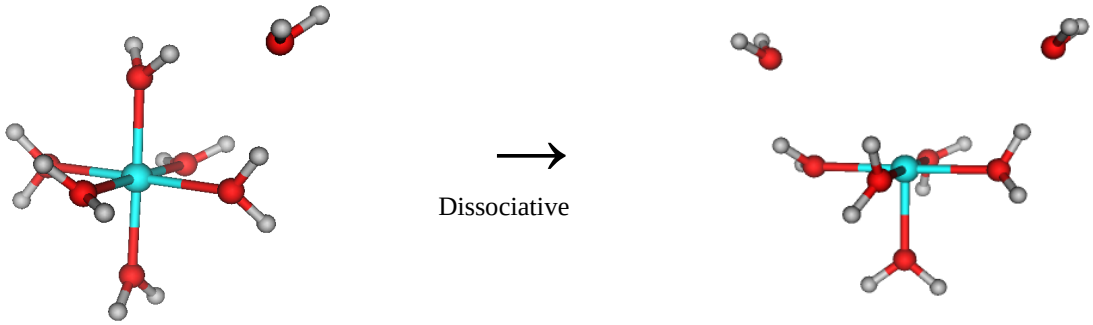

Figure 4-3 Dissociative (D) exchange and intermediate

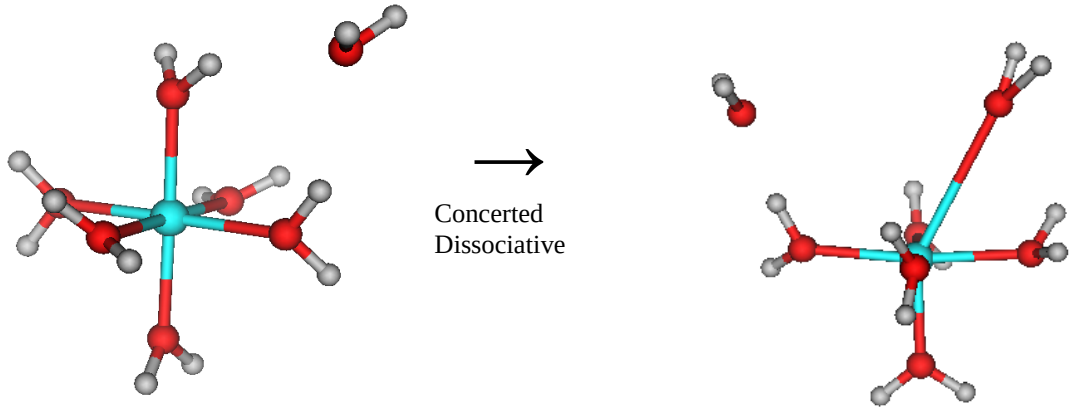

Figure 4-4 Interchange, dissociatively activated (I_d)

While the above mechanisms are not in contention, the assigment of these mechanisms to transition metal systems has long been disputed.

The early experimental work assigned the exchange mechanism for these systems based on the relative volume of activation, with all first row transition metal complexes being assigned a D mechanism[4-6]. However, later work by Merbach[7-10] showed that the exchange process of Mn^{2+} in water proceeded by an I_a mechanism.

The volume of activation is found from the pressure dependence of the rate constant *k*.

$$\left(\frac{\delta \ln k}{\delta p}\right)T = -\frac{\Delta V^{\dagger\dagger}}{RT}$$

Equation 4-1 Relationship between volume of activation and rate constant

This was not the end of the discussion and various groups published their own results on the assignment of the mechanism of exchange in water. It was then Aakesson[11], some twenty years after the original publication, who used theoretical methods to assign the exchange mechanisms. In this later publication a D/I_d mechanism was defended for all first row transition metal complexes in water. It only took a few years for these results to be argued both experimentally and theoretically. Most notably this was done by Rotzinger[2], who has provided many papers[3,12-15] on the topic of water exchange and the mechanistic changeover from an I_a mechanism at V to an I_d mechanism at Ni.

The investigation of the exchange processes of these systems has, so far, only been attempted computationally by QM methods. The reasons for using QM over MM include, QM can locate and minimise to a transition state with no extra parameterisation and QM is a more trusted method for the modelling of bond breaking processes because it explicitly treats electrons.

Modelling water exchange

It has been shown previously that LFMM gives comparable results for conformational structures and conformer energies as the corresponding QM methods do when applied

to the same systems. For this reason a QM like approach was chosen for the work using LFMM.

Previous work[2,3] on the subject of water exchange at a metal centre provides two possible starting conformers of the type $[M^{2+}(H_2O)_6].H_2O$, where the seventh water molecule is located in the second coordination sphere (the primary solvation shell).

The two different structures for these complexes are, Vertex (V) and Edge (E) which are defined by the position of the seventh water and its method of association with the complex. In a V type complex the seventh water molecule is hydrogen bonded to only one of the primary coordination shell water molecules. In the E type complex the seventh water molecule is hydrogen bonded to two primary coordination shell molecules.

It was decided that these calculations should be repeated using PW91 and COSMO, as this was the internally validated and consistently used functional for the DFT work. During the DFT comparison a third structural type Face (F) was found. The F type complex, which had previously not been reported, has the seventh water molecule bound to the complex through three of the primary coordination sphere water molecules.

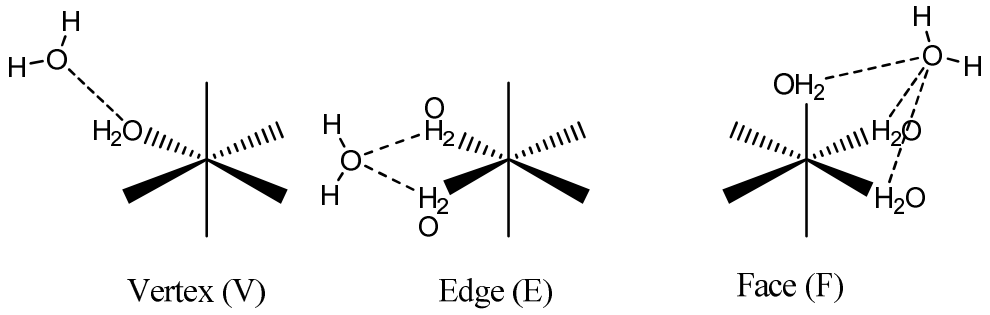

Figure 4-5 Diagrammatic representation of the three different binding modes

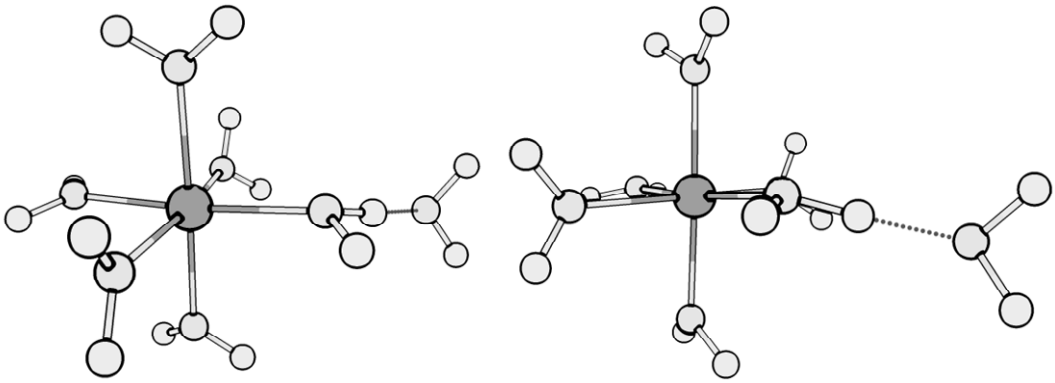

Figure 4-6 DFT minimised structures of $[V(H_2O)_6]^{2+}$, V type binding

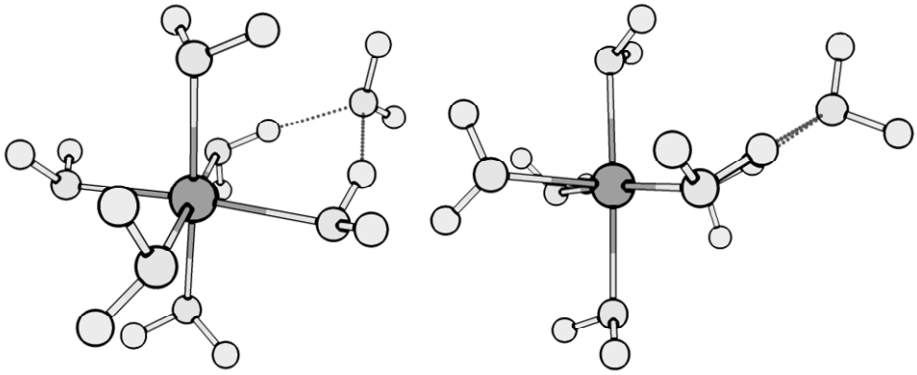

Figure 4-7 DFT minimised structures of $[V(H_2O)_6]^{2+}$, F type binding

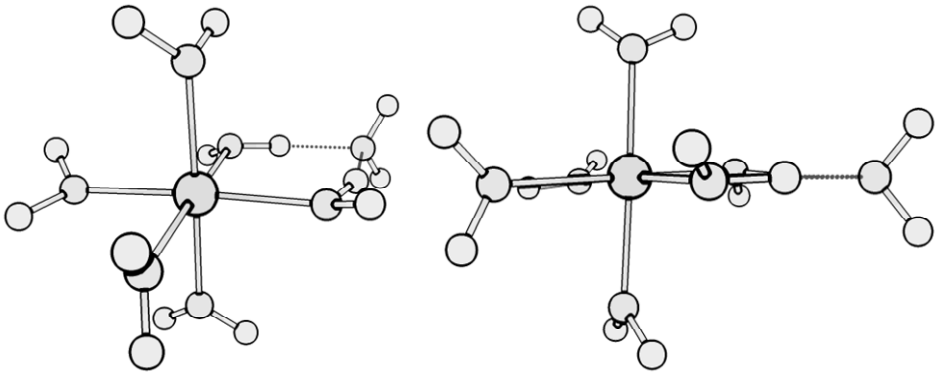

Figure 4-8 DFT minimised structures of $[V(H_2O)_6]^{2+}$, E type binding

The energy of the V,E and F forms of the complex were computed using PW91, with COSMO to account for the solvation, for the $[M(H_2O)_6]^{2+}.H_2O$, where M is either V, Mn or Ni.

Metal	E_{rel}(**V**)	E_{rel}(**E**)	E_{rel}(**F**)
V	0.5	0.0	2.5
Mn	1.1	0.0	2.8
Ni	0.6	0.0	1.9

Figure 4-9 Relative energies (Kcal mol^{-1})

In each case the E type complex was the lowest in energy (set at relative zero in Figure 4-9) with the V type just slightly higher and finally our newfound F type complexes were the highest in energy.

	DFT V	LFMM V	DFT Ni	LFMM Ni	DFT Mn	LFMM Mn
M-O 1	2.14	2.12	2.08	2.06	2.18	2.18
M-O 2	2.15	2.12	2.08	2.06	2.18	2.18
M-O 3	3.74	3.87	3.64	3.79	3.95	3.96
H-H	2.22	2.44	2.18	2.3	2.42	2.42

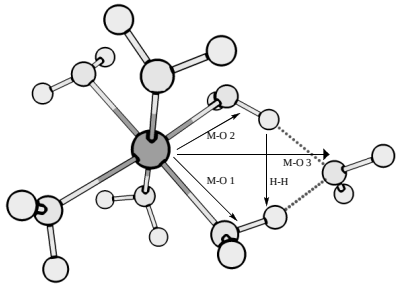

Figure 4-10 Comparison of selected structural parameters (Angstroms/Å) from DFT and LFMM optimisations.

In the simple six coordinate complexes, the distance between neighbouring hydrogen atoms is at least 3.25 Å, whereas in the seven coordinate systems that distance is contracted by at least half an angstrom. From Figure 4-10 it can be seen that the LFMM structures are indeed very close to the calculated DFT structures. It should be remembered at this point that the parameters used were developed solely on "ground state" data.

The above data shows that the LFMM method is stable for the $[M(H_2O)_6]^{2+}.H_2O$ systems. However, some of the processes to be modelled may well be A or at least I_a in nature, which means that the LFMM systems would need to be stable when the seventh water is explicitly connected to the metal. Systems where the seventh water is explicitly connected are defined as $[M(H_2O)_6.H_2O]^{2+}$ type complexes.

If the LFMM method is to stand any chance of successfully treating the exchange processes in these systems then it must be stable with seven connected ligands. It could be expected that when a seventh ligand is connected the molecule will minimise to one of three possible structures; pentagonal bypyramid, capped octahedron, capped trigonal prism.

It is of significance that the LFMM minimised structure does not differ greatly from the unbound structure.

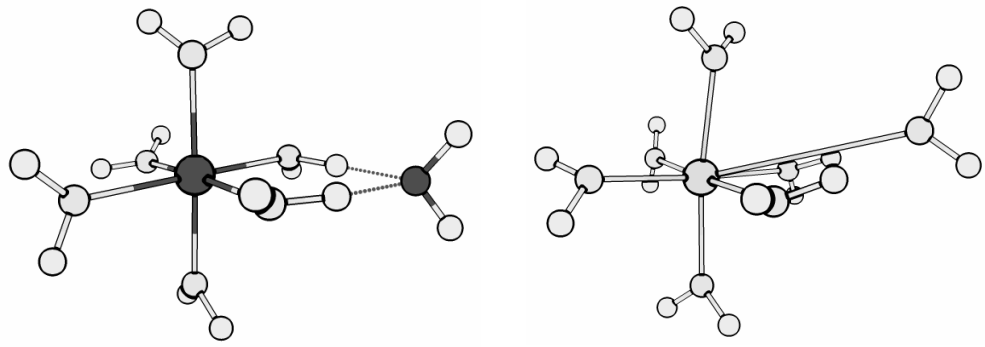

Figure 4-11 Bound and unbound LFMM structures with seventh water

LFMM exchange energy

The initial aim was not to model the explicit exchange process but to use idealised "transition states" as a model for calculating the relative energies of the exchange mechanisms for the different metals Figure 4-12. True transition states are covered in Chapter 5.

For the I_a process the TS is relatively easy to locate manually from the principle of microscopic reversibility, which states that the environment of entering and leaving groups must be chemical identical.

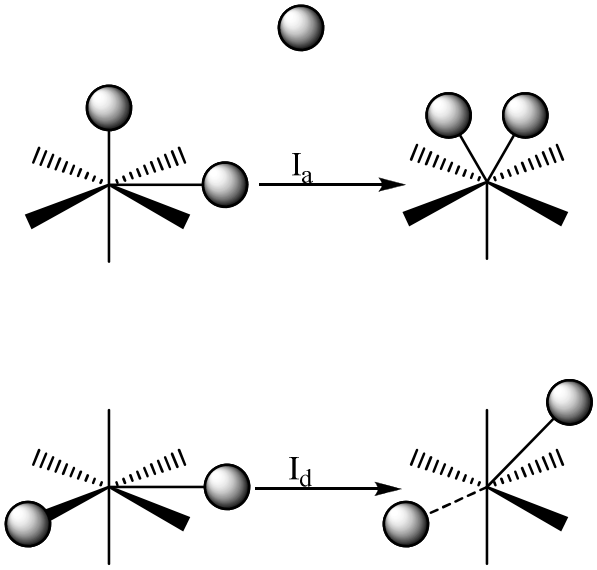

Figure 4-12 Schematic representation of the of how basic exchange process were modelled.

However, it is more complicated to define a model geometry for the calculation of the dissociative pathways energetics. It is not as simple as breaking a M-O bond to give a $[M(H_2O)_5]^{2+}.H_2O$ complex, as the number of bonds in the reactant and the "transition state" are not equal.

The remaining option was to reposition the sixth water ligand over an octahedral face. This new configuration was a true minimum for all species except Mn^{2+} and Zn^{2+}. In the Mn^{2+} and Zn^{2+} cases the complexes always collapse back to the octahedral. The solution for the Mn^{2+} was to put the sixth bound ligand over a face as before, but include the seventh water ligand, in the now vacant sixth ligand position but explicitly disconnected as the dissociating molecule. This type of complex is referred to as a

$[M(H_2O)_5(H_2O)]^{2+}.H_2O$ complex. This model "pseudo transition state" is in fact a local minimum for all complexes except Zn^{2+}. It is not clear why zinc behaved anomalously for the dissociative pathway but it is omitted from the analysis and discussion.

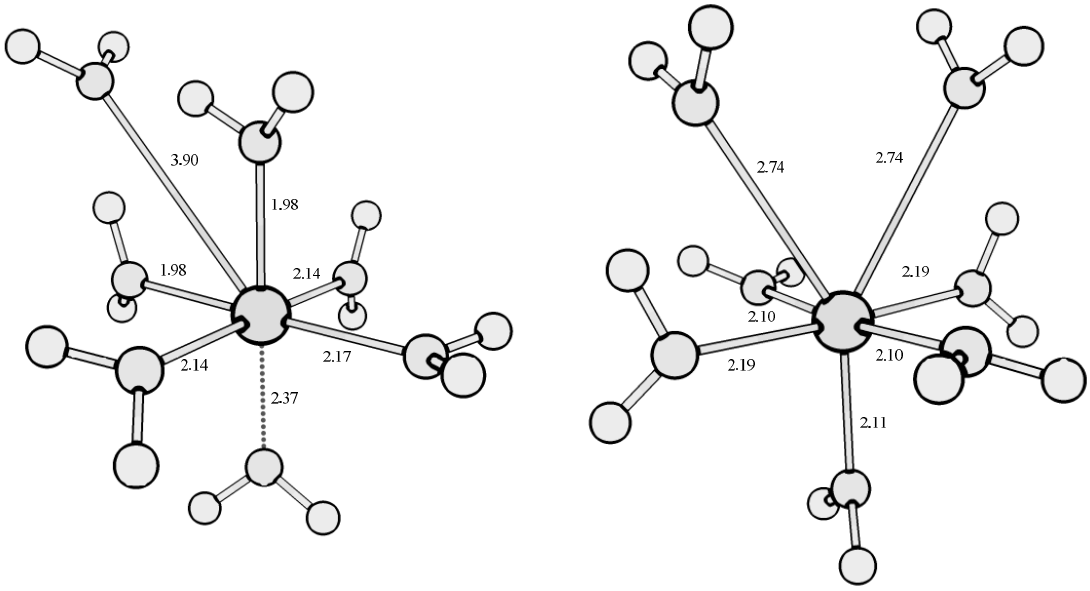

Figure 4-13 Structures with structural parameters (Å) for model complexes of $[V(H_2O)_6]^{2+}.H_2O$

The "activation energy" for a given complex is defined as the difference between the ground state, in these cases the seven coordinate ground state, and the transition state, in these cases the model geometries proposed above, for the associative mechanism.

For the dissociative process the "activation energy" is defined as the energy difference between the ground state, with six explicitly connected ligands and one "free" ligand, and the pseudo transition state again with six explicit bonds.

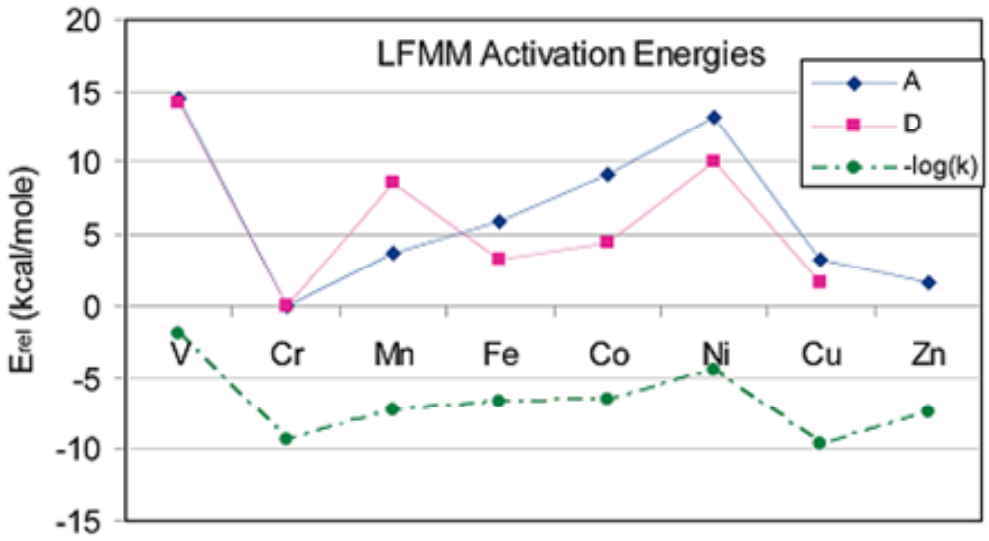

Figure 4-14 Activation energies (calculated/kcal mol^{-1}) for the first row divalent elements, for both A and D pathways compared to the experimental –log*k*, where *k* is the experimental exchange constant.

The activation energy of the Cr^{2+} system always gave a negative value: -1.3 kcal mol^{-1} for associative and -2.3 kcal mol^{-1} for dissociative. Cr^{2+} having the lowest activation energy is consistent with the observed fast exchange rates. However, a negative value does not seem reasonable. Consequently, and as an aid to the comparison and discussion, the calculated activation energies are adjusted relative to Cr^{2+} being at baseline zero for both associative and dissociative pathways.

The computed activation energies show a surprisingly good correlation with the experimental rate constants. For example, it was shown by high level quantum chemistry calculation performed by Rotzinger, that the associative and dissociative pathways should have nearly identical energies for V^{2+}. In addition to the relative energies of the V^{2+} system and more importantly, the calculations predict a mechanistic changeover from associative to dissociative from Fe^{2+} onwards. This changeover in mechanism is consistent with the changeover in sign of the volume of activation data from experiment.

The mechanisms for the Cr^{2+} and Cu^{2+} systems are expected to be somewhat ambiguous due to the strong Jahn-Teller distortion in these systems and given that the simple model pathways used only a nominal octahedral base for the calculations. This is seen in Figure 4-14 as a nearly indistinguishable difference between the two different mechanistic pathways. For Zn^{2+} the dissociative pathway is expected to be the most favoured. However, a dissociative mechanism of the type found for the other metals is not found for Zn, also Zn has a slower exchange rate than Cu but is calculated in this method to have a lower exchange energy, therefore a faster exchange.

The calculated qualitative exchange energies are reasonably robust given the empirical nature of the methodology and the approximations used.

The overall result of this work is positive but it has to be restated that the parameters developed were not unique and other parameter sets may be used. The parameters used, while qualitatively good, do not show any discernable trends when the energetic terms are broken down into individual contributions.

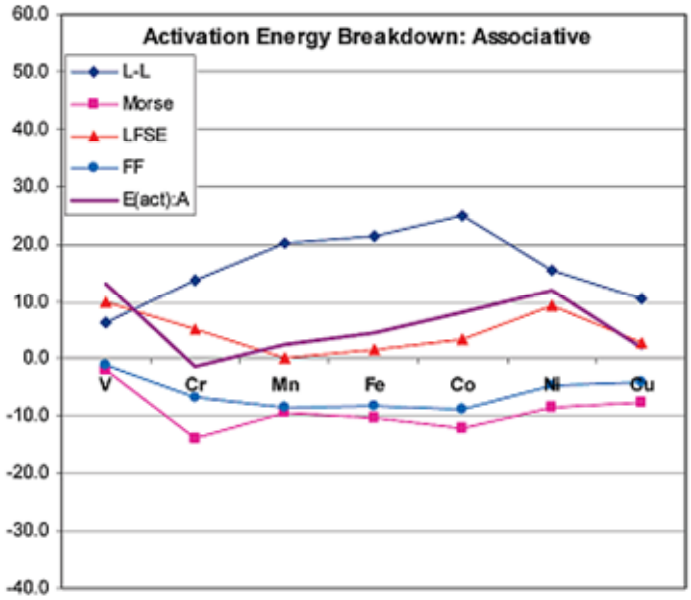

Figure 4-15 Breakdown of associative activation energy into individual components (kcal mol^{-1}): ligand-ligand repulsion (L-L), M-L bond stretching (Morse), LFSE and the parent force field terms.

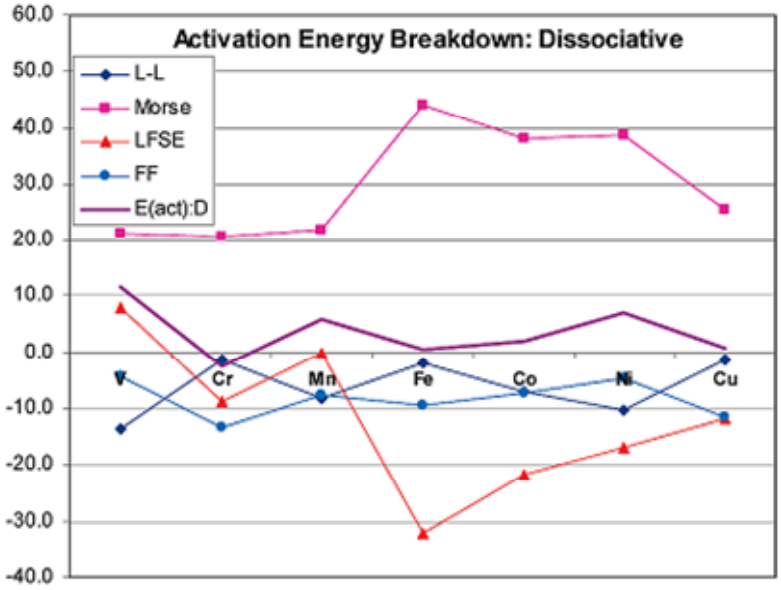

Figure 4-16 Breakdown of dissociative activation energy into individual components (kcal mol^{-1}): ligand-ligand repulsion (L-L), M-L bond stretching (Morse), LFSE and the parent force field terms.

Small changes in the force field parameters can lead to relatively large changes in the energy of a complex, ~ 6 kcal mol^{-1}. However, there is significant cancellation of errors and the energy of the resultant pathway changes by a lot less, ~ 1 kcal mol^{-1}.

Taking the lowest calculated exchange energy for each metal, associative for V, Cr, Mn and dissociative for Fe, Co, Ni and Cu, and platting them against the logarithm of the rate constant gives a good correlation with an R^2 value of 0.94.

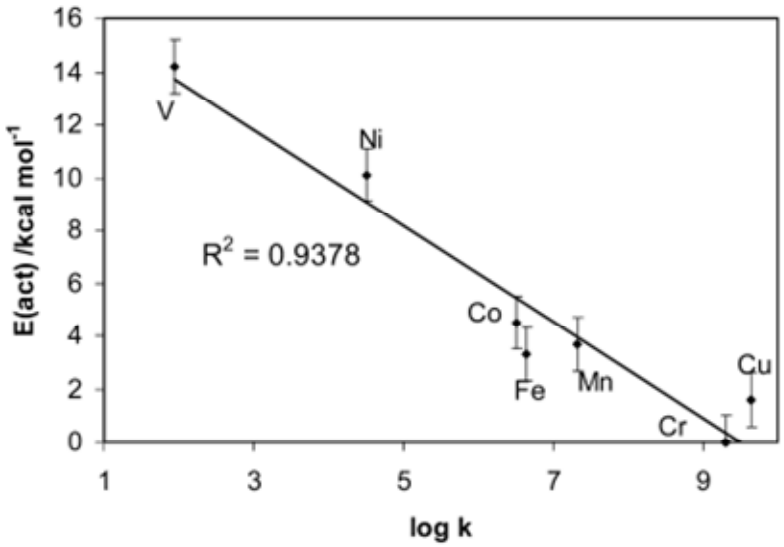

Figure 4-17 Correlation between log *k* values and calculated activation energies, showing a 1 kcal mol^{-1} error

Conclusions

The LFMM method has been shown able to qualitatively reproduce the energies of the water exchange processes for the first row divalent metals. This is a significant achievement as the force field parameters were developed based solely on six coordinate structures. The LFMM method has proved applicable to "transition states" with different explicit connectivity than the training geometries. Also the method shows stability to "second sphere" ligands and does not collapse or abnormally distort in an attempt to deal with these species.

It should be noted that the method has, so far, been unsuccessful in treating Zn^{2+} using the two model pathways detailed. A more detailed investigation into the exact behavior of this moiety by DFT and then LFMM is required.

Finally the negative activation energy for the Cr^{2+} species also requires a more detailed analysis of the system and the models used. However, this is sadly beyond the scope of the current project.

References

(1) Basolo, F.; Pearson, R. G. *Mechanisms of Inorganic Reactions, A Study of Metal Complexes in Solution. 2nd Ed*, 1967.
(2) Rotzinger, F. P. *J Am Chem Soc* **1996**, *118*, 6760-6766.
(3) Rotzinger, F. P. *J Am Chem Soc* **1997**, *119*, 5230-5238.
(4) Merbach, A. E.; Vanni, H. *Helv Chim Acta* **1977**, *60*, 1124-1127.
(5) Ducommun, Y.; Earl, W. L.; Merbach, A. E. *Inorg Chem* **1979**, *18*, 2754-2758.
(6) Ducommun, Y.; Zbinden, D.; Merbach, A. E. *Helv Chim Acta* **1982**, *65*, 1385-1390.
(7) Meyer, F. K.; Newman, K. E.; Merbach, A. E. *J Am Chem Soc* **1979**, *101*, 5588-5593.
(8) Vanni, H.; Merbach, A. E. *Inorg Chem* **1979**, *18*, 2758-2762.
(9) Ducommun, Y.; Newman, K. E.; Merbach, A. E. *Inorg Chem* **1980**, *19*, 3696-703.
(10) Ducommun, Y.; Zbinden, D.; Merbach, A. E. *Helv Chim Acta* **1982**, *65*, 1385-90.
(11) Aakesson, R.; Pettersson, L. G. M.; Sandstroem, M.; Wahlgren, U. *J Am Chem Soc* **1994**, *116*, 8705-8713.
(12) Rotzinger, F. P. *Chimia* **1997**, *51*, 97-99.
(13) Rotzinger, F. P. *Helv Chim Acta* **2000**, *83*, 3006-3020.
(14) Rotzinger, F. P. *Chem. Rev.* **2005**, *105*, 2003-2038.
(15) Rotzinger, F. P. *J Phys Chem B* **2005**, *109*, 1510-1527.

Chapter 5 - Transition states and Minimum Energy Crossing Points (MECP)

Introduction

The work in previous chapters has led to the realisation that Molecular Mechanics can be used to investigate properties and systems not usually treated with such methods.

However, a lot of the work so far reported has been on model or qualitative work.

The results for the water exchange pathways while very encouraging and qualitatively correct, did not yield information about the "actual transition states" except for the case of the I_a mechanism for $[V(H_2O)_6]^{2+}$. In addition to this the model used for the pseudo transition state study required an understanding of the chemical process as it required a trial model "transition state" geometry to be used.

The Holy Grail of this chapter's work was to find out if it was possible within LFMM to search for actual transition states and if possible to arrive at these transition states without prior knowledge of the mechanism.

There already exist within the literature a few methods for the location of transition states within a MM framework. Each of the methods locates structures that lie close to the true transition state, if they do not find the actual transition state. Of the methods available, the ones that find the true transition state are Empirical Valence Bond (EVB)[1,2], Multi Configuration Molecular Mechanics (MCMM)[3,4] and Reactive Force Field (ReaxFF)[5,6]. The ones that find the crossing point are Seam and MECP[7,8]. To allow the MECP methodology implemented within DOMMIMOE to find the true transition state an additional minimisation is required after the MECP search. This minimisation uses a

modified Newton-Raphson technique to go from the MECP to the transition state. The remaining Q2MM[9,10] method locates a structure that is considerably higher in energy than the transition state. However, it still provides useful information of the transition state mechanism (Figure 5-1).

The EVB, MCMM and RFF methods all use the same underlying ideas, that of mixing the force fields for the reactant and the product with a given mixing term. The difficulty with this is that the mixing term is not known *a priori* and is not transferable from one reaction to another.

The Seam and MECP methods both use a minimisation technique to follow the intersection of the component force fields to the crossing point. The benefit of these methods is that the intersection between the two PES's is fairly easy to locate, even from bad starting geometries.

The Q2MM method constructs a modified PES from the area contained within both of the PES's from the parent force field and performs a simple minimisation within this new PES. This is done by replacing the actual negative frequency in the calculated hessian matrix with an arbitrarily large positive value, and minimizing with respect to that eigen value.

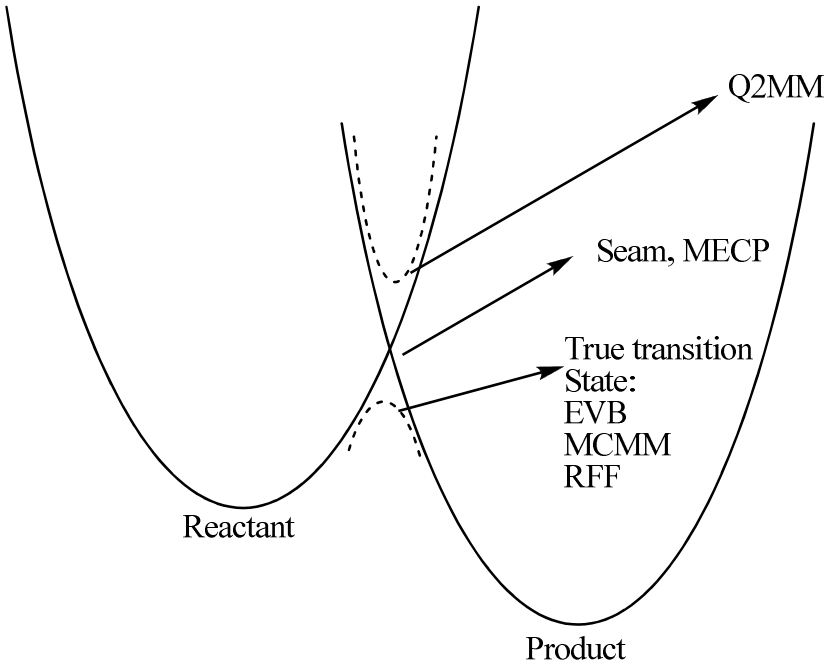

Figure 5-1 Schematic representation of what structures on the PES different methods locate

Computational details

All calculations in this chapter were performed using DOMMIMOE and ADF.

Geometry optimisations performed using ADF were done using various gradient corrected functionals; PW91, BLYP, RPBE, as well as the LDA. LDA calculations were performed using the Vosko-Wilke-Nusair equations for the electron correlation energy.

ADF allows imposed symmetries; however, due to the exact symmetry of the hexaaqua complexes, there are complications, which are discussed in full detail later in the chapter.

The default ADF options were used for all minimisations, with the COSMO scheme being employed where solvation was to be included. An integration level of 4.0 was used for simple minimisations and a level of 6.0 for frequency calculations.

All structures (both minimum and transition state) reported in this chapter were calculated either with ADF and the PW91 GGA, or with DOMMIMOE and the parameters stated at the end of the previous chapter.

Minimum Energy Crossing Points (MECP)

The method that was chosen as the one that could be integrated into LFMM was that of the MECP (see Computational Chemistry Chapter 2).

An appealing feature of the MECP implementation in LFMM is that it does not require knowledge of the transition state in the process being studied. It requires an idea of the possible mechanism of the reaction but not of the actual transition state. What is required for the MECP search are guesses at the starting and ending geometries, the MECP code drives these structures together looking for the transition state between the two.

True Transition states

The earlier work on modelling the energetics of exchange processes used only a basic model of the transition state structures. To be scientifically more rigorous, we need a way to locate transition states without knowing them before hand.

The MECP methodology that was referred to earlier is a way to achieve this. However, to gauge the successes of the LFMM method good descriptions of the actual transition states is needed first. To this end a set of DFT transition states were optimised using the same functionals and program that were used for the earlier parameter development

work. This was to ensure an internally consistent comparison and also to look at some of the reported inconsistencies regarding negative frequencies in the literature.

For the initial foray into true transition states only three metals were chosen: V^{2+}, Mn^{2+} and Ni^{2+}. These were chosen as they have relatively simple transition states being orbitally non-degenerate. They do not suffer from the complexities of the Jahn-Teller active metals especially the extreme case of Cu^{2+} for which the discussion still continues as to what the exact coordination number is when solvated[11-13]. The chosen metals also did not suffer from the complications of the Zn^{2+} seen in the earlier work.

The expectation based on a literature review[14-16] is that the mechanism for V^{2+} will be associative and for Ni^{2+} it will be dissociative with Mn^{2+} being ambiguous. For these reasons we used DFT to try to locate only four types of transition state; associative (Figure 5-2, Figure 5-4, Figure 5-7, I_a), associative-trans exchange (Figure 5-3, I_a), dissociative (Figure 5-5, Figure 5-8, I_d) seven aqua molecules, dissociative (Figure 5-6, I_d) six aqua molecules.

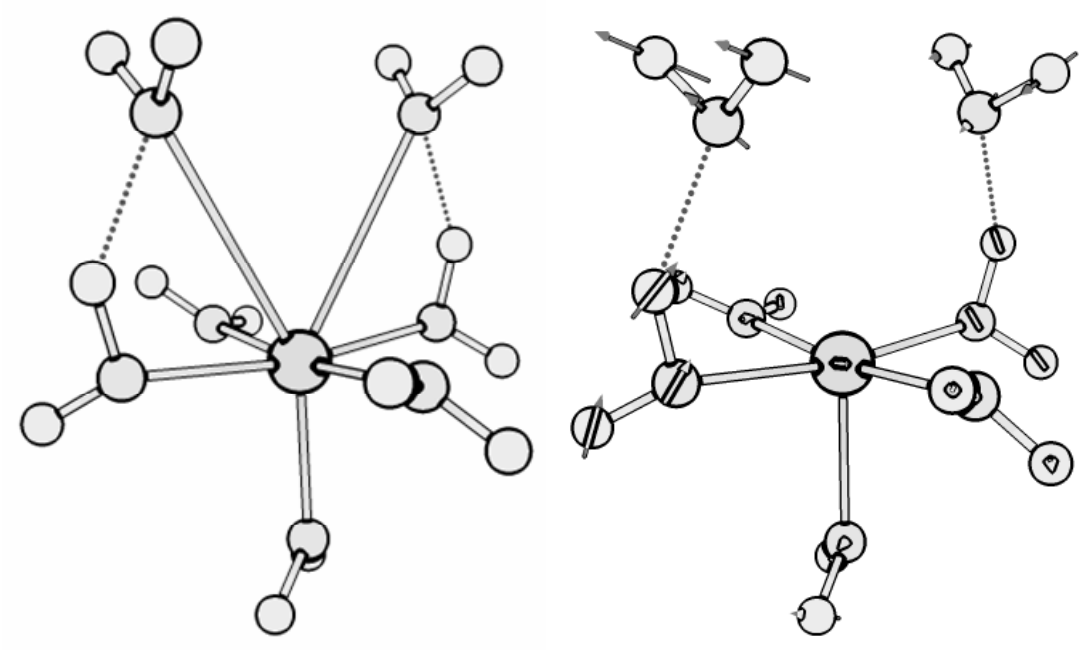

Figure 5-2 DFT transition state for $[V(H_2O)_5.(H_2O)_2]^{2+}$, Associative mechanism and with displacement vectors

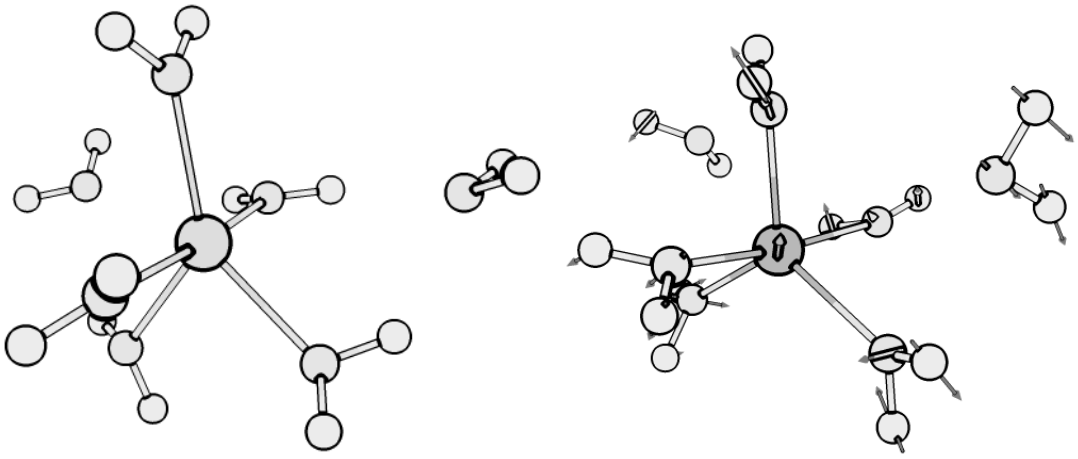

Figure 5-3 DFT transition state for $[Mn(H_2O)_5.(H_2O)_2]^{2+}$. A mechanism, trans ligands exchanging

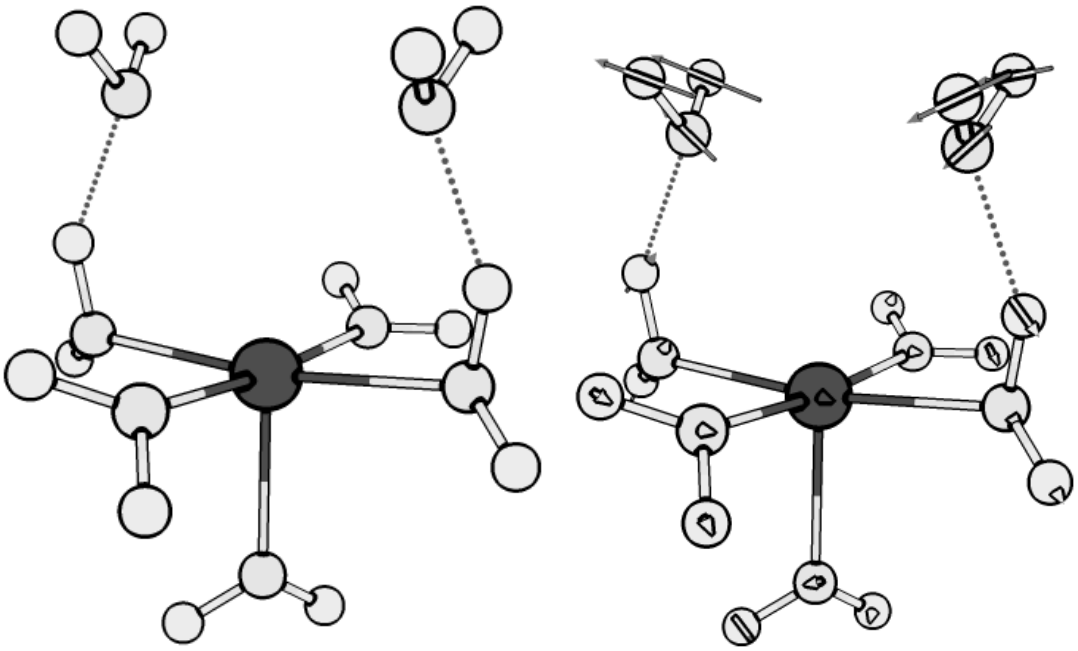

Figure 5-4 DFT transition state for $[Mn(H_2O)_4.(H_2O)_2]^{2+}$, Associative mechanism and with displacement vectors

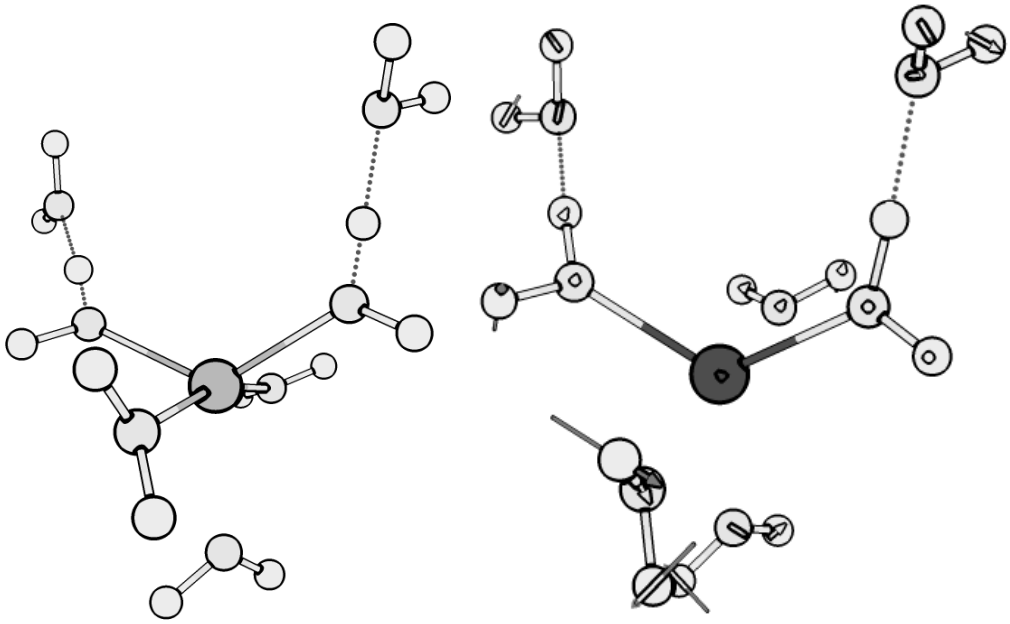

Figure 5-5 DFT transition state for $[Mn(H_2O)_5...(H_2O)_2]^{2+}$, D mechanism and showing displacement vectors. However still based on seven water system

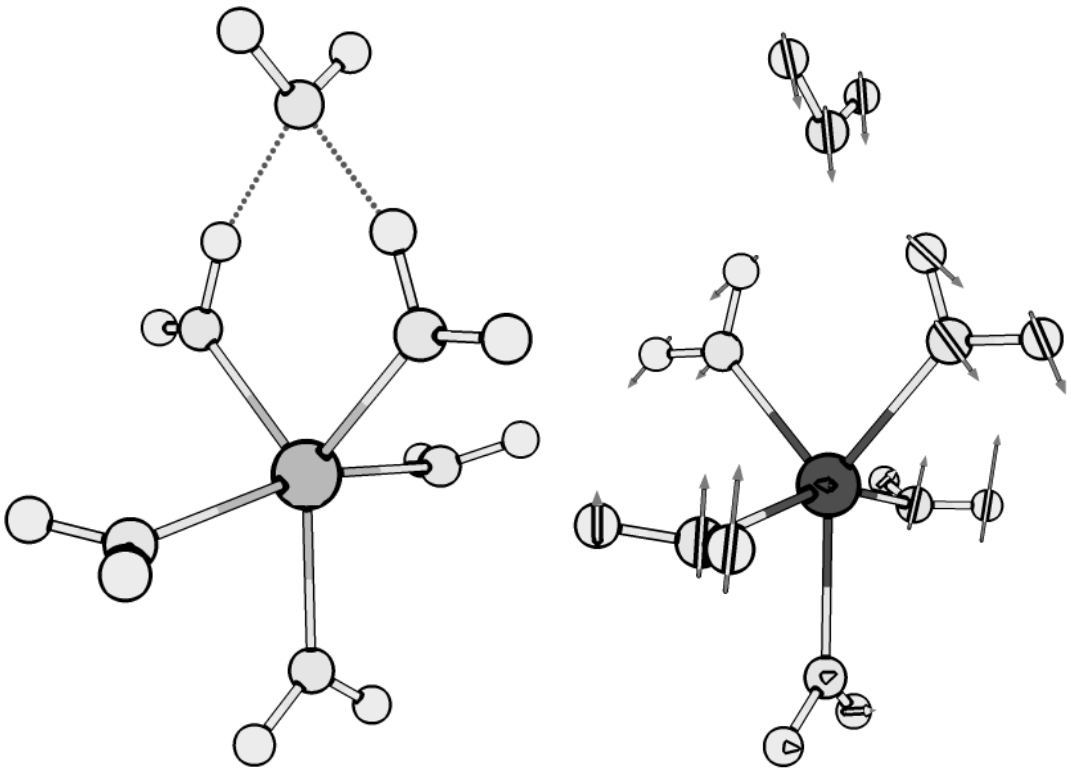

Figure 5-6 DFT transition state for $[Mn(H_2O)_5...H_2O]^{2+}$, D mechanism and with displacement vectors, based on a six water system

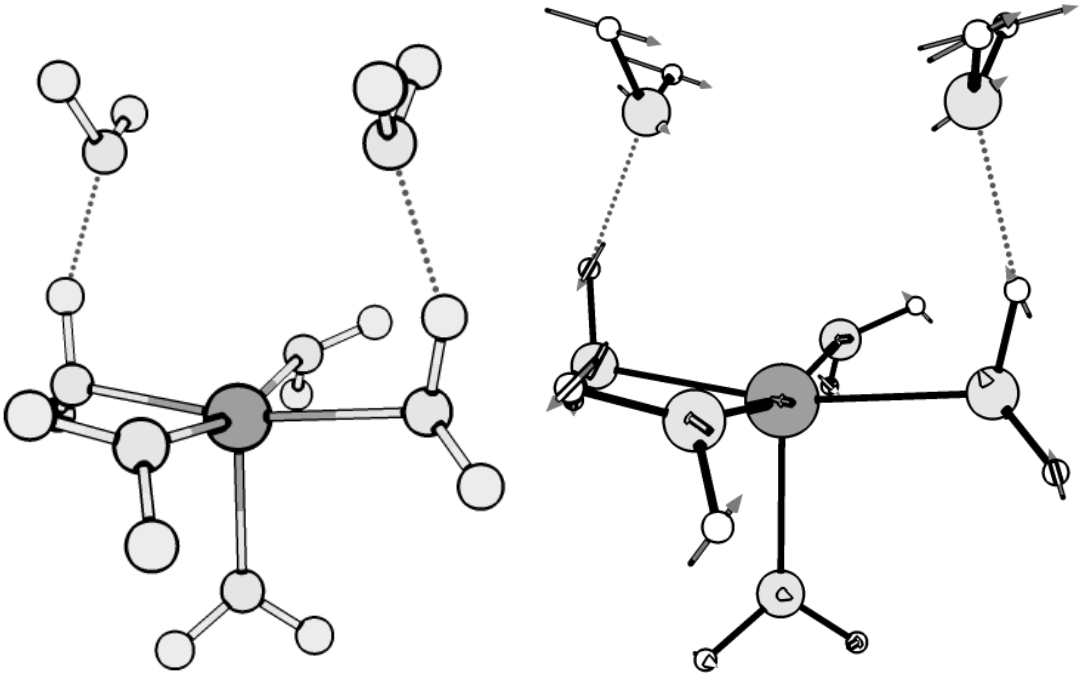

Figure 5-7 DFT transition state for $[Ni(H_2O)_4.(H_2O)_2]^{2+}$, A mechanism and with displacement vectors

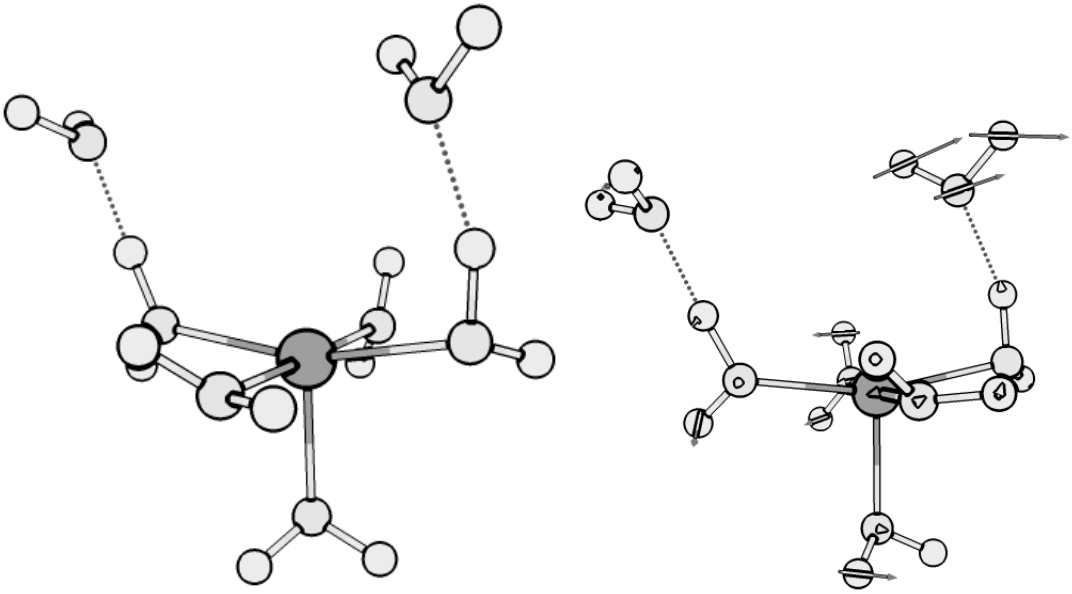

Figure 5-8 DFT transition state for $[Ni(H_2O)_4...(H_2O)_2]^{2+}$, D mechanism and with displacement vectors

Complex	Frequency cm^{-1}
$[V(H_2O)_5.(H_2O)_2]^{2+}$	-98.15
$[Mn(H_2O)_5.(H_2O)_2]^{2+}$ trans	-87.03
$[Mn(H_2O)_5.(H_2O)_2]^{2+}$	-76.54
$[Mn(H_2O)_5...(H_2O)_2]^{2+}$	-71.24
$[Mn(H_2O)_5...H_2O]^{2+}$	-43.57
$[Ni(H_2O)_5.(H_2O)_2]^{2+}$	-67.44
$[Ni(H_2O)_5...(H_2O)_2]^{2+}$	-43.06

Table 5-1 Collection of the single negative frequencies found in the above geometries calculated with DFT

Metal	Associative	Dissociative	Ground state	Associative exchange	Dissociative exchange
Ni	-2065.50	-2068.21	-2079.87	14.37	11.66
Mn	-2204.74	-2177.06	-2213.65	8.91	36.59
V	-2181.85	-2174.92	-2199.46	17.61	24.54

Table 5-2 Table showing comparison of energies (kcal mol^{-1}) for the different transition state pathways calculated with DFT

As Table 5-2 shows, the expected pathways for V^{2+} and Ni^{2+} are associative and dissociative respectively. However, the case for Mn^{2+} is not as simple, more transition states for water exchange at a Mn^{2+} centre can be found. Based on the difference between the energies of the associative and dissociative pathways it is expected that Mn^{2+} should undergo associative exchange. This energetic argument for the exchange mechanism at a Mn^{2+} centre is in agreement to the volume of activation[17-19], which is a negative value, suggesting a contracted transition state when compared to the starting geometry. However, as not all of the different exchange pathways for Mn^{2+} were located it is possible that one of the other pathways could be lower in energy and change this conclusion.

The energies and frequencies above (Table 5-1, Table 5-2) were calculated using DFT, rather than using the values in the literature. This was to make sure that the methods used were internally consistent and as the initial parameterisation was done based on personal DFT work then similar methods were followed throughout.

Transition States with LFMM

The MECP code written within MOE for use with the LFMM force field simply requires starting "reactant" geometry and "product" geometries. This had to be done in a specific way within MOE due to the assignation of unique atom keys to the molecule.

Firstly a minimised LFMM geometry was taken. In most cases this was a E type complex (see Chapter 3). The outgoing ligand (most often the nominal axial ligand) is removed to mirror the incoming ligand, then the incoming ligand is bound to the metal in the now vacant site.

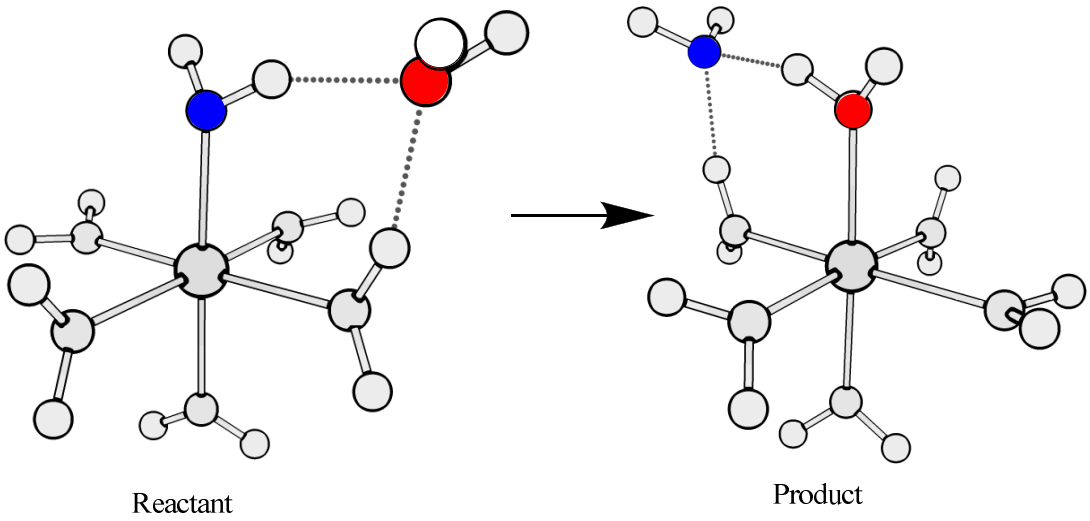

Figure 5-9 "Reactant" and "product" geometries used in standard MECP runs. Associative pathway

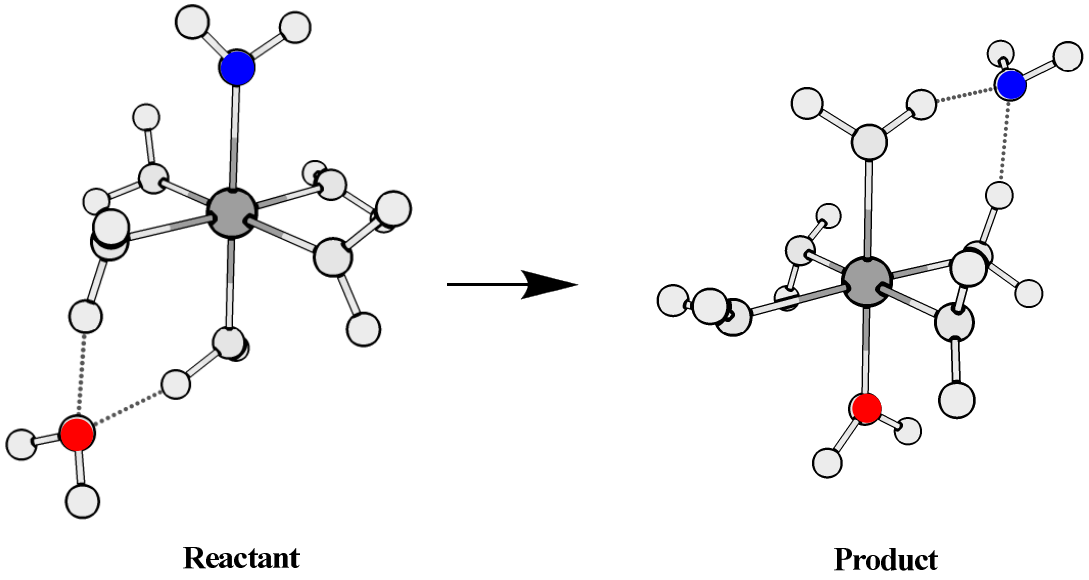

Figure 5-10 “Reactant” and “product” geometries used in standard MECP runs. Associative pathway – trans mechanism

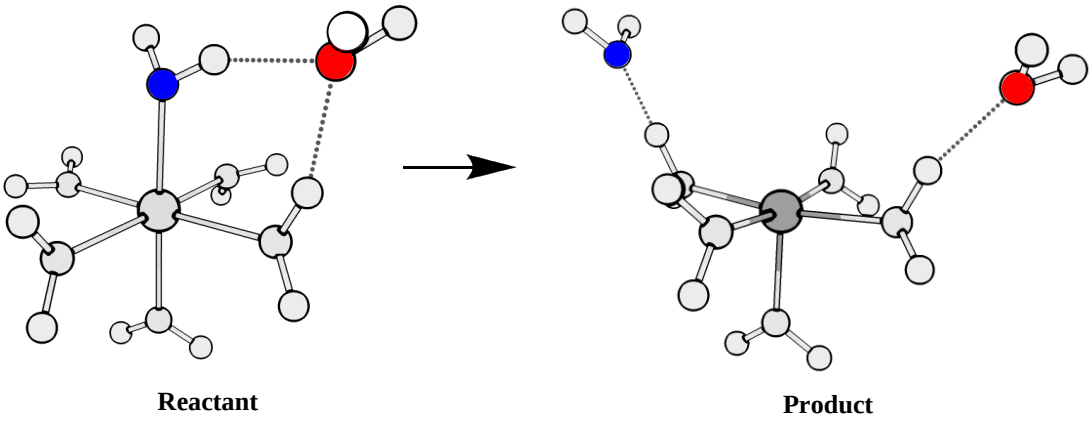

Figure 5-11 “Reactant” and “product” geometries used in standard MECP runs. Dissociative pathway

The use of the above (Figure 5-9, Figure 5-10, Figure 5-11,) as starting and ending species for MECP runs yields the following LFMM structures for the transition states of the exchange reaction for V^{2+}, Mn^{2+} and Ni^{2+}.

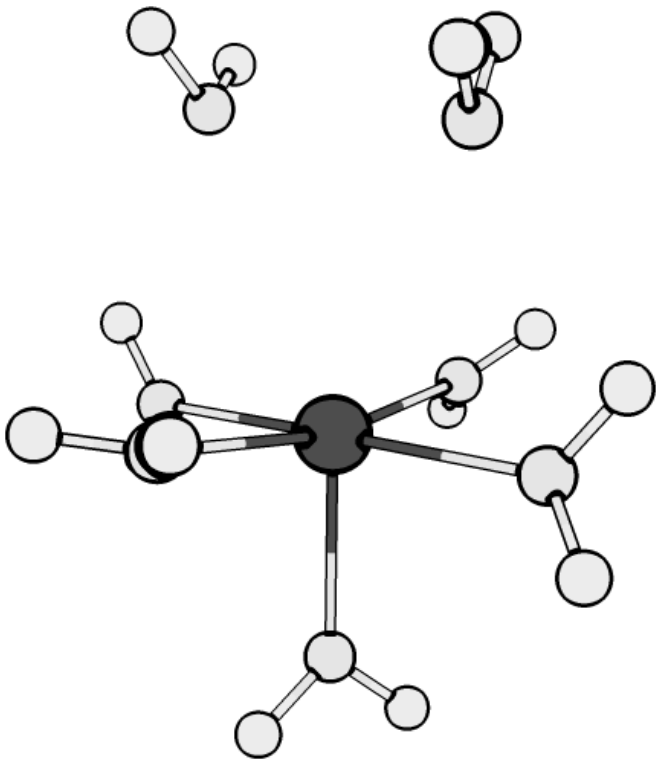

Figure 5-12 LFMM transition state for V^{2+}, Associative mechanism

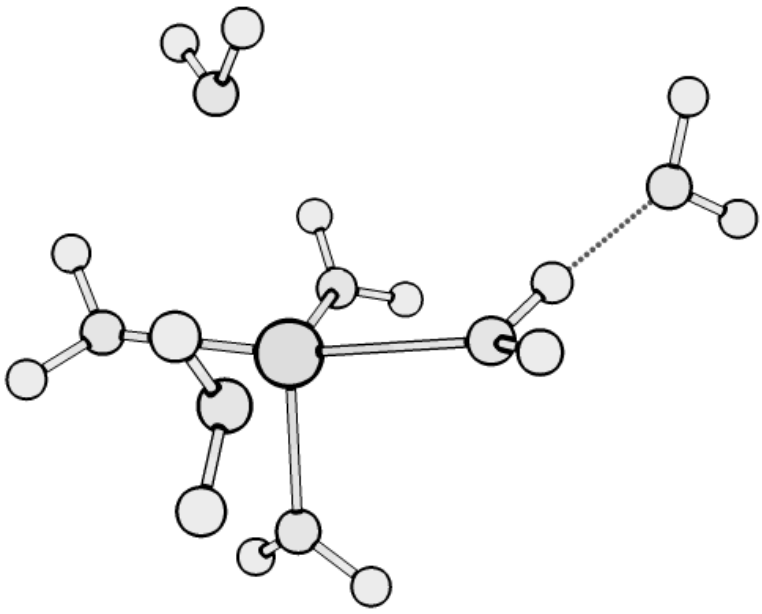

Figure 5-13 LFMM transition state for V^{2+}, Dissociative mechanism

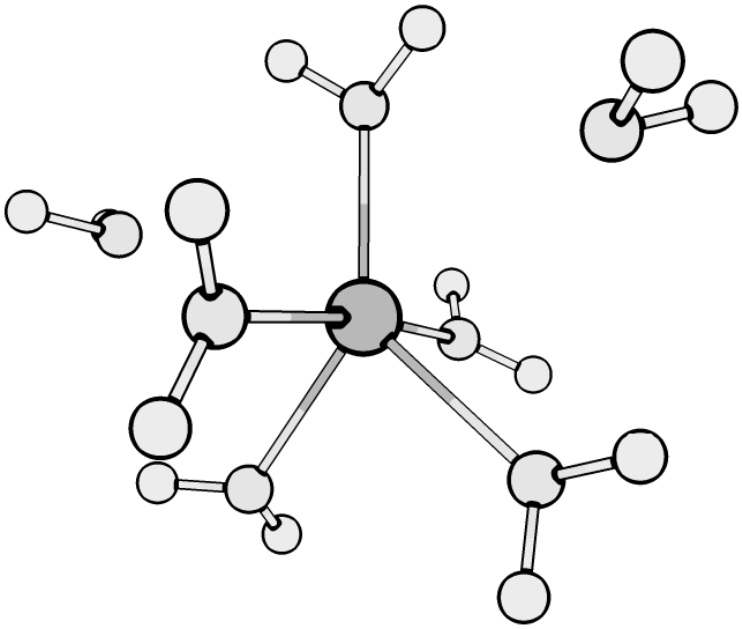

Figure 5-14 LFMM transition state for Mn^{2+}, Associative mechanism

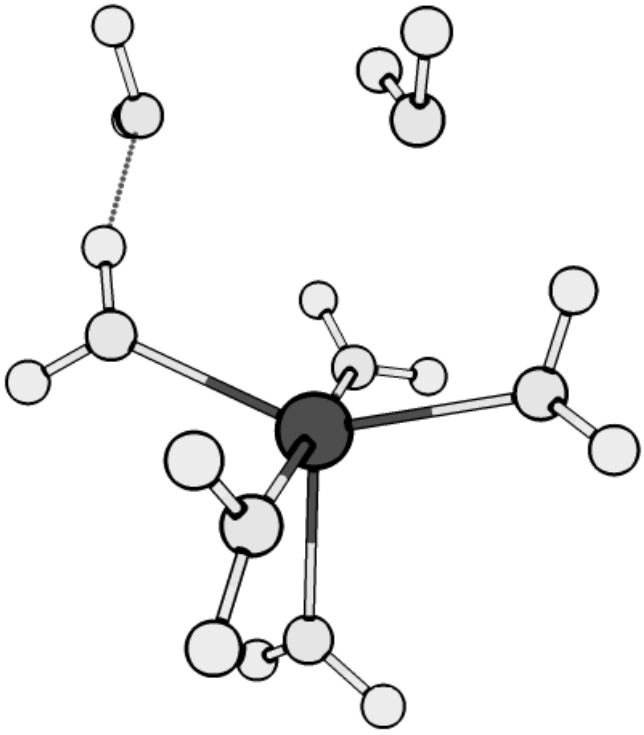

Figure 5-15 LFMM transition state for Mn^{2+}, Dissociative mechanism

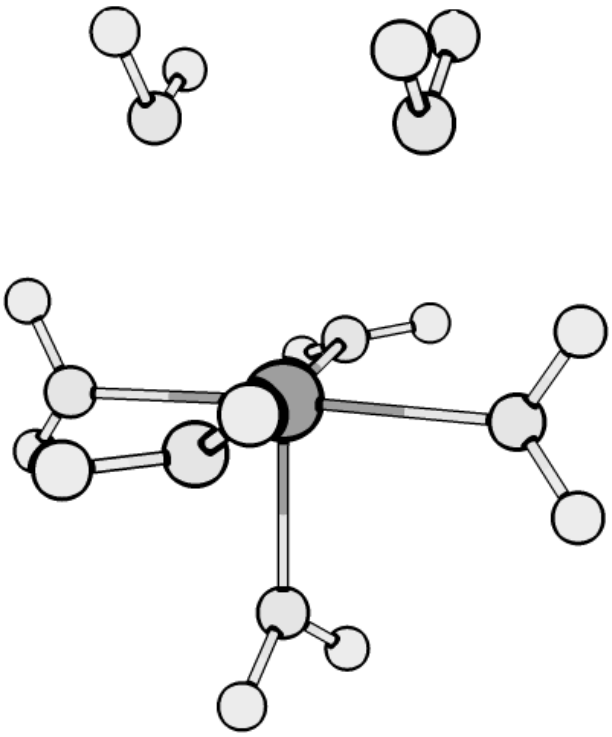

Figure 5-16 LFMM transition state for Mn^{2+}, Associative mechanism

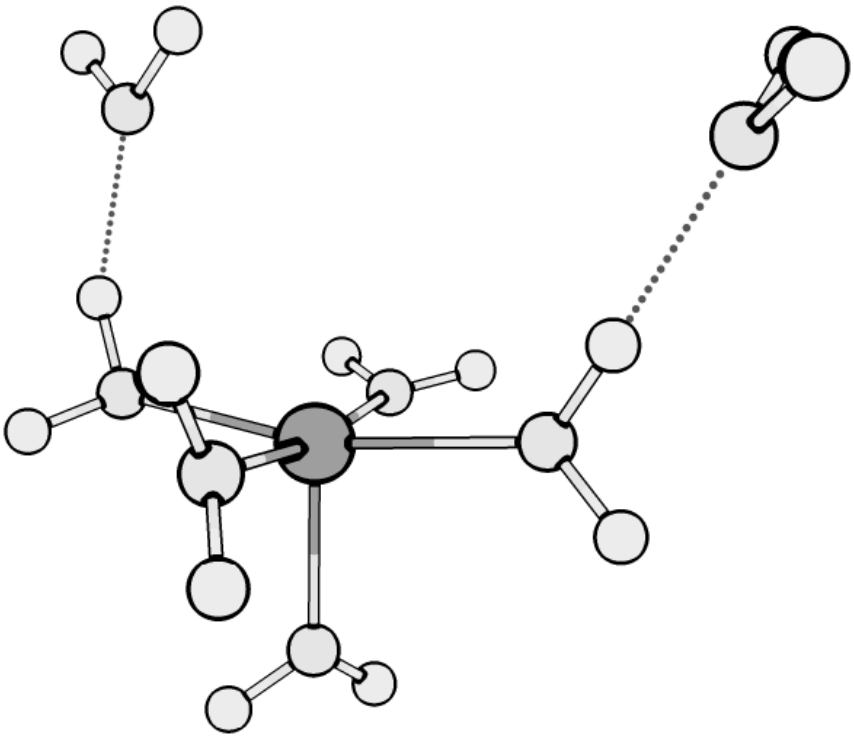

Figure 5-17 LFMM transition state for Ni^{2+}, Dissociative mechanism

Metal	Associative	Dissociative	"Reactant" 6 Bonds	"Reactant" 5 Bonds	LFMM exchange I_a	DFT exchange I_a	LFMM exchange I_d	DFT exchange I_d
Ni	-271.05	-244.72	-300.35	-233.57	29.30	14.40	11.15	11.70
Mn	-226.58	-186.97	-237.14	-209.82	10.56	8.90	22.85	36.60
V	-238.07	-229.78	-258.14		20.07	17.60	28.36	24.50

Table 5-3 LFMM energies (kcal mol^{-1}) for the different calculated MECP structures

The energies calculated for the LFMM MECP structures agree remarkably well with the calculated energies and structures from DFT.

For each of the metals considered the correct expected pathway is found to be lowest in energy and the ordering of the energy gaps between reactant species and transition state is consistent with the ordering of the exchange rates from experiment.

Each of the above structures generated by the MECP routine was minimised using a LFMM Newton-Raphson minimiser. This Newton-Raphson minimisation is required because the MECP is designed to find the seam and then the intersection of a reaction. However, the actual transition state is not found at the intersection and lies slightly lower in energy. Performing a Newton-Raphson optimisation on an MECP structure leads to the true transition state, confirmed by frequency calculation. Also the MECP method implemented within DOMMIMOE is based on a connectivity argument and so the structure it generates is based on product/reactant. So in the I_a processes the generated MECP will have six explicit bonds (whereas, it should have seven), also the correct connectivity is required for the LFMM to calculate the energy correctly. Likewise

in the I_d process the LFMM MECP will have six bonds (whereas, it should have five). It is worthwhile to note that the LFMM method gets exceptionally close to the true transition state, even though it is based on a approximate system.

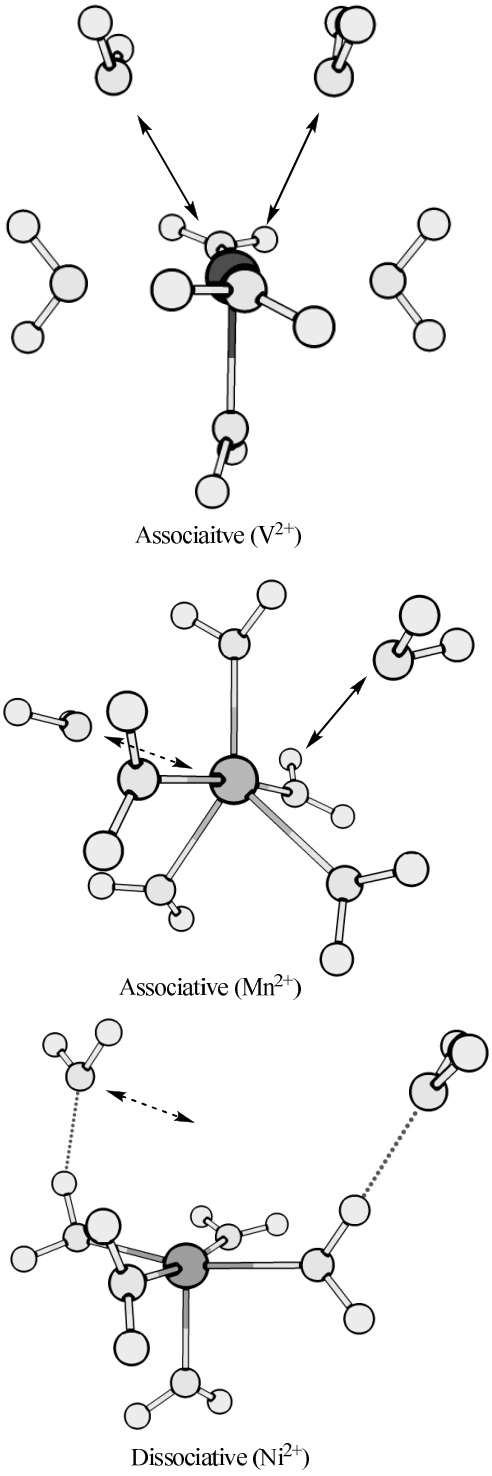

Figure 5-18 Showing the dominant motion in each of the calculated LFMM transition states.

	Coordinated Bonds (Å)	Incoming Ligand (Å)	Outgoing Ligand (Å)	Frequency cm^{-1}
DFT starting geometry V^{2+}	2.14	3.88	2.14	
LFMM starting geometry V^{2+}	2.14	3.92	2.14	
DFT TS geometry V^{2+}	2.14	2.99	2.99	-98.15
LFMM TS geometry V^{2+}	2.14	3	3.01	-108
DFT starting geometry Mn^{2+}	2.22	3.75	2.22	
LFMM starting geometry Mn^{2+}	2.19	4.07	2.19	
DFT TS geometry Mn^{2+}	2.22	3.22	3.22	-76.54
LFMM TS geometry Mn^{2+}	2.21	3.43	3.42	-84
DFT starting geometry Ni^{2+}	2.01	3.63	2.01	
LFMM starting geometry Ni^{2+}	2.05	3.92	2.05	
DFT TS geometry Ni^{2+}	2.06	4.06	3.28	-43.06
LFMM TS geometry Ni^{2+}	2.06	4.3	3.27	-62

Table 5-4 Comparison of DFT and LFMM calculated structures and frequencies of the most favourable pathway for each metal.

Conclusions

A method for locating the transition state of an exchange pathway has been successfully implemented within DOMMIMOE. This method, the MECP, has been used to find the structures of the crossing point species. These species have then been minimized using a modified Newton-Raphson minimiser to find the transition state. These species were then confirmed as true transition states using a combination of the DOMMIMOE frequency routine and DFT.

The true transition states were used to find the energy of the exchange process and hence find out which exchange process was favoured with the LFMM force field. The calculated energies compared qualitatively well with published exchange mechanisms, correctly predicting the mechanistic change over from V^{2+} to Mn^{2+} to Zn^{2+}. The LFMM energies also compare quantitatively well to the calculated DFT exchange energies.

The predominant motion in the one negative frequency in the LFMM transition state was confirmed to be that of the exchange process.

References

(1) Hwang, J. K.; King, G.; Creighton, S.; Warshel, A. *J. Am. Chem. Soc.* 1988, *110*, 5297-5311.
(2) Warshal, A. *Computer Modeling of Chemical Reactions in Enzymes and Solutions*; John Wiley & Sons: New York, 1991.
(3) Albu, T. V.; Corchado, J. C.; Truhlar, D. G. *J. Phys. Chem. A* 2001, *105*, 8465-8487.
(4) Tishchenko, O.; Truhlar, D. G. *J. Phys. Chem. A* 2006, *110*, 13530-13536.
(5) van Duin, A. C. T.; Dasgupta, S.; Lorant, F.; Goddard, W. A. *J. Phys. Chem. A* 2001, *105*, 9396-9409.
(6) Nielson, K. D.; van Duin, A. C. T.; Oxgaard, J.; Deng, W. Q.; Goddard, W. A. *J. Phys. Chem. A* 2005, *109*, 493-499.
(7) Bearpark, M. J.; Robb, M. A.; Schlegel, H. B. *Chem. Phys. Lett.* 1994, *223*, 269-74.
(8) Harvey, J. N.; Aschi, M.; Schwarz, H.; Koch, W. *Theor. Chem. Acc.* 1998, *99*, 95-99.
(9) Norrby, P. O.; Rasmussen, T.; Gillies, M. B. *Abstr. Am. Chem. Soc.* 2002, *224*, 048-054.
(10) Jensen, F.; Norrby, P. O. *Theor. Chem. Acc.* 2003, *109*, 1-7.
(11) Pasquarello, A.; Petri, I.; Salmon, P. S.; Parisel, O.; Car, R.; Toth, E.; Powell, D. H.; Fischer, H. E.; Helm, L.; Merbach, A. E. *Science (Washington, DC, U. S.)* 2001, *291*, 856-859.
(12) Neubrand, A.; Thaler, F.; Korner, M.; Zahl, A.; Hubbard, C. D.; van Eldik, R. *Dalton Trans* 2002, 957-961.
(13) Bryantsev, V. S.; Diallo, M. S.; van Duin, A. C. T.; Goddard III, W. A. *J. Phys. Chem. A* 2008, *112*, 9104-9112.
(14) Rotzinger, F. P. *J. Phys. Chem. A* 1999, *103*, 9345-9348.
(15) Tsutsui, Y.; Wasada, H.; Funahashi, S.*J. Mol. Struct. Theochem.*1999, *462*, 379-390.
(16) Rotzinger, F. P. *Helv. Chim. Acta* 2000, *83*, 3006-3020.
(17) Ducommun, Y.; Newman, K. E.; Merbach, A. E. *Inorg. Chem.* 1980, *19*, 3696-703.
(18) Kang, S. K.; Lam, B.; Albright, T. A.; O'Brien, J. F. *New J. Chem.* 1991, *15*, 757-62.
(19) Hermansson, K.; Wojcik, M. *J. Phys. Chem. B* 1998, *102*, 6089-6097.

Chapter 6 - Cobalt (III) and Nitrogen donor cage complexes

Introduction

Cobalt (III) hexammine is regarded as an octahedral "rock", with its quite rigorously unchanging metal ligand bond length, due to the very stable low spin d^6 electron configuration. However, cobalt am(m)ines have shown a diverse set of uses and properties ranging from templates in synthesis[1,2] to targeted drug chaperones[3].

The structures of these cobalt complexes are not as unchanging as the stable electronic configuration would have us believe; suitably restricted ligands can cause distortions from the nominal bond length (~1.96 Å). The ligands that are capable of causing this distortion are mainly polydentate ligands with multiple backbone linkages. Figure 6-1, shows a ligand which causes a large distortion from the assumed octahedron. The distortion is due to the constraining nature of the ligand. The deformation caused by this ligand is a trigonal twist, going away from the octahedral shape towards the trigonal prism.

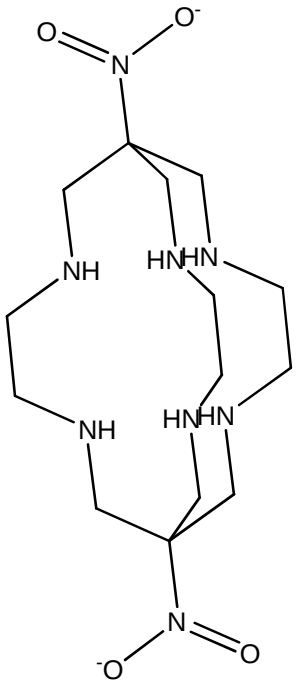

Figure 6-1 *Diamsar* a hexadentate ligand that causes distortion away from nominal octahedral shape with Co^{+3}

The cobalt analogues of these cage complexes are of significant interest as they have shown many desirable properties for use in the pharmaceutical industry; such as stability to strongly acidic conditions (such as those found in the mammalian gut). The cage complex is also stable enough to allow selective breakdown of the complex given the correct conditions. Lastly the complexes are very stable in the bloodstream with little or no excretion in the faeces (only in the urine)[3]. An important role for cobalt cages is their possible use as anticancer agents due to their DNA binding affinities[4], and the robust chemical substitutions that can be performed upon the cages to allow possible biological targeting (Figure 6-2). The diversity of possible cage complexes that could be developed are in part due to one of the last features of cobalt ammine complexes, which is cobalt(III)'s ability to template smaller ligands prior to synthesis and its stability to common reaction conditions (acidic, basic, alcohols) due to its "rock" nature.

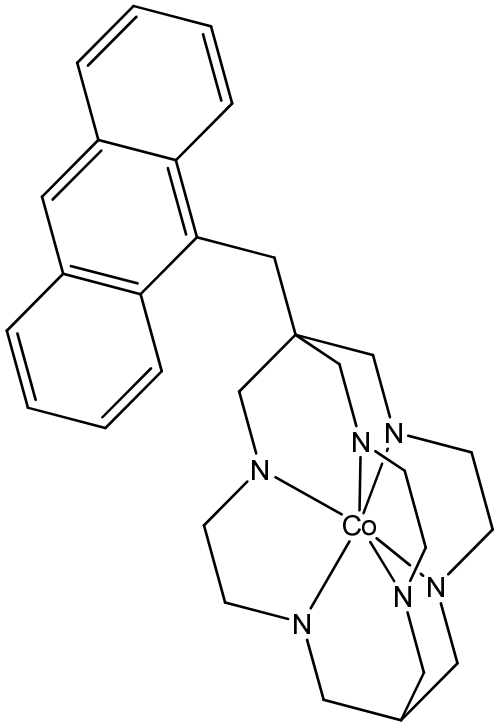

Figure 6-2 Cobalt cage complex showing significant DNA targeting and binding characteristics.

For these reasons cobalt cage complexes, and by extension cobalt ammines, are very interesting complexes as targets for computational modelling.

Cobalt ammine complexes were one of the "cornerstone" complexes in inorganic chemistry, being one of the complexes that was highly researched by Gibbs and Genth, then by Jorgensen some 20 years later and finally extensively used by Alfred Werner in his coordination chemistry theory. Given that these compounds were known so long ago it may be considered surprising that work is still carried out on these species. However, considering the properties of these compounds and the importance of active drug development, the recent interest is understood. Work has been done to investigate these complexes both experimentally and theoretically, and the advantages of applying theoretical methods to drug discovery problems are well publicised. The main methods

used for high throughput studies are based on Molecular Mechanics (MM). The reasons for this are that MM is a lot faster than Quantum Mechanical methods (QM) and is as accurate for structures, coupled with the large numbers of compounds that can be found in prodrug libraries makes MM often the only choice. Also many drugs are designed to interact with proteins, enzymes or DNA in the body, all of which are inherently large systems. Such system sizes are not easily dealt with in QM (although there are methods emerging that allow some QM access to large scale problems) and so we fall back to relying on MM. However, is not initially a technique you would trust in dealing with cobalt complexes, as MM takes no account of the electrons in the system, which often means that MM treatments of transition metals fall woefully short of the real system. To this end we use our in house add-on to the Molecular Operating Environment (MOE), called D Orbital Molecular Mechanics In MOE (DOMMIMOE).

LFMM uses Ligand Field Theory (LFT) via the Angular Overlap Model (AOM) to account for the d orbital effects and energies (such as the Ligand Field Stabilisation Energy, (LFSE)) in transition metal complexes, and has already been shown to deal accurately with relatively complex problems such as the Jahn-Teller effect in copper (II) and cobalt (II) complexes, as well as fast theoretical access to transition states, not previously thought accessible via MM, (see Chapters 3 and 4).

Computational Details

All LFMM calculations were performed using our in-house code applied to the MOE 2007 platform.

All DFT calculations were performed using the 2006 version of the Amsterdam Density Functional (ADF) program. Geometry optimisations were performed using the frozen

core approximation, 1s-2p on the metal and 1s on the nitrogen, carbon and other "heavy" elements, with triple ζ plus polarisation (TZP) on the metal and donating ligand atoms, and double ζ plus polarisation (DZP) on all others, default SCF and optimisation convergence limits were used.

Frequency calculations were performed again using ADF 2006 with the frozen core approximation. However, triple ζ plus polarisation basis sets were used on all atoms and a default integration level of 6 was used (rather than the default 4).

Results and discussion

Parameter development

The LFMM force field parameters were developed much in the same way as they were for the earlier water work (See Chapter 3).

A baseline for the comparison was calculated using DFT and cobalt III hexaammine complexes.

	Early parameters	Final parameters	Target
r_0 (Å)	1.94	1.99	
D (kcal mol^{-1})	75	65	
α	1.55	1.05	
A_{LL} kcal mol^{-1}	7000	7000	
a_5 e_σ kcal mol^{-1} $Å^{-5}$	216841	216841	
M-N (Å)	1.99	2.00	2.01
Symmetric stretch cm^{-1}	770	402	409

Table 6-1 Early LFMM parameters and the final refined set based on full system property analysis (see later in this chapter)

The early set of parameters (Table 6-1) were tested on a database of Co(III) complexes where the donors where simple saturated nitrogen atoms. This was to see how the force field performed on systems more complicated than the $[Co(NH_3)]^{3+}$ that the parameters were developed on.

Refcode	M-L(rms) Å	Heavy Atom rmsd Å	Refcode	M-L(rms) Å	Heavy Atom rmsd Å
ABIXIT	0.013	0.120	JESCIT	0.007	0.140
ACHXCO	0.013	0.108	JESCOZ	0.015	0.101
BAJZUI	0.014	0.135	LITREL	0.005	0.107
BEKJOQ	0.002	0.103	LIYMUB	0.010	0.080
BIGNOU	0.007	0.074	LOMRAG	0.009	0.072
BIGNOU01	0.007	0.075	NITNEJ	0.008	0.186
BUKKIB10	0.005	0.117	OAZCOC	0.008	0.120
BUTPIP	0.006	0.097	PDAMCO	0.011	0.173
BUTPIP01	0.015	0.099	PEVXAP	0.011	0.086
CAKQIP	0.006	0.109	PIBFOV	0.009	0.089
COPTNC	0.008	0.124	POVPEV	0.011	0.093
EDANEC	0.013	0.098	SAYKUY	0.008	0.094
ENCOCD	0.016	0.089	SOZFIW	0.011	0.106
ENCOCT	0.007	0.093	TAKHOD	0.016	0.102
ENCOCT01	0.007	0.095	TEACOC	0.005	0.082
ENCOPN	0.007	0.071	VIMWOD	0.013	0.108
FIRQIH	0.012	0.090	WACMIX	0.008	0.109
FOPLOL	0.013	0.178	XAZSEW	0.013	0.080
GAPHUA	0.009	0.078	YUXPOW	0.010	0.117
GUZNOE	0.008	0.087	ZEKNUY	0.009	0.090

Table 6-2 Calculated LFMM structures compared to crystal structures, sorted by CCDC reference code

Our method has been validated on many transition metal systems where there is a strong electronic LFSE controlling the behaviour of the system. However, in the case of these cobalt complexes the LFSE (strongly low spin, d^6, strongly octahedral) and the sterically demanding ligand (distorted octahedral, often trigonal prismatic) Figure 6-3, are in direct competition, and it has been shown that many other MM methods for dealing with transition metals do not in fact treat these systems adequately. There is not enough variation in the bond lengths computed, most likely due to the parameters that keep the complex octahedral.

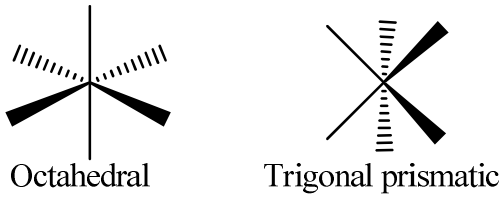

Figure 6-3 Octahedral geometry preferred by cobalt(II) complexes and trigonal prism often preferred by donor atoms in the pro-ligand

A recent review[5] in the area has made comparisons of available methods (that are supposedly able to deal with transition metals) for the calculation of structures and energies of cobalt cage complexes. It was from this paper that we built our starting database, 6-3, of test cases to see how the LFMM method compares and performs. The set of structures was said, by the original authors, to be representative and very reliable (based on the crystallographic parameters).

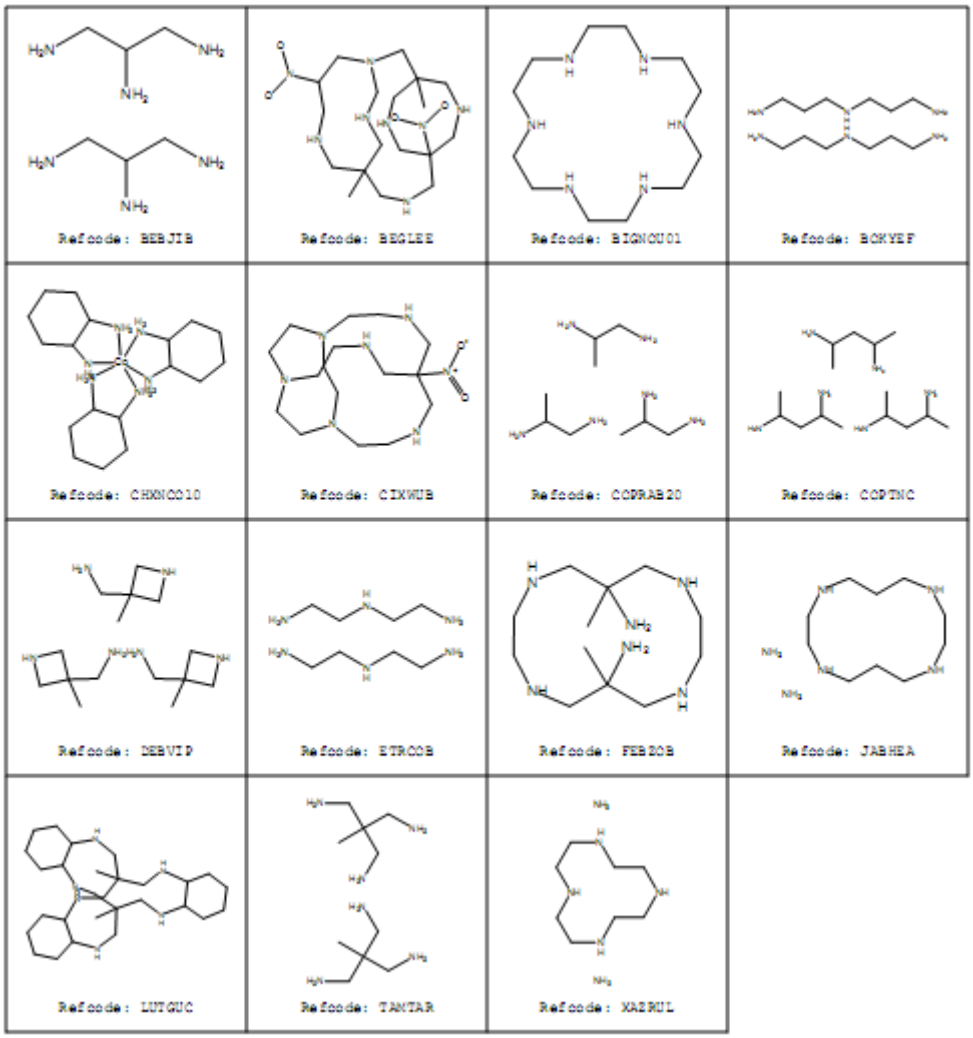

6-3 Composition of starting test set, alphabetical by ccdc refcode

Each molecule in this database was minimised using LFMM(using parameters developed based solely on hexa-ligated cobalt am(m)ine complexes) and the resulting minimised structures were compared to the original crystallographic structures (Figure 6-4).

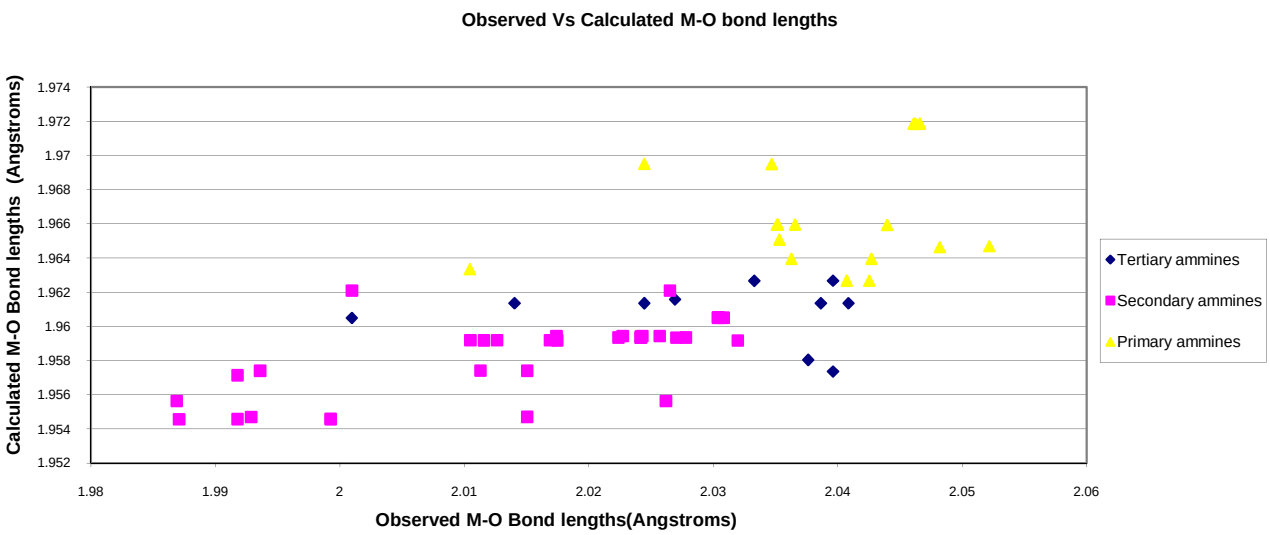

Figure 6-4 comparison of LFMM structures with crystallographic structures

It appears at first glance that our LFMM method "fails" for looking at these complex and biologically relevant systems, but both methods predict that secondary M-N bonds are shorter than tertiary M-N bonds which in turn are shorter than primary M-N bonds. Although, the LFMM results have a much tighter spread than the experimental results. However, these systems are much more complicated than the original parameterisation set, and so a more involved method of defining the MM parameters was decided upon.

To further refine and improve the parameters it was decided that some handle on the vibrational frequencies was needed (as the cage complexes are particularly strained in comparison to cobalt hexammine). A frequency component to the force field development was the most logical choice as the results shown (Figure 6-4) do not show enough flexibility.

The vibrational frequencies of cobalt hexammine were calculated using the ADF package and compared to the frequencies calculated within LFMM, and the normal modes were used to parameterise the LFMM force field Figure 6-5. This was done using a manual iterative procedure. After this parameter re-optimisation the performance of LFMM for

our test set was re-evaluated, Figure 6-6. The frequencies shown in Figure 6-6 all showed the same predominant motions in the compared pairs. The normal mode symmetric stretch for this system is the highest point on the LFMM scale (~400 cm^{-1}).

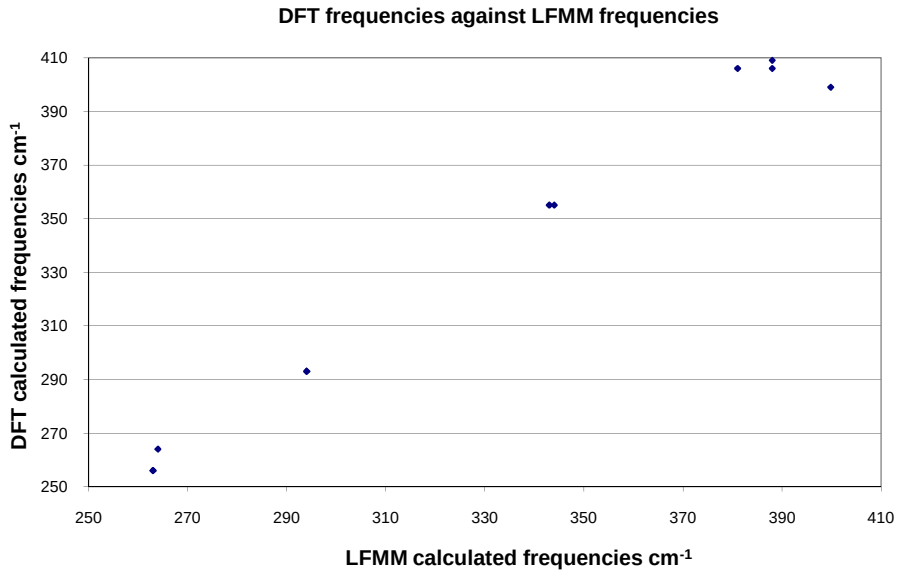

Figure 6-5 Comparison of ADF and LFMM calculated frequencies (cm^{-1}) for cobalt hexamine

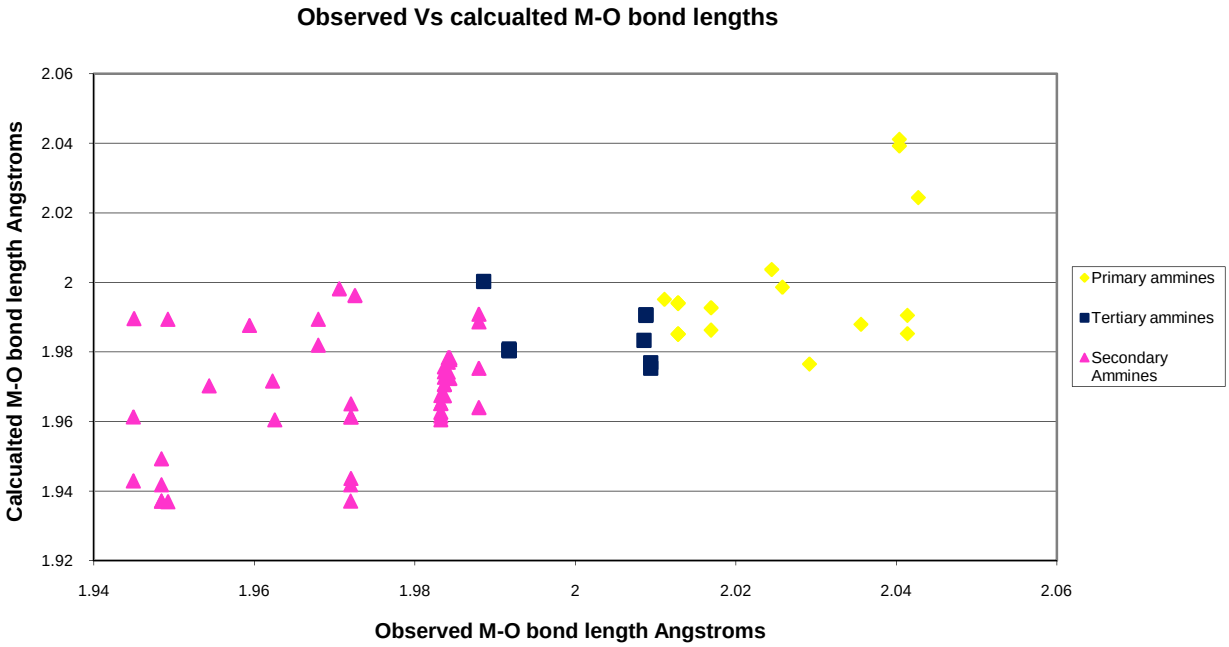

Figure 6-6 Comparison of M-O bond lengths in LFMM and the Crystallographic data

In the comparison after the parameter re-optimisation LFMM does perform better than in the initial trial. However, it is still not good enough, as the spread for the LFMM data is still too tight. This leads to one of the following conclusions: one, our method is not as accurate as we would like for the systems being looked at currently, or two, the "representative" structures in our original test set are not as representative, diverse or accurate as we need, and perhaps should be looked at in more detail. The ways to look into the latter of the above points are, assume our method is correct and that the cases we are "worse" for are in fact special cases and need more investigation, or, the initial database is not diverse at all and needs broadening to accurately test our method. One of the major strengths of our LFMM method is its ability to deal with mixed systems and system changes without needing a new force field (once a force field has been developed).

Not accepting that our method is inadequate, the database was re-evaluated, with a more critical look at the structures. This revealed that the database was not as diverse or accurate as first expected. All of the structures included in the initial search were unsaturated amines and were often found to have large counter ions in the crystallographic file. To remedy this, the Cambridge crystallographic database was used to find other cobalt systems which could be designated as cage complexes. This search resulted in nearly 100 extra complexes which could be included in our database for comparison. These extra structures allowed to have a more systematic look at our performance against a broad range of structures, not just against a handpicked test set from the literature.

The expanded database included a much broader range of complexes that incorporated many new types of nitrogen donor that were not considered in the initial study, as well as a few mixed ligand systems .

Continuing on the assumption that LFMM is not actually doing something wrong, then there must be something else that is being missed in the structures we are comparing too. As we are using crystallographic structures as our baseline we must consider the likelihood of crystal effects, such as packing and counter ions.

To investigate the effects of packing we can simply (at least to a first approximation) use DFT to minimise the structures and compare LFMM to these.

To investigate the effects of counterions, the easiest thing to try first is to explicitly include a counterion in the LFMM simulation and see if this has a marked effect on the geometry.

Initially the expanded database of crystallographic structures was minimised in LFMM and the results compared.

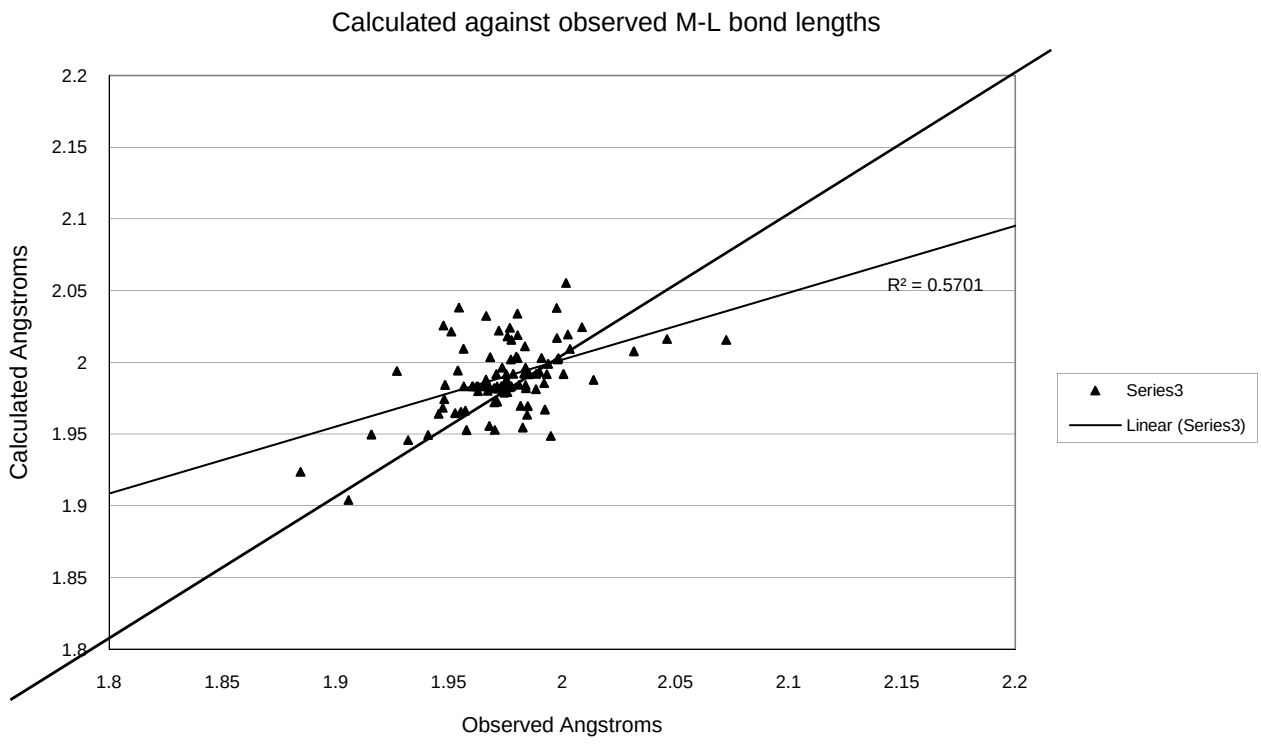

Figure 6-7 Graph of LFMM M-N bond lengths against the crystal M-N bond lengths

From the above figure it is clear that, while LFMM is a valid treatment for a large number of these diverse cobalt amine complexes. There is still some work to be done to validate the method as a generic tool, as there are a handful of rather extreme outliers that need some explaining.

DFT with ADF: a new baseline

The baseline database has many structures in it, too many for an exhaustive DFT study, so the structures that showed the largest difference in calculated bond lengths were chosen and were minimised using ADF. The resulting structures were compared to the LFMM minimised structures and the results were very encouraging.

The new structures obtained from the DFT calculations were a much closer match to the LFMM structures than the crystal structures were. This lead to the conclusion that some crystal effect that we had not yet accounted for was causing these distortions and so the crystal structures were not as valid a baseline as was originally suspected.

In the original test set, one of the complexes that LFMM did the poorest on was CIXWUB, a complex comprised of a hexadentate ligand with six nitrogen donors linked by ethylene bridges with a NO_2^- capping group linking 3 of the bridges. However, the alignment between the ADF structure and the LFMM structure was much stronger, this partially validates our idea either something was missing in our earliest simulation or that there are some strong crystal effects in play.

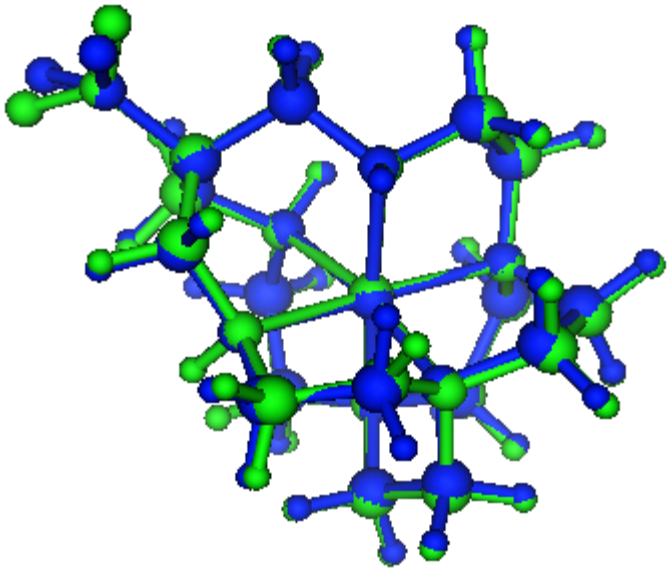

Figure 6-8 Overlay of the LFMM(blue) and ADF (green) structures of (Cambridge crystal database refcode)

To clarify this point further the counterion from the crystallographic structure was added to both the LFMM structure and the ADF structure, and both were again minimised using that respective method. This resulted, in both cases, to a geometry much closer to the crystallographic structure Figure 6-9 and greatly explains why the LFMM calculations were apparently so different to the crystal structures in the initial study.

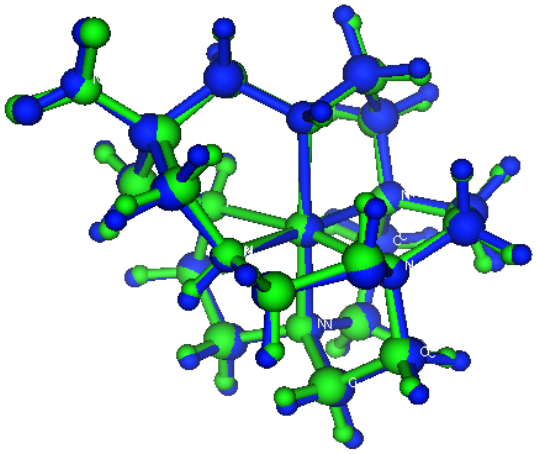

Figure 6-9 Overlay of LFMM structure (calculated with counterion, ClO_4^-) with original crystal structure of CIXWUB

Bond with atom	LFMM Bond length (Å)	DFT Bond length (Å)	Angle Between bonds	LFMM Bond Angle (°)	DFT Bond Angle (°)
1	2.02	2.04	1 - 5	85.60	85.20
2	2.02	2.02	1 - 4	100.01	98.80
3	2.02	2.06	1 - 6	172.60	169.40
4	1.99	2.00	1 - 3	89.40	89.12
5	1.99	1.99	1 - 2	90.10	90.10
6	1.33	1.98	1 - 7	54.30	54.60
7	3.05	3.04			

Table 6-4 Comparison of LFMM and DFT structural parameters for CIXWUB (Key for bond numbering shown below)

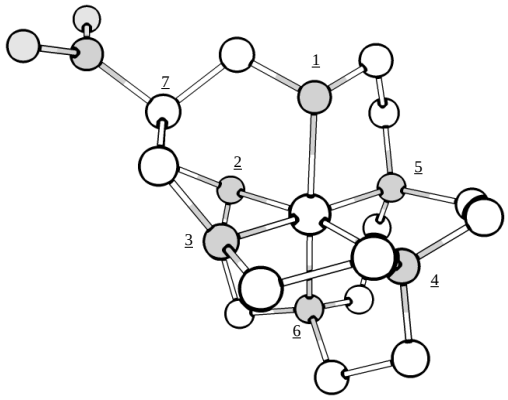

Figure 6-10 Key for Table 6-4

This correction was applied to the database, and the comparison redone, the graph Figure 6-11 clearly shows that in difference to the earlier graph the major outliers have been removed, just by correcting this one structure.

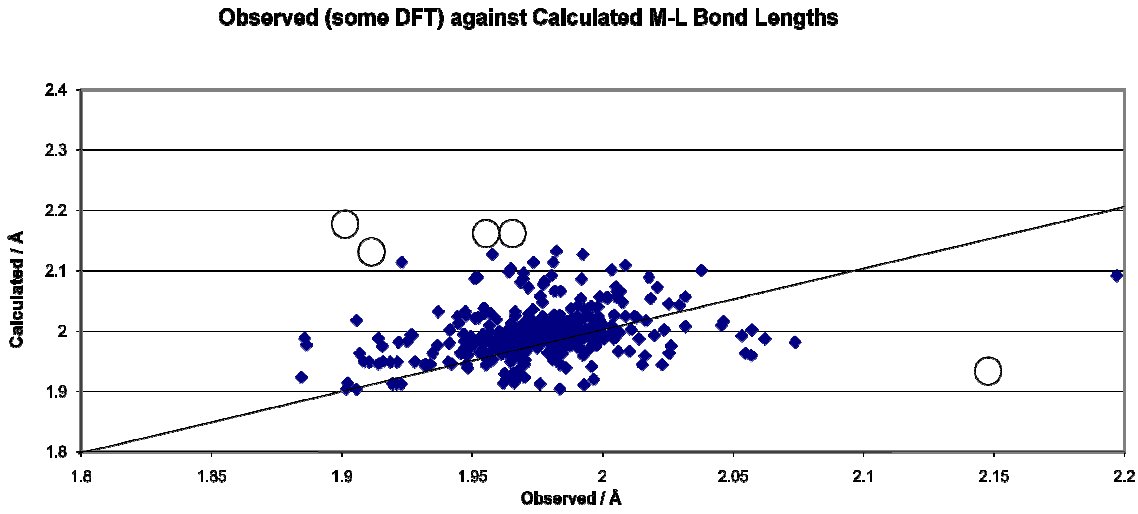

Figure 6-11 comparison of M-O bond lengths given the above stated correction, the circles highlight the outliers that were removed just on the correction of the two above structures.

Expanded ligand types

The expanded database included all of the complexes from the initial study as well as a significant number of extra complexes. The original database contained only complexes with saturated, single bonded, nitrogen donors. The expanded set also contained additional nitrogen donor types (defined as different MM force field types). The expanded set also added some mixed type systems, which were another type of complex missing from the initial work.

Bond with	Crystal (Å)	LFMM (Å)	Type
All bonds	1.90 - 1.92	1.92	N=C
1 - 6	1.71	173	N=C
1 - 2	1.79	1.81	N=C
1 - 5	1.95	1.95	N=C
2 - 5	1.95	1.94	N=C
4 - 5	1.80	1.81	N=C

Table 6-5 Comparison of structural features for OXAMCO from the crystal structure and the LFMM structure

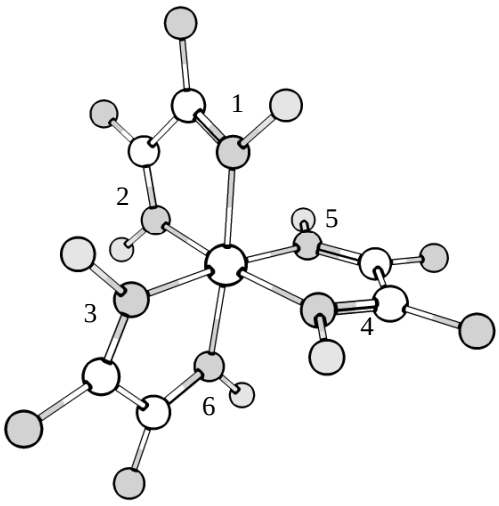

Figure 6-12 OXAMCO structure (hydrogen atoms removed for clarity) with labeling key

Bond with	Crystal (Å)	LFMM (Å)	Type
1	1.88	1.86	N5B
2	1.98	1.98	N=C
3	1.93	1.96	N=C
4	1.9	1.89	N5B
5	1.91	1.89	N5B
6	1.95	1.97	N=C

Table 6-6 Comparison of structural features for CAFHUN from the crystal structure and the LFMM structure

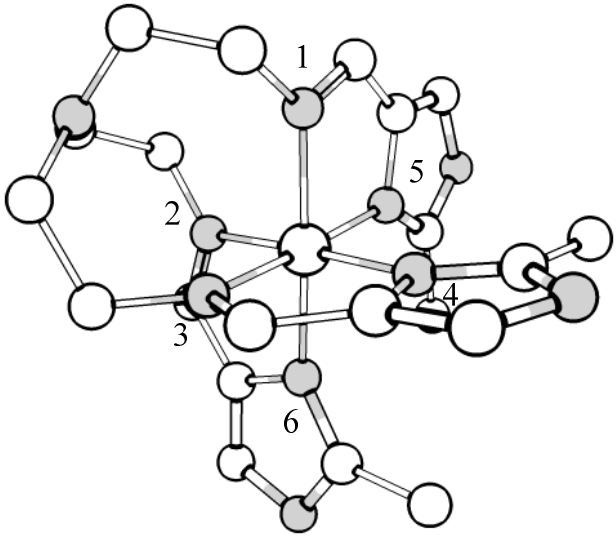

Figure 6-13 CAFHUN structure (hydrogen atoms removed for clarity) with labeling key

Bond with	Crystal (Å)	LFMM (Å)	Type
1	1.91	1.93	N=C
2	1.96	1.98	N
3	1.96	1.95	N=C
4	1.92	1.93	N=C
5	1.87	1.89	N=C
6	1.99	2.01	N
Angle 1-6	167	166	

Table 6-7 Comparison of structural features for WUGNUH from the crystal structure and the LFMM structure

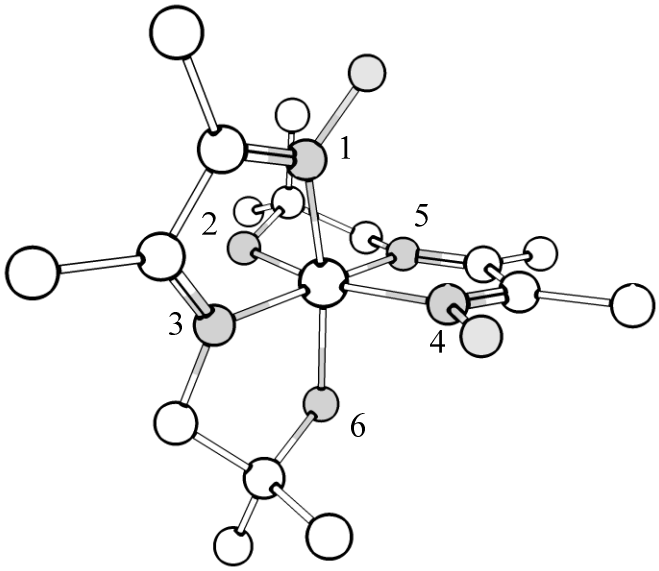

Figure 6-14 WUGNUH structure (hydrogen atoms removed for clarity) with labeling key

Conclusions

A set of LFMM force field parameters has been developed for the Co^{3+} complexes with nitrogen donors. Initially the parameters were arrived at based solely on crystal structure data. However, it was found that this was not sufficient to accurately capture all of the required details of these systems.

After DFT calculations were also utilised the ability of the LFMM method to reproduce the target data improved. However, this was still insufficient to account for all of the structures available.

This led to the realization that the available crystal data may have external factors affecting the observed geometries. To test this observation two things were done. Firstly: select crystal structures were minimised, in an attempt to remove any crystal packing artifacts present on the reported geometries. These single molecule DFT structures were accurately reproduced using the LFMM method. Secondly the LFMM calculations were run including a counter ion, these calculated structures agreed much more favourably with the crystal structures. From this it looks hopeful that the LFMM method would be applicable to solid state problems based on single molecule parameterisation, although this is pure speculation at this point.

References

(1) Comba, P.; Hormann, A.; Martin, L. L.; Zipper, L. *Helv Chim Acta* **1990**, *73*, 874-882.
(2) Lundberg, M.; Siegbahn, P. E. M. *J Phys Chem B* **2005**, *109*, 10513-10520.
(3) Sargeson, A. M. *Coord Chem Rev* **1996**, *151*, 89-114.
(4) Richards, A. D.; Rodger, A. *Chem Soc Rev* **2007**, *36*, 471-483.
(5) Bygott, A. M. T.; Sargeson, A. M. *Inorg Chem* **1998**, *37*, 4795-4806.

Chapter 7 – Mixed Ligand Systems of Cr^{3+}

Introduction

As stated in the computational chemistry chapter (Chapter 2), one of the greatest strengths of the LFMM method is that the force field developed should be applicable to any system that contains the atom types that have developed parameters. As discussed earlier the exchange mechanism at transition metals is of utmost interest and it was found that the LFMM can adequately deal with this fundamental process, not just in a qualitative but in a quantitative manner.

To test the limit of this work, a new test system was investigated as a mixed ligand benchmark (Figure 7-1).

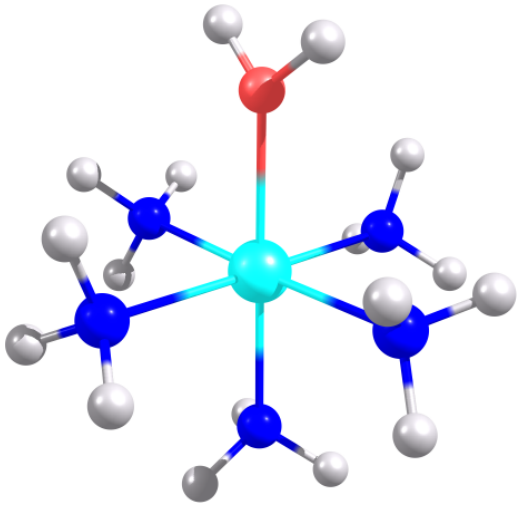

Figure 7-1 $[Cr(NH_3)_5(H_2O)]^{3+}$

The above system (Figure 7-1) was selected as a target because it is a mixed ligand system comprised of ligands that had been treated successfully with the LFMM force field. Also the earlier computational work on this species was performed by Rotzinger[1-4], and as our previous study has been extensively compared to his research it made sense to pick a test system where we knew the methods used and how they compared to LFMM.

The $[Cr(NH_3)_5(H_2O)]^{3+}$ system contains the two ligands that have been previously studied in this research (Chapters 2,3,4 and 5). However, the metal centre is a Cr^{3+} ion, which has not been included as a target in this work, meaning that a new parameter set was required.

Parameter development

The parameters were developed based on a set of DFT calculations on the pure Cr^{3+} species, $[Cr(NH_3)_6]^{3+}$ and $[Cr(H_2O)_6]^{3+}$. The parameter development occurred as detailed in the first results chapter utilising: the solvation energy, interaction energy, geometric features and normal mode frequencies.

	Mulliken	Hirshfeld	Voronoi
Cr^{3+}	1.45	0.7695	0.632
O	-0.48	-0.14	-0.21
H	0.37	0.25	0.3

Table 7-1 Charges calculated for the $[Cr(H_2O)_6]^{3+}$ complex.

	Mulliken	Hirshfeld	Voronoi
Cr^{3+}	1.43	0.614	0.506
N	-0.17	-0.148	-0.197
H	0.14	0.182	0.205

Table 7-2 Charges calculated for the $[Cr(NH_3)_6]^{3+}$ complex

The charges used were based on the Mulliken[5] population analysis. Although, the other methods are more mathematically sound they did not reproduce the roll, pitch and yaw which was found to be important in the earlier work.

Atom	Charge
Cr	1.44
O	-0.48
N	-0.17
H (O)	0.37
H (N)	0.145

Table 7-3 Charges used for all LFMM work that follows

	$[Cr(H_2O)_6]^{3+}$		$[Cr(NH_3)_6]^{3+}$	
	adf	lfmm	adf	lfmm
Energy kcal mol^{-1}	-313.59	-313.49	-389.08	-390.23
Frequency cm^{-1}	435	437	374	377
M-O Distance Å	1.99	2.01	2.15	2.16

Table 7-4 Table of key parameters calculated in both ADF and with LFMM using the developed parameter set.

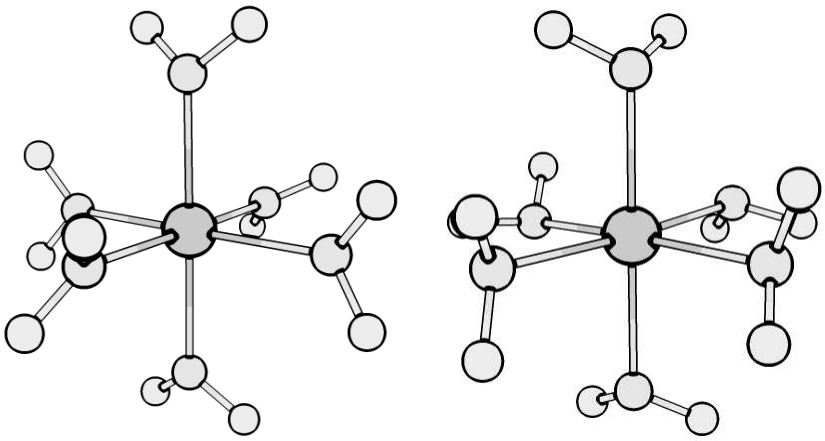

Figure 7-2 LFMM (left) and ADF (right) structures for the hexaqua complexes of Cr^{3+}, both showing the roll, pitch and yaw found in earlier work

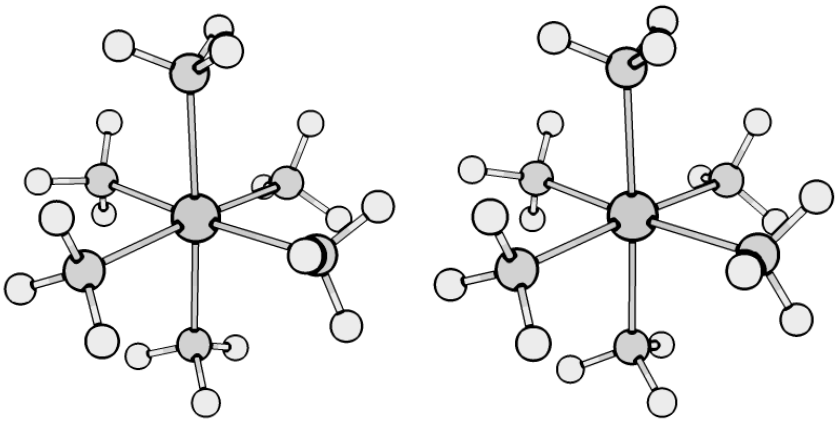

Figure 7-3 LFMM (left) and ADF (right) structures for the hexaammine complexes of C r^{3+}

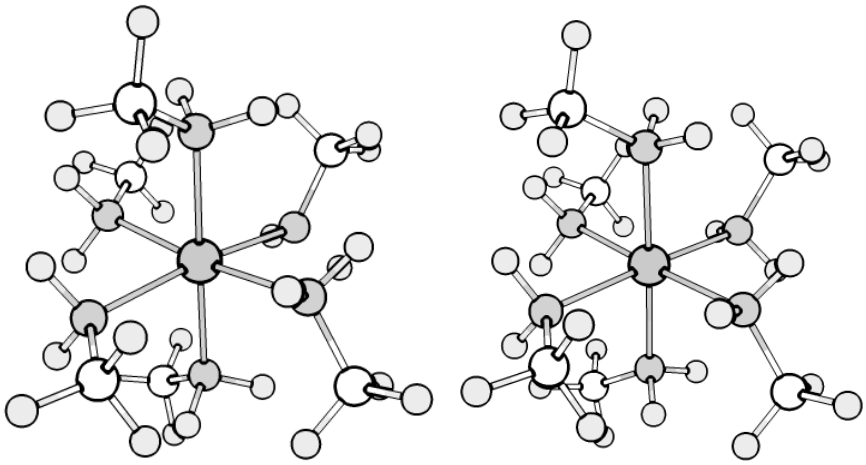

Figure 7-4 LFMM (left) and ADF (right) structures for the methalyted hexaamine complexes of Cr^{3+}

As these parameters are to be used to assess the LFMM method's ability with mixed ligand systems and exchange at these centres. It is important that the method performs correctly for the starting species. The behaviour above shows that the method deals with the six coordinate species, but the seven coordinate species need to be validated. All of the work presented deals with water exchange on these ammine complexes. The work of Rotzinger[1-3,6] has been used as a comparison for the calculated structures as the work contains high level theoretical calculations of the geometries, methods that were beyond the scope of this work.

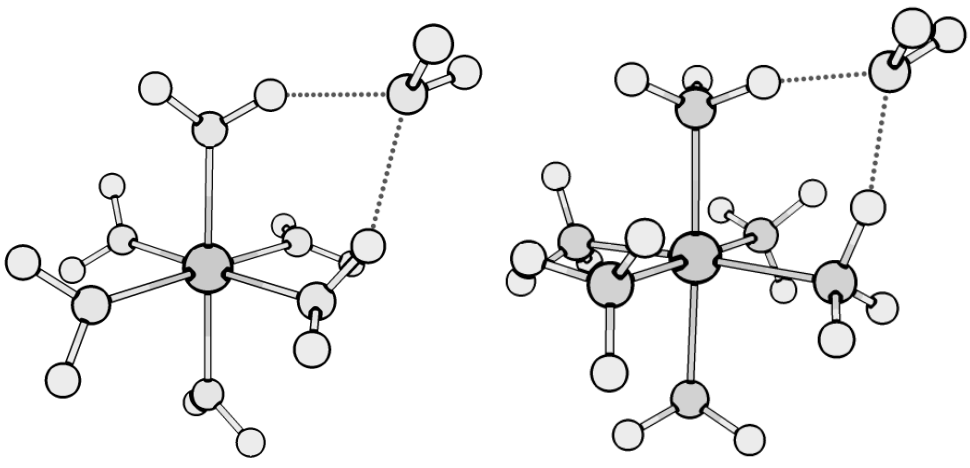

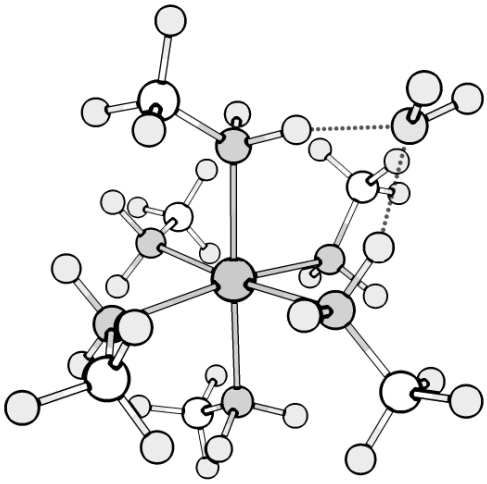

Figure 7-5 diagrams of LFMM structures of the complexes with an associated seventh water molecule

	LFMM	DFT
$[Cr(H_2O)_6]^{3+}$	3.78	3.82
$[Cr(NH_3)_6]^{3+}$	3.61	3.55
$[Cr(NH_2CH_3)_6]^{3+}$	3.80	3.90

Table 7-5 Comparison of LFMM and DFT M-O bond lengths (Å) to the seventh ligand (in these a molecule of water)

The above structures show stability to the presence of the seventh ligand. The changes to the general structure are minor but include the important features from the QM calculations, such as the contraction of the bite angle between the two first coordination sphere ligands by about 5 degrees as well as a lengthening of the metal ligand bonds by approximately 0.05 Angstroms.

Finally the LFMM force field was used to calculate the water exchange process as stated in the earlier chapters.

	I_a	I_d
ground state	-333.76	-267.61
transition state	-341.96	-278.36
reaction barrier	8.20	10.75

Table 7-6 Energy comparison (kcal mol^{-1}) of different pathways for water exchange at $[Cr(H_2O)_6]^{3+}$

The LFMM method calculates the I_a process to be the most favoured for the $[Cr(H_2O)_6]^{3+}$. This is in agreement with the previously published results. However, the calculated geometry for the I_a process does not agree with that calculated in the literature. The literature geometry gives a bond length for the exchanging ligands of 2.4 Angstroms, whereas the LFMM method calculates the bond lengths to be 3.00 Angstroms. Similarly the I_d process also has a longer M-O bond length than in the literature reported one; 4.2 Angstroms instead of 3.49 Angstroms. Although, this difference in bond lengths is to be expected as the literature work was all done with a significant water shell, and solvation shell effects often cause a contraction of the ligand sphere. Also as stated earlier it appears that the charge scheme used in this work (based on the pure ligand systems) is not optimal for the mixed ligand system.

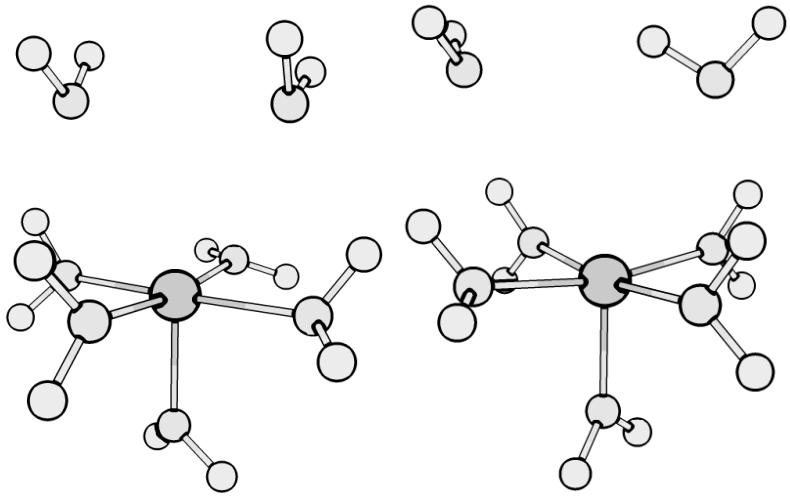

Figure 7-6 I_a and I_d respectively, structures calculated with the LFMM MECP method

The Mixed System

Having developed a set of parameters that perform adequately on the single ligand systems it was now time to apply this force field to the full mixed system. The mixed system $[Cr(NH_3)_5(H_2O)]^{3+}$ was minimised with the LFMM method. The resulting structures were stable both with and without the seventh ligand.

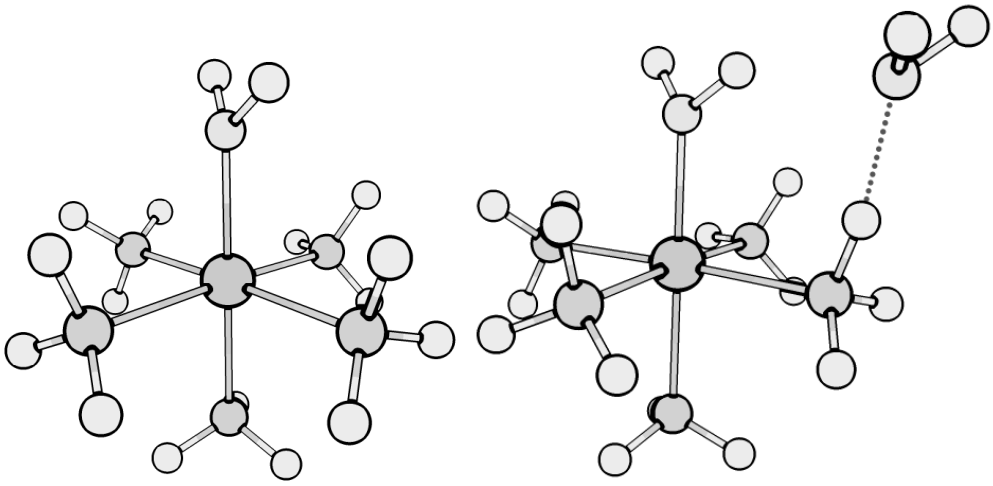

Figure 7-7 LFMM structures for the $[Cr(NH_3)_5(H_2O)]^{3+}$ complex and the $[Cr(NH_3)_6(H_2O)]^{3+}$

The LFMM calculated structure is fairly accurate but shows a noticeable contraction in the M-O bond length.

	LFMM M-O	DFT M-O	LFMM M-N	DFT M-N
$[Cr(NH_3)_5(H_2O)]^{3+}$	1.99	2.09	2.11	2.16
$[Cr(NH_3)_5(H_2O).(H2O)]^{3+}$	3.87	4.01		

Table 7-7 Comparison of M-O bond lengths (Å) in the $[Cr(NH_3)_5(H_2O)]^{3+}$ complex

Both the M-O and the M-N bonds show slight shortening compared to the DFT value. This may mean that the charge scheme used for the individual ligands is not the optimum one for the mixed system. An improvement may be to use a charge a scheme that is an average of the ones reported above (Table 7-2, Table 7-2). However, the results are acceptable and so the developed parameters were used in the further investigation.

The exchange of the water ligand at these metal centres was investigated using the methods outlined earlier; MECPs and NR optimisation, the results were as follows.

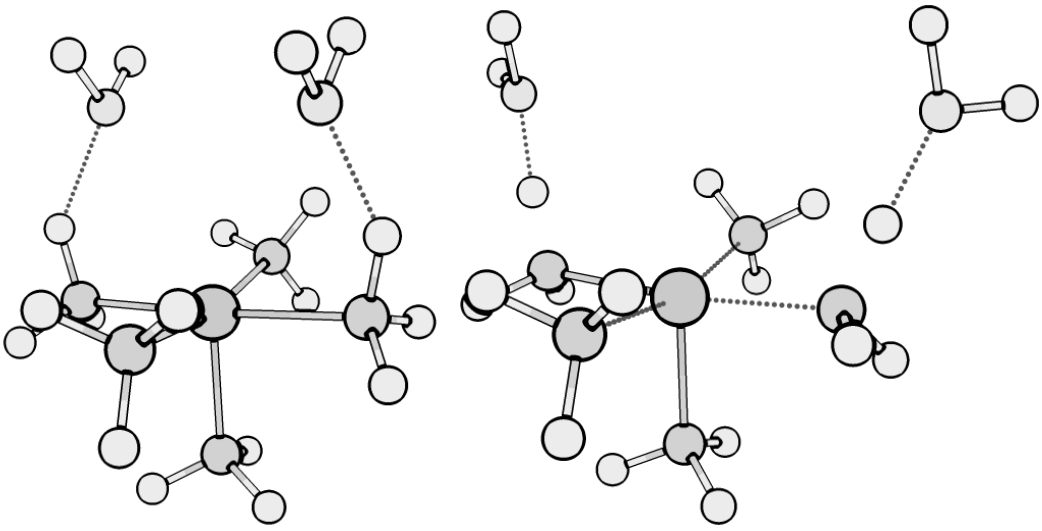

Figure 7-8 I_a and I_d transition states calculated with the LFM method

	LFMM I_a	LFMM I_d	Literature I_a	Literature I_b
Ground state	-500.38	-410.66		
Transition state	-483.33	-386.79		
Reaction barrier	17.05	23.88	25.41	28.3

Table 7-8 Comparison of exchange route energies (kcal mol^{-1}) from LFMM

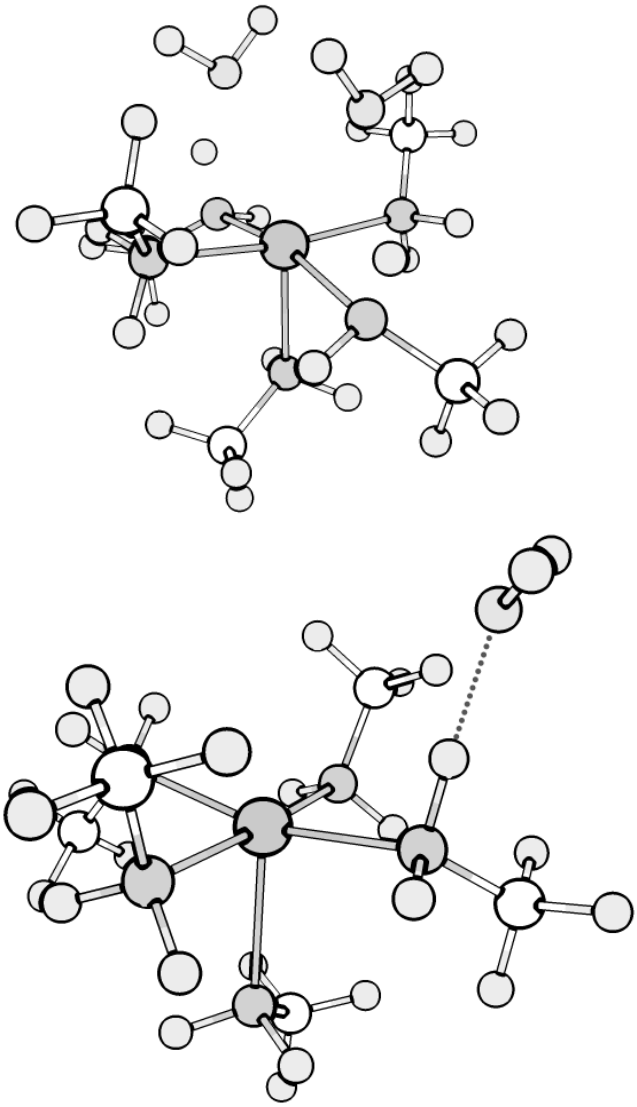

Figure 7-9 I_a and I_d MECP structures for the exchange at $[Cr(NH_2CH_3)_5H_2O]^{3+}$

	LFMM	Literature
Incoming I_a	3.20	3.38
Outgoing I_a	3.20	3.26
Outgoing I_d	3.75	3.55

Table 7-9 Comparison of LFMM and Rotzinger calculated bond lengths (Å) for the exchange pathways of $[Cr(NH_2CH_3)_5H_2O]^{3+}$

	LFMM I_a	LFMM I_d	Literature I_a	Literature I_d
Ground state	-369.16	-324.038		
Transition state	-338.00	-313.227		
Reaction barrier	31.16	10.81	30.54	24.26

Table 7-10 Comparison of exchange route energies (kcal mol^{-1}) from LFMM

The LFMM method correctly predicts the different exchange mechanisms for the systems above, including the mechanistic difference between the ammonia and methylated ammonia complex.

The LFMM method was unable to find a transition state for the I_a pathway for the trans exchange. The trans exchange is shown in the literature to be difficult to locate and energetically less favourable than the adjacent I_a mechanism.

Conclusions

Using the knowledge and insight gained throughout the earlier chapters a set of LFMM parameters has been developed for the $[Cr(H_2O)_6]^{3+}$ and $[Cr(NH_3)_6]^{3+}$ complexes. These parameters were derived based solely on DFT calculations.

The LFMM force field was then used to calculate the exchange mechanism of the $[Cr(H_2O)_6]^{3+}$ complex. The structures and energies generated agreed with those shown in the literature.

Having succeeded on the simple pure ligand systems the method was tested on a set of mixed ligand systems, $[Cr(NH_3)_5(H_2O)]^{3+}$ and $[Cr(NH_2CH_3)_5(H_2O)]^{3+}$. The LFMM generated transition states agreed qualitatively with the published QM work. However, the geometries were not as accurate as in the earlier water exchange work. This may be correctable by a re-optimisation of charge schemes and then the parameters.

The LFMM generated structures and energies were in agreement with the QM work for the associated mechanisms. Even predicting the mechanistic difference between the $[Cr(NH_3)_5(H_2O)]^{3+}$ and $[Cr(NH_2CH_3)_5(H_2O)]^{3+}$ complexes, the $[Cr(NH_3)_5(H_2O)]^{3+}$ being associative in nature and the $[Cr(NH_2CH_3)_5(H_2O)]^{3+}$ being dissociative.

References

(1) Rotzinger, F. P. *Inorg. Chem.* **1999**, *38*, 5730-5733.
(2) Rotzinger, F. P. *J. Phys. Chem. A* **2000**, *104*, 8787-8795.
(3) Rotzinger, F. P. *J. Phys. Chem. A* **2000**, *104*, 6439-6446.
(4) Rotzinger, F. P. *J. Phys. Chem. A* **2000**, *104*, 8787-8795.
(5) Mulliken, R. S. *J. Chem. Phys.***1955**, *23*, 1833-1840.
(6) Rotzinger, F. P. *J. Phys. Chem. B* **2005**, *109*, 1510-1527.

Chapter 8 – Conclusions

General conclusions

This thesis and the research done to produce it have been interested in the applications of the Ligand Field Molecular Mechanics (LFMM) method to problems not typically tractable within a Molecular Mechanics (MM) framework. These problems have included: absolute energies, d electron effects, reaction mechanism investigation and generation of transition states.

In the course of this research, new force field parameter sets have been generated for a range of metal ligand interactions: first row divalent metal ions with aqua ligands (V^{2+} - Zn^{2+}), cobalt (III) with a selection of nitrogen donors and chromium (III) with both aqua and ammine ligands.

This thesis includes a brief overview of the LFMM method and previous work of the group. For a more complete picture the recent review by this group is included in the appendix.

In Chapter 3, a force field for treating complexes of the type $[M(H_2O)_6]^{2+}$ was developed. The $[M(H_2O)_6]^{2+}$ system was chosen due to the relatively large amount of available experimental data and due to the amount of interest in this fundamental system. To augment the parameter development a series of DFT calculations was performed. The first calculations were to ascertain if one of the gradient corrected functionals (the Generalised Gradient Approximation, GGA) was more accurate or precise for the hexaaqua complexes. The GGA functionals all performed equally well and showed significant improvement over the Local Density Approximation (LDA). The PW91 functional was chosen from this and used to calculate a series of geometries, energies and frequencies for the complexes. The frequency analysis showed that the T_h (D_{2h})

hexaaqua complexes were not in fact ground states. Further DFT calculations were performed to find true ground state structures. The true ground state structures were located and key distortions were seen in the DFT geometries that became an integral part of the LFMM parameterisation process. Having integrated a large amount of DFT and experimental data into the parameterisation, the LFMM force field performed exceptionally well in reproducing all of the required data, including absolute energies and vibrational modes.

In Chapter 4 the validated LFMM force field was used with a set of model structures to calculate the energies of the different exchange mechanisms for aqua complexes. The LFMM force field accurately predicted the mechanistic change over from I_a to I_d after Mn^{2+}. However, there were complications with the method as it could not treat the Zn^{2+} system and it calculated a negative energy barrier for the exchange process with Cr^{2+}. The research presented in this chapter spurred the integration of a method for the calculation of transition states and exchange pathways within the DOMMIMOE program.

In Chapter 5 the Minimum Energy Crossing Point (MECP) method, now implemented with DOMMIMOE, was used to calculate the LFMM exchange pathways for the V^{2+}, Mn^{2+} and Zn^{2+} complexes. To maintain consistency with the previous research, new DFT data were generated for the seven coordinate starting geometries as well as the transition states. The calculation of the complexes structures using DOMMIMOE led to the discovery of a third possible geometry that had not before been mentioned in the literature. This alternative geometry was confirmed to be a true ground state by DFT frequency analysis. The complex's with a seventh water ligand ($[M(H_2O)_6.\ H_2O]^{2+}$)were found to be stable with the LFMM method, even when the seventh water molecule was explicitly connected to the metal. From the $[M(H_2O)_6.\ H_2O]^{2+}$ complexes a series of target "product" geometries was built. These included both I_a products, where the ligand had exchanged with the seventh ligand, and an I_d product, where a previously bound water

ligand had left the primary coordination sphere but with the seventh water remaining nearly unmoved. These structures were used as the input for the MECP calculations to find the TS of the process. The MECP geometries were not the true transition states because the MECP minimises to the crossing point (which lies slightly higher in energy than the transition state) and so a Newton-Raphson (NR) optimiser was implemented allowing the LFMM method to minimise to a first order saddlepoint. The NR structures were confirmed to be true TSs by frequency analysis.

The LFMM TS energies were used to find the lowest energy pathway for the the ligand exchange mechanisms. Again the LFMM force field correctly predicted the mechanistic changeover as well as the energies of the process (against DFT energies for the exchange process).

In Chapter 6, a set of LFMM parameters was developed for the $[Co(NH_3)_6]^{3+}$ complex. This parameterisation was done using the ideas and process developed in earlier work. The LFMM force field was then used on a test set of cobalt am(m)ine cage complexes. The initial results were a little disappointing considering the earlier successes. However, the structures in the test set were scrutinised in a more thorough way. This led to the discovery that the complexes that LFMM performed worst on showed significant solid state or counter ion effects. DFT was then used to provide alternative geometries for these complexes as a new baseline for the LFMM force field. LFMM performed much better on this new baseline and the force field was also extended to include additional nitrogen donor types (different MM force field typing). On the extended set LFMM accurately calculated the geometries of the complexes, including mixed ligand systems.

In Chapter 7 the ability to fully treat mixed ligand systems was explored using a series of chromium complexes ($[Cr(NH_3)_5(H_2O)]^{3+}$ and $[Cr(NH_2CH_3)_5H_2O]^{3+}$). The LFMM parameters for these systems were developed based on six coordinate homoleptic systems ($[Cr(H_2O)_6]^{3+}$ and $[Cr(NH_3)_6{}^{3+}]$. The LFMM force field was then used to model

the exchange process of the $[Cr(H_2O)_6]^{3+}$ complex, which it correctly predicted as I_a. The compiled parameters were then used to calculate the MECP and hence NR geometries for the ligand exchange on the mixed ligand systems. The LFMM method correctly calculated the lowest energy pathway for each of the complexes, including the mechanistic difference between the ammine complex and the methyl ammine one (the ammine complex being I_a the methyl ammine complex being D)

Although this chapter showed many successes it did not reproduce the geometries or the energies quantitatively compared to DFT. This was speculatively attributed to the chosen charge scheme.

Future Work

The charge scheme for the chromium complexes needs to be optimised to see if this improves the calculated energies and geometries.

The MECP method needs to be trialled with systems where the "products" and "reactants" are not energetically the same, to develop the energetic considerations made by the MECP optimisation routine.

Also, now that the MECP routine has been tested for "simple" complexes, a more involved system with a more complicated ligand sphere would be interesting as a target. Trying to model the ligand exchange at an enzyme centre would be the final goal of this method, as the big benefit of the MM framework is that it is not too computationally costly to deal with large systems that are not practical to treat with QM.

Final Conclusions – LFMM

The LFMM method is a versatile way to treat the d electron effects seen in transition metal complexes. As well as being able to reproduce the Jahn-Teller effect it is capable of accurately reproducing frequencies and energies of ground states and TS.

LFMM is capable of calculating the quantitative properties of a complex system, using parameters developed on ground state data.